



Datrier, Laurence Élise Hélène (2018) *Investigating the prospects for constraining the Hubble constant using compact binary coalescences as standard sirens*. MSc(R) thesis.

<https://theses.gla.ac.uk/30621/>

Copyright and moral rights for this work are retained by the author

A copy can be downloaded for personal non-commercial research or study, without prior permission or charge

This work cannot be reproduced or quoted extensively from without first obtaining permission in writing from the author

The content must not be changed in any way or sold commercially in any format or medium without the formal permission of the author

When referring to this work, full bibliographic details including the author, title, awarding institution and date of the thesis must be given

Enlighten: Theses

<https://theses.gla.ac.uk/>
research-enlighten@glasgow.ac.uk

Investigating the prospects for constraining the Hubble constant using compact binary coalescences as standard sirens

Laurence Élise Hélène Datrier
B.Sc.

Submitted in fulfilment of the requirements for the
Degree of Master of Science (By Research)

School of Physics and Astronomy
College of Science and Engineering
University of Glasgow



University
of Glasgow

March 2018

Abstract

The use of gravitational wave observations from compact binary inspirals as standard sirens was first proposed by Schutz in 1986. Following the recent observations of compact binary coalescences by the Advanced LIGO detectors and the first standard siren measurement of the Hubble constant with the binary neutron star merger GW170817, and in anticipation of future detections during upcoming observing runs, it is useful to further investigate standard sirens, the gravitational wave analogues of standard candles, as an alternative way to measure the Hubble constant. Compact binary inspirals are well modelled, and their luminosity distance can be obtained from GW observations. From these distance measurements and using redshifts from EM galaxy catalogues and Bayesian inference, it is possible to assign a probability to each host galaxy, and a value for the Hubble constant can be obtained. While a redshift can sometimes be obtained from multi-messenger observations of binary neutron star coalescences, binary black hole mergers are not expected to produce electromagnetic signals, making statistical approaches an important tool in cosmology using gravitational waves. In this project, an investigation of statistical methods of measuring the Hubble constant with standard sirens is carried out using simulated data, to find out how well we can constrain the Hubble constant and to characterise the biases due to selection effects coming from the incompleteness of EM galaxy catalogues. Results are obtained for a range of aLIGO sensitivities, using both binary black hole and binary neutron star mergers as standard sirens. This constitutes an independent measurement of the Hubble constant that is competitive with other methods.

Contents

Abstract	i
Acknowledgements	viii
Declaration	ix
1 Introduction	1
1.1 General Relativity and Gravitational Waves	2
1.1.1 General Relativity	2
1.1.2 Gravitational Radiation	4
1.1.3 Generation of Gravitational Waves	5
1.1.4 Astrophysical Sources of Gravitational Waves	6
1.1.5 Observables of Gravitational Waves	8
1.1.6 Parameter Estimation from Gravitational Wave Signals	8
1.2 Gravitational Wave Detectors	9
1.2.1 Resonant Mass Detectors	9
1.2.2 Laser Interferometry for Gravitational Wave Detection	9
1.2.3 First Generation Gravitational Wave Detectors	11
1.2.4 Second Generation Gravitational Wave Detectors	11
1.2.5 Space-Based Detectors	13
1.2.6 Third Generation Detectors	13
1.3 Detections	15
1.3.1 Indirect Detection	15
1.3.2 Direct Detection	16
1.3.3 Future Observing Runs and Detections	18
2 Bayesian Data Analysis	20
2.1 Introduction	20
2.1.1 Probability Theory	20
2.1.2 History of Bayes' theorem	20
2.1.3 The Bayesian and Frequentist Approaches	21

2.1.4	The Role of Bayesian Inference in Physical Sciences	22
2.2	Basics of Bayesian Inference	24
2.2.1	Notations	24
2.2.2	Deriving Bayes' Theorem	25
2.2.3	Marginalisation	26
2.3	Model Selection	27
2.4	Parameter Estimation	27
3	Overview of Modern Cosmology	28
3.1	The Road to Precision Cosmology	28
3.2	Cosmological Principle and Standard Cosmological Model	29
3.3	The Expanding Universe	29
3.3.1	The Accelerating Universe	34
3.4	Measuring the Hubble Constant	34
3.4.1	The Hubble Flow	36
3.4.2	Peculiar Velocities	36
3.4.3	Cosmography	37
3.5	Methods for Measuring the Hubble Constant	39
3.5.1	The Cosmic Microwave Background	39
3.5.2	Standard Candles	40
3.6	Discrepancies in Measurements of the Hubble Constant	42
4	Measuring the Hubble Constant using Standard Sirens	44
4.1	Standard Sirens	44
4.1.1	Theory	44
4.1.2	Previous Work	47
4.2	Electromagnetic Galaxy Catalogues	48
4.2.1	Current Galaxy Catalogues for the EM follow-up of Gravitational Waves	48
4.2.2	Comparison of Simulated Galaxy Catalogue to Real Galaxy Catalogues	49
4.3	Identifying the Host Galaxy	50
4.4	Events Outside the Galaxy Catalogue	51
4.5	Bayesian Inference	51
4.6	Choice of Priors	52
4.6.1	Prior on H_0	53
4.6.2	Priors for the Electromagnetic Data	53
4.6.3	Priors for the Gravitational Wave Data	54
4.7	Derivation of Bayesian formalism	55
4.7.1	Probability of the Data Given the Host Galaxy is Within the Galaxy Catalogue: $p(\hat{\rho} G, H_0, D, I)$	56

4.7.2	Probability of the Host Galaxy Being in the EM Catalogue Given a Hubble Constant : $p(G H_0, D, I)$	58
4.7.3	Probability of the Data Given the Host galaxy is Outwith the Galaxy Catalogue : $p(\hat{\rho} \bar{G}, H_0, D, I)$	60
4.7.4	Probability of the Host Galaxy Being Outwith the EM Catalogue Given a Hubble Constant :: $p(\bar{G} H_0, D, I)$	61
5	Results	62
5.1	Parameters	62
5.2	Binary Black Hole Merger Scenario	63
5.3	Binary Neutron Star Merger Scenario	66
5.4	Probability of the Host Being in the Galaxy Catalogue	68
5.5	Posterior with no Bias Corrections	71
5.6	Interpretation of Results	72
5.7	Limitations of the Model	75
6	Conclusions and Future Work	78
6.1	Conclusions and Insights from the Toy Model Experiment	78
6.2	Towards a Precise Measurement of the Hubble Constant Using Standard Sirens	79
6.3	Cosmology Using Multi-Messenger Astronomy	79
6.3.1	Cosmology with Third Generation Gravitational Wave Detectors	80
6.4	GW170817 and the First Gravitational Wave Standard Siren Measurement of the Hubble Constant	80
A	Code	83

List of Tables

1.1	Detector sensitivities	18
1.2	Detector phases	18
4.2	Sensitivity range for aLIGO	55
5.2	Final results for BBH observing scenarios	63
5.4	Final results for BNS observing scenarios	67

List of Figures

1.1	Different phases of plus-polarisation and cross-polarisation of gravitational waves	5
1.2	Joseph Weber with a resonant mass (bar) detector	10
1.3	Advanced LIGO optical configuration	12
1.4	Sources of noise for aLIGO	12
1.5	Global network of gravitational wave observatories (second generation)	13
1.6	LIGO upgrade timeline	14
1.7	Shift in periastron time for PSR 1913+16	16
1.8	The measured signal at LIGO Hanford and LIGO Livingston for GW150914	17
1.9	Characteristic strains of compact binary coalescences	19
2.1	The frequentist approach and Bayesian approach illustrated by Randall Munroe	22
2.2	A schematic representation of the scientific method	24
3.1	The SDSS map of the universe	30
3.2	Expansion of coordinate grid, with $a(t)$ the scale factor of the universe	32
3.3	Edwin Hubble's redshift-luminosity distance relationship	35
3.4	Map of the CMB from 2013 Planck results	40
3.5	Angular power spectrum by WMAP	40
3.6	Discrepancies in current measurements of the Hubble constant	42
4.1	GW150914 template vs. numerical relativity	46
4.2	Masses in the stellar graveyard	47
5.1	Results for 2000 events at $D_L(\rho_{th}) = 1640\text{Mpc}$, with a H_0 bin width of $1 \text{ kms}^{-1}\text{Mpc}^{-1}$	64
5.2	Results for 3000 events, $D_L(\rho_{th}) = 1640\text{Mpc}$	65
5.3	Results for 3000 events, $D_L(\rho_{th}) = 1300\text{Mpc}$	65
5.4	Results for events with $\hat{\rho} < 20$ at $D_L(\rho_{th}) = 900\text{Mpc}$	66
5.5	Results for 2000 events, $D_L(\rho_{th}) = 100\text{Mpc}$	67
5.6	Results for 2000 events, $D_L(\rho_{th}) = 100\text{Mpc}$	68
5.7	Typical distribution of apparent magnitude and luminosity distance (for $H_0 = 70\text{kms}^{-1}\text{Mpc}^{-1}$) of galaxies	69

5.8	$p(G H_0, D, I)$ and $p(\bar{G} H_0, D, I)$ for $D_L(\rho_{th}) = 1300\text{Mpc}$	70
5.9	$p(G H_0, D, I)$ and $p(\bar{G} H_0, D, I)$ for $D_L(\rho_{th}) = 190\text{Mpc}$	70
5.10	$p(H_0 \hat{\rho}, I)$ for $D_L(\rho_{th}) = 190\text{Mpc}$	71
5.11	$p(H_0 \hat{\rho}, I)$ for $D_L(\rho_{th}) = 900\text{Mpc}$	71
5.12	$p(H_0 G, \hat{\rho}, I) * p(G H_0, I)$ for $D_L(\rho_{th}) = 190\text{Mpc}$	72
5.13	$p(H_0 G, \hat{\rho}, I)$ for $D_L(\rho_{th}) = 190\text{Mpc}$	72
5.14	$p(H_0 G, \hat{\rho}, I) * p(G H_0, I)$ for $D_L(\rho_{th}) = 900\text{Mpc}$	72
5.15	$p(H_0 G, \hat{\rho}, I)$ for $D_L(\rho_{th}) = 900\text{Mpc}$	72
5.16	90% confidence intervals derived from the posterior on H_0 for $D_L(\rho_{th}) = 100\text{Mpc}$	73
5.17	90% confidence intervals derived from the posterior on H_0 for $D_L(\rho_{th}) = 1640\text{Mpc}$	73
5.18	90% confidence intervals derived from the posterior on H_0 for $D_L(\rho_{th}) = 150\text{Mpc}$	74
5.19	90% confidence intervals derived from the posterior on H_0 for $D_L(\rho_{th}) = 190\text{Mpc}$	74
5.20	90% confidence intervals derived from the posterior on H_0 for $D_L(\rho_{th}) = 900\text{Mpc}$	74
5.21	Confidence intervals derived from the posterior on H_0 for $D_L(\rho_{th}) = 1300\text{Mpc}$	75
5.22	$\frac{1}{K(H_0)}$ for $D_L(\rho_{th}) = 100\text{Mpc}$	76
5.23	$\frac{1}{K(H_0)}$ for $D_L(\rho_{th}) = 190\text{Mpc}$	76
5.24	Noisy individual posteriors, with comparatively smooth posteriors at low $D_L(\rho_{th})$	76
6.1	Sky localisations of gravitational wave signals detected by LIGO-VIRGO	80
6.2	GW standard siren measurement of H_0 using GW170817	81
6.3	Timeline of measurements of the Hubble constant	82

Acknowledgements

Thank you to my supervisors, Martin and Chris, for giving me the opportunity to do this masters, and for their continuous help, from long hours of debugging to long discussions about cosmology.

Thank you to all my friends for being an amazing source of both support and inspiration during this degree, and previous ones.

I'd also like to thank the IGR, and everyone in the School of Physics and Astronomy for being such a wonderful group to work in. Thanks especially to my fellow research students for the moral support and bizarre conversations at coffee.

Thanks to Astrosoc for being my wonderful space family for the last three years, and endlessly reminding me of why I chose to study astronomy in the first place, even though after three years we have yet to see clear skies during our observing evenings.

I'd also like to thank the Glasgow University Fencing Club for being a great source of support and providing some often much needed stress release throughout this project, along with being a fantastic way to exercise only one of my legs.

Thank you to my family for their incredible support throughout my entire time at university; this was only made possible thanks to their help.

Merci à ma famille pour leur aide et leur soutien, non seulement durant ce diplôme mais aussi au fil des dix longues années depuis que j'ai quitté la France.

"One of the interesting things about space [...] is how dull it is.

[...]

Yes, staggeringly dull. Bewilderingly so. You see, there's so much of it and so little it. Would you like me to quote you some statistics?

[...]

Please, I would like to. They, too, are quite sensationally dull."

- Douglas Adams, *Life, the Universe, and Everything*

Declaration

This thesis is an account of work carried out from October 2016 to October 2017 as part of the Institute for Gravitational Research and the LIGO Scientific Collaboration at the University of Glasgow.

The Marcum Q function which replaces the built-in python function in Appendix A was written by Chris Messenger. Parts of the code were re-written with the help of Daniel Williams in order to make it run in parallel form on a computer cluster.

Unless stated otherwise, the work presented in this thesis is my own, and has not been presented in support of any other degree or qualification at this institution or any other.

Chapter 1

Introduction

Gravitational waves are disturbances in spacetime that propagate at the speed of light. Generated by some of the most violent astrophysical events in the universe, they can teach us more about our cosmos. Gravitational wave astronomy is a new and rapidly growing field: while efforts in the development of theory and detectors had been ongoing for many years, the first direct detection of gravitational waves, in September 2015, marked the true advent of the era of gravitational wave astronomy. [1] Since this first detection, and subsequent ones, the field and its scientific returns and applications to astronomy and astrophysics have grown considerably.

Gravitational waves were predicted in 1916, one year after Einstein proposed his theory of general relativity, which revolutionised physics. A direct consequence of the theory, it took nearly a century to finally directly detect gravitational radiation for the first time. The search for these tiny ripples spanned several decades, and was a colossal international effort. For most of the history of astronomy, observations were limited to the optical realm. This first changed in 1932, when Karl Jansky, then working at the Bell Telephone Laboratories, made the first observations of the Milky Way in the radio band. [2] Consequently, throughout the 20th century, new windows of the electromagnetic spectrum kept opening up, and with each new window came new revelations about our universe: X-ray, radio, gamma rays... Likewise, the discovery of gravitational waves marked the dawn of a completely new way of observing our cosmos, and with it came an abundance of new science. Whereas EM observations were fundamentally biased towards the observation of hot, glowing matter, with gravitational waves, astronomers can probe violent astrophysical processes and massive, dense objects like black holes and neutron stars. While electromagnetic radiation is easy to detect due to its strong coupling to charges, 96% of the mass-energy of the universe carries no charge. This could make gravitational radiation a better probe for the astrophysical, and physical phenomena linked to this mostly unexplored part of the universe. [3]

This chapter presents an overview of gravitational waves as a consequence of general relativity. We also discuss the astrophysical sources of gravitational waves, and what we can learn from them. Finally, an overview of past, current and future gravitational wave detectors is presented,

along with a summary of the current state of the search for gravitational waves.

1.1 General Relativity and Gravitational Waves

It seems probable that most of the grand underlying principles have been firmly established and that further advances are to be sought chiefly in the rigorous application of these principles to all the phenomena which come under our notice. [...] An eminent physicist remarked that the future truths of physical science are to be looked for in the sixth place of decimals."

These words, often misattributed to Lord Kelvin, were spoken by physicist Albert A. Michelson during an address to the Ryerson Physical Laboratory in July 1894. [4] This seemed to be, at the time, the general consensus amongst even the most eminent physicists. It was only a few years after this statement was made that two revolutions were made in the world of physics.

Einstein revolutionised physics when he proposed his theory of special relativity, inspired by Maxwell's work on electromagnetics. [5–7] Published in 1905 under the name "On the electromagnetics of moving bodies", the theory introduced some concepts that would later become fundamental to our understanding of the universe. In this paper, Einstein postulates that light will always propagate at velocity c in a vacuum, regardless of the velocity of the emitting body. [7]

Einstein's work removed the need for a universal reference frame, thus making the luminiferous aether, a theoretical substance through which light propagated and which would provide a reference frame common to the entirety of the cosmos, unnecessary.

The theory of special relativity relies on two important postulates:

- The principle of relativity: 'the laws by which the states of physical systems undergo change are not affected, whether these changes of state be referred to the one or the other of two systems of co-ordinates in uniform translatory motion.'
- Invariant light speed: light moves at a fixed velocity c in the stationary system of co-ordinates, regardless of whether the emitting source is stationary or not. [7]

After releasing his work on special relativity, Einstein started extending his theory to gravitational fields. From this work came general relativity, with what would become known as Einstein's field equations published in 1915. [8] One year later, in 1916, gravitational radiation was predicted as a direct consequence of the theory.

1.1.1 General Relativity

The main idea behind general relativity can be easily summarised by this memorable quote by John Archibald Wheeler: "*Spacetime tells matter how to move; matter tells spacetime how to curve.*" [9]

Before Einstein developed his theory of general relativity, our understanding of gravity was Newtonian; gravity was understood as a force which acted on massive objects. While Newtonian dynamics are a good approximation of everyday phenomena, certain problems remained with Newton's approach, especially on astrophysical scales: discrepancies would appear between Newton's theory and some observed astrophysical phenomena. The main issue with Newton's understanding of gravity was the seemingly instantaneous aspect of the force.

In 1907, two years after he proposed the theory of special relativity, Einstein started extending his work to gravitational fields. He first proposed that free fall was an inertial motion, an idea which would later be known as the equivalence principle. [10] This is fundamentally different from previous theories, including special relativity, in which gravity is treated as a force acting upon an object. This concept means that free-falling test particles follow geodesics: the shortest path in a curved spacetime.

Einstein first published the field equations he derived for general relativity in 1915. [8] These equations describe the interaction of spacetime and matter; that is, they describe how the metric responds to energy and momentum. [11]

$$R_{\mu\nu} - \frac{1}{2}Rg_{\mu\nu} = 8\pi GT_{\mu\nu}, \quad (1.1)$$

where $R_{\mu\nu}$ is the Ricci curvature tensor, R is the scalar curvature, $g_{\mu\nu}$ is the metric tensor, G is Newton's gravitational constant and $T_{\mu\nu}$ is the stress-energy tensor.

In 1916, Einstein proposed a number of tests of general relativity. [12]

- The perihelion precession of Mercury; observations of the orbital motion of Mercury presented some discrepancies with the Newtonian predictions, which could be explained by Einstein's theory.
- The bending of light in a strong gravitational field, such as starlight being deflected by the Sun during a solar eclipse.
- The gravitational redshift of light.

The first observational evidence of general relativity came from British scientist Arthur Eddington, in 1919. [13] According to GR, light bends when passing through the gravitational field of a massive astrophysical object. This bending is also predicted by Newtonian dynamics; however, the bending of light predicted by GR is twice that of the Newtonian one. What this means is that when observed near a very massive object, objects like stars or galaxies are observed to be in a different location than they truly are.

By observing a star field at night and during a solar eclipse, Eddington showed that the bending of light by massive objects was consistent with predictions made by Einstein's theory of general relativity; the predicted bending was twice that of the bending of light predicted by

Newton's theory. This result remained controversial for many years, with suspicions of underlying political motivations and erroneous analysis. Some believed that Eddington was biased in favour of general relativity and that the experiment only served as a pacifist act of reconciliation between Britain and Germany following World War I. [14] However, since 1919, general relativity has triumphed and withstood many other experimental tests. So far, no inconsistencies have been found between Einstein's theoretical predictions and observations.

The observation of gravitational radiation serves as one of many tests of general relativity. The search for gravitational waves has been a colossal scientific enterprise going back to the 1960s, and involving thousands of people and institutions across the globe.

1.1.2 Gravitational Radiation

Gravitational radiation arises as a natural consequence of general relativity. In 1916, one year after he introduced general relativity, Einstein proposed a wave solution to his equations. [15]

In the weak field limit, the metric can be decomposed into the flat Minkowski metric of special relativity $\eta_{\mu\nu}$ and a small perturbation $h_{\mu\nu}$.

$$g_{\mu\nu} = \eta_{\mu\nu} + h_{\mu\nu}, \quad |h_{\mu\nu}| \ll 1 \quad (1.2)$$

There is a lot of freedom to the choice of gauge for $h_{\mu\nu}$. However, one gauge is of particular interest to general relativity: that is the transverse traceless (TT) gauge. In this gauge, the coordinates are marked out by the world lines of free-falling test masses. The TT gauge embodies the idea of gravity as a phenomenon of geodesic motion through curved space time. [16]

When using the transverse traceless gauge in the weak field limit, Einstein's field equations become a wave equation.

$$(\nabla^2 - \frac{1}{c^2} \frac{\partial^2}{\partial t^2}) h_{\mu\nu} = 0 \quad (1.3)$$

$h_{\mu\nu}$ represents a perturbation travelling at the speed of light, c .

$$h_{\mu\nu} = \begin{pmatrix} 0 & 0 & 0 & 0 \\ 0 & a & b & 0 \\ 0 & b & -a & 0 \\ 0 & 0 & 0 & 0 \end{pmatrix} \quad (1.4)$$

$$h = a\hat{h}_+ + b\hat{h}_x \quad (1.5)$$

There are therefore two possible polarisations for $h_{\mu\nu}$, denoted by \hat{h}_+ and \hat{h}_x . These are

called, respectively, plus polarisation and cross polarisation.

$$\hat{h}_+ = \begin{pmatrix} 0 & 0 & 0 & 0 \\ 0 & 1 & 0 & 0 \\ 0 & 0 & -1 & 0 \\ 0 & 0 & 0 & 0 \end{pmatrix} \quad \hat{h}_\times = \begin{pmatrix} 0 & 0 & 0 & 0 \\ 0 & 0 & 1 & 0 \\ 0 & 1 & 0 & 0 \\ 0 & 0 & 0 & 0 \end{pmatrix} \quad (1.6)$$

These act as basis tensors for the two orthogonal polarisations of waves propagating along the \hat{z} -axis.

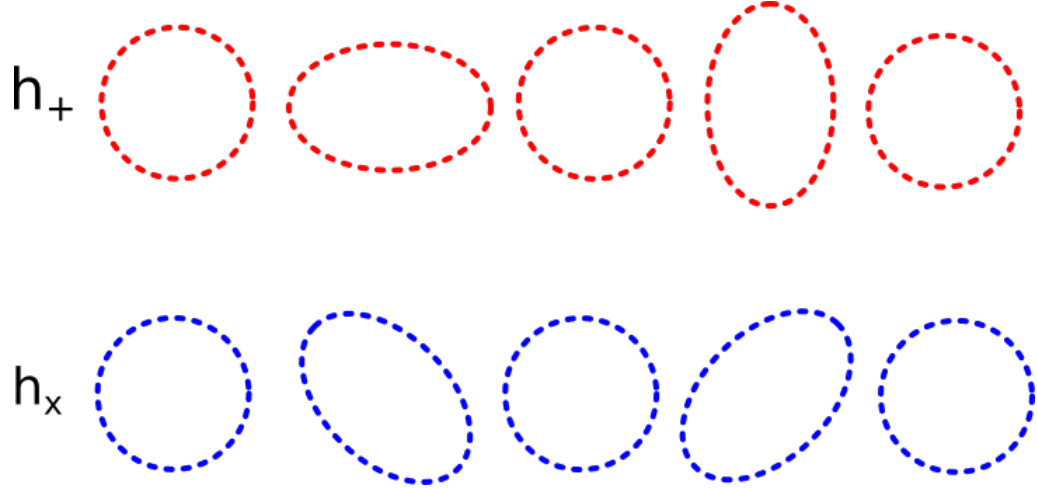


Figure 1.1: Different phases of plus-polarisation and cross-polarisation of gravitational waves

Figure 1.1 shows a representation of these two polarisations, by showing the effect of a gravitational wave in a plus polarisation and a cross polarisation on a ring of test particles. Most detected gravitational wave signals will be a combination of these two polarisations.

The existence of a wave solution to Einstein's equations is a profound statement about our universe: it demonstrates the existence of oscillations in the spacetime metric that propagate at the speed of light. This was the first theoretical prediction of the existence of gravitational waves.

1.1.3 Generation of Gravitational Waves

Similarly to the way electromagnetic waves are produced by accelerating charges, gravitational waves are produced by accelerating mass-energy. [17] While electromagnetic waves are produced by the dipole moment of electric charges, gravitational waves are produced by the quadrupole moment of mass.

For gravitational radiation to be generated, the mass quadrupole moment of the system needs to undergo variations in time. In other words, for gravitational waves to be generated, we need a non-spherically and non-cylindrically symmetrical accelerating mass. [18]

1.1.4 Astrophysical Sources of Gravitational Waves

Any massive object with a non-zero quadrupole moment is a source of gravitational waves. However, due to the small effect of these waves, only massive astrophysical objects accelerating rapidly produce detectable gravitational radiation. Spacetime is remarkably stiff; this means that only very massive, dense objects, or cataclysmic events can produce detectable gravitational wave signals.

We can expect to observe four different types of gravitational wave signals: compact binary coalescence, burst, stochastic and continuous.

Compact Binary Coalescence

At the time of writing, all detections of gravitational wave signals have been from compact binary coalescences (CBC). Two types of CBC have been detected: binary black hole coalescences (BBH), and one binary neutron star coalescence (BNS). We also expect to be able to observe black hole-neutron star systems in the future.

Compact objects are very dense, heavy astrophysical objects. Black holes (BH) and neutron stars (NS) are such objects; these objects are compact stellar remnants.

Black holes are compact objects with a gravitational field that is so strong no object or signal can escape their gravitational pull. They were first mathematically predicted in 1916 by Schwarzschild, who proposed a solution to Einstein's field equations for the gravitational fields of point masses. [19]

Neutron stars are extremely dense stars made primarily of neutrons. Their masses range from 0.5 to 3 M_{\odot} with radii of around 10km. [20]

White dwarfs (WD) are another type of compact astrophysical object, and white dwarf mergers, or WD-NS/BH are expected to be common in our galaxy. [21] However, such compact binary coalescences do not have a strong signature, and their frequencies make them more appropriate targets for space-borne detectors like LISA. [22]

Stellar mass binary black hole mergers are the most commonly detected systems to date. Stellar binary black holes can form in a number of ways; for example, they could result from binary systems comprised of two massive stars which collapsed into black holes, or they could form in dense stellar environments through dynamic processes in which a black hole is captured into orbit around another black hole. [23] Stellar mass black holes range from 5 M_{\odot} to several tens of M_{\odot} , as seen in figure 4.2.

The characteristic signature of compact binary coalescences is a "chirp" signal, named for the "chirping" sound of the signal when translated into sound. This signal can be seen in Figure 1.8.

Burst

Gravitational wave bursts are, along with compact binary coalescences, a type of transient gravitational wave signal. Bursts are weakly-modelled transients of short duration; burst searches make fewer assumptions on the shape of the waveform, identifying instead significant excess-power transient signals. [24, 25] They also require a coherence of the signals between several detectors. [26]

Gravitational wave bursts are "generic" transient signals. Targeted astrophysical objects for burst searches include core-collapse supernovae, pulsar glitches, cosmic string cusps and magnetar flares. [25, 27]. It is also possible that astrophysical systems that are not yet known will be sources of gravitational wave bursts.

Stochastic

Stochastic gravitational waves are the astrophysical gravitational wave background made up of a multitude of incoherent signals.

If we consider a gravitational wave detector in the frequency band above 10Hz then two black holes merge roughly every 200s, while binary neutron star mergers occur roughly every 15s within the range of the entire universe. [28] These estimates are limited by uncertainties in the rates. These events form a stochastic gravitational wave background.

Another potential source of stochastic signals is primordial gravitational waves from the Big Bang. These would form a stochastic background similar to the Cosmic Microwave Background in EM. Processes in the very early universe, such as vacuum fluctuations can generate a weak gravitational wave background. [29]

Continuous

Continuous gravitational waves are signals of a defined frequency produced over a long period of time.

Spinning neutron stars with an asymmetry with regards to the rotation axis are a source of continuous gravitational waves. [30] This asymmetry would manifest as a deformation on the surface of the neutron star.

At the time of writing, no continuous waves have been detected from pulsars and neutron stars; however, the lack of detection allows for constraints to be placed on the strain (as defined in equation 1.7) of the gravitational waves produced by the asymmetries of neutron stars. These constraints translate to a limit on the height of the largest possible deformation, or mountain, in these objects.

The lack of continuous gravitational wave detection in all-sky searches puts a limit on the maximum strain of these signals. At most frequencies, this upper limit is estimated to be 10^{-24} to 2×10^{-23} . [31]

1.1.5 Observables of Gravitational Waves

The variable measured by gravitational wave detectors is called the strain. The strain of a gravitational wave can be thought of as an oscillating tidal force between two distant masses. [32] It's measured transversely to the direction of propagation of the wave, and has an amplitude h . Another measured variable is the signal-to-noise ratio (SNR), which scales inversely with the distance. [33]

The strain is a measure of the distortion of space by the gravitational wave: for two objects separated by a length L , it is defined as twice the change in displacement caused by the gravitational wave ΔL divided by the length.

$$h = \frac{2\Delta L}{L} \quad (1.7)$$

As defined in equation 1.5, gravitational waves can be polarised in a cross or a plus configuration; typically, a measured gravitational wave will be a combination of both polarisations.

For a system radiating an energy E in gravitational waves over a time T , at a frequency f and distance r , the amplitude of the signal goes as [3]

$$h \sim \frac{1}{\pi f r} \sqrt{\frac{E}{T}}. \quad (1.8)$$

Therefore, the parameters of the system can be inferred from measuring the strain of gravitational waves.

1.1.6 Parameter Estimation from Gravitational Wave Signals

A number of parameters can be estimated from the observables of gravitational waves, which are measurements of the time evolution of the strain of the gravitational wave. Localisation information can also be obtained from the use of a network of detectors.

Parameter estimation from gravitational wave signals coming from binary black hole coalescences has been made possible thanks to recent breakthroughs in the field of numerical relativity. [34–37] Using numerical relativity equations, templates can be made for different parameters of the astrophysical systems, and real signals are matched to those templates, therefore allowing for parameter estimation of the system. Parameters that can be inferred from the signal include the spin of the binary, mass ratios, chirp mass, inclination and polarisation angles, luminosity distance and localisation. [34] In the case of BNS mergers like GW170817, efforts in analytical relativity and post-Newtonian approximations made parameter estimation possible. [38, 39]

1.2 Gravitational Wave Detectors

When Einstein first introduced the wave solution to his equations, predicting the existence of gravitational radiation, it was thought that the minuscule effect of such perturbations would mean that gravitational waves would never be detected.

Despite this prognosis, physicists decided to search for these tiny gravitational waves, starting in the 1960s with bar detectors. In 1960, Joseph Weber started developing methods for detecting gravitational waves and measuring the Riemann tensor using resonant mass detectors. [40]

1.2.1 Resonant Mass Detectors

The first gravitational wave detectors were not interferometers, but resonant mass detectors, also called bars.

The resonant mass gravitational wave detectors developed by Weber were made to detect the short pulses of gravitational radiation predicted from the collapse of supernovae. [17]

Gravitational waves can be thought of as a tidal relative force between two masses, or across an extended object. [16]. The gravitational wave sends the pair of masses vibrating about their common centre of mass.

In 1969, Joseph Weber announced, during a conference on general relativity, the detection of gravitational waves. [41,42] After the controversial announcement, several teams built their own bar detectors. However, Weber's result was never duplicated. Other teams never saw anything but random noise in their own detectors, casting even more doubts on the the controversial claim, and the supposed detection of gravitational waves was put down to a flawed data analysis.

1.2.2 Laser Interferometry for Gravitational Wave Detection

After the unsuccessful resonant mass detectors, physicists started exploring other possibilities in gravitational wave detection.

Another way of measuring the separation of two distant objects is to determine the time of travel of light between the two objects. [16] This can be done with the use of Michelson interferometers.

Michelson interferometers were famously used in the Michelson-Morley experiment in 1887, designed to detect the luminiferous ether, the substance through which physicists believed electromagnetic waves travelled. [43] At the time, it was believed that EM waves needed a medium to travel through; the aim of the experiment was to detect the Earth's motion through that medium.

The use of interferometry in gravitational wave detection was first proposed by Forward and Weiss. [44,45] Laser interferometers are more sensitive than resonant mass detectors, and over a wider detection bandwidth.



Figure 1.2: Joseph Weber with a resonant mass (bar) detector

In order to detect a gravitational wave strain of 10^{-21} to 10^{-22} , the optical path length L_{opt} needs to be of the order of 1000km. [16]

However, there is no need for building interferometers of such large scale. The dominant noise source in such interferometers is shot noise, which only depends on the light power and total optical length. This means the light can be reflected on mirrors as many times as necessary without increasing the shot noise. This is called optical path folding, and leads to the following equation for the length of the interferometer arms

$$L = \frac{L_{opt}}{2N}, \quad (1.9)$$

where L is the new length of our interferometer arms, and N is the number of round trips the laser makes.

Laser interferometers for gravitational wave detection are long-baseline interferometers, working as a world-wide network of antennae. A network of separated interferometers is essential in order to locate the sources of gravitational wave signals in the sky using time delays. [46]

1.2.3 First Generation Gravitational Wave Detectors

The first generation of gravitational wave detectors includes the first interferometric GW detectors built.

LIGO, the Laser Interferometer Gravitational-Wave Observatory, was built in the 1990s, and was operating at design sensitivity in its data acquisition mode from November 2005 to September 2007. [32] Consisting of two identical interferometers in Louisiana and Washington, each with 4km arms, LIGO was built to detect and study gravitational wave signals from astrophysical sources. [47] Astronomical research was not the only scientific goal of the detectors. The observation of gravitational waves could also be a way to tackle some fundamental questions about the physics of our universe, such as characterising the graviton, testing nonlinear gravity, or investigating dark matter. [47]

Another detector, the GEO 600 laser interferometer with 600m arms, is located in Germany. [48]

Like resonant mass detectors, the first generation of interferometric gravitational wave detectors did not succeed in its search for gravitational radiation; detecting the tiny ripples would require the updated technology of second generation gravitational wave detectors.

1.2.4 Second Generation Gravitational Wave Detectors

Following Initial LIGO, the interferometers underwent an update, Advanced LIGO, bringing them into the second generation of gravitational wave detectors. Another second generation detector, VIRGO, is located in Italy. [49]

The design of Advanced LIGO is based around a Michelson interferometer with each arm containing a Fabry-Perot cavity to build up the phase shift produced by the change in length of the arms. [50]

Currently, the aLIGO detectors comprise of two identical instruments based in Hanford (Washington) and Louisiana. The Advanced LIGO detectors started their data acquisition in 2015. The first direct detection of gravitational waves was in both instruments made during the engineering run of O1. [1] After the success of aLIGO's first observing run, a third identical detector was approved for construction in India, IndiGO, and will join the network of LIGO detectors. [51]

The sensitivity of aLIGO detectors is limited by noise. Sources of noise include seismic noise, thermal noise, quantum noise (made up of radiation noise and shot noise) and others, see figure 1.4. The noise floor of the interferometers is determined by quantum noise and thermal noise. [50]

Currently, three second-generation gravitational wave detectors are operating: the two aLIGO detectors, and VIRGO, in Italy. KAGRA is a second-generation cryogenic gravitational wave detector currently under construction in Japan. [52]

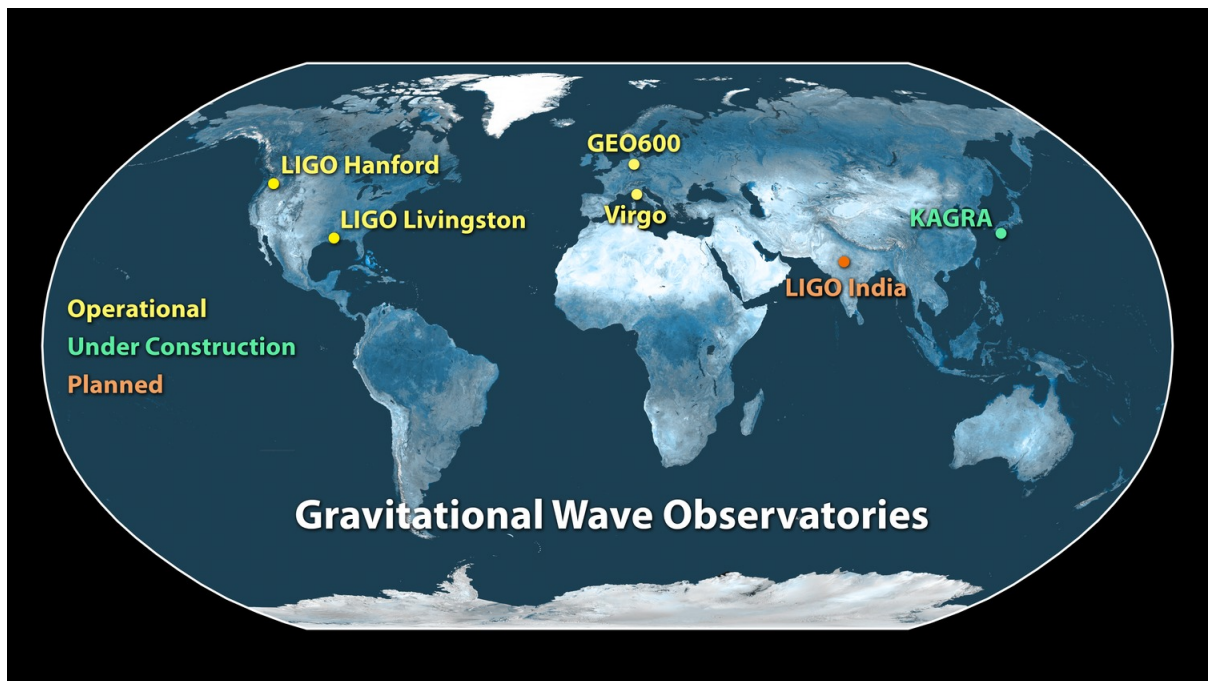


Figure 1.5: Global network of gravitational wave observatories (second generation). [51] This map shows currently operational detectors and future detectors that will soon join the global network of gravitational wave observatories.

1.2.5 Space-Based Detectors

The Earth is a considerably noisy place for gravitational wave detectors. Seismic activity, tidal waves, and many other everyday terrestrial occurrences are a significant source of noise in ground-based interferometers, making it impossible to detect gravitational waves at certain frequencies, as seen in figure 1.4. These sources include, for example, the mergers of supermassive black holes. [54]

This means that in order to open new windows of the gravitational wave spectrum, detectors need to be taken away from these noise sources. This is what space-based detectors will be attempting to accomplish.

The LISA mission seeks to explore the gravitational wave spectrum in a frequency window of 0.1 to 100mHz. It is designed as an interferometer with a 3-arm configuration, with each arm separated by 2.5 million km. Its orbit will be an Earth-trailing heliocentric orbit. [54] The LISA Pathfinder mission launched in December 2015, and successfully demonstrated the technology that will be used for the LISA spacecraft. [55]

1.2.6 Third Generation Detectors

Following the success of Advanced LIGO and Advanced Virgo, the third generation of detectors is under way. The next generation of gravitational wave detectors will be able to detect compact

binary sources with high SNR (> 20) at redshifts > 10 . [56]

The Einstein Telescope

The Einstein Telescope is a planned third generation gravitational wave detector. Funded by the, European Commission, it is currently under study. The target for ET is an improvement in sensitivity of 10 over a wide range of frequencies; this would improve the detection rate by a factor of 1000. [57]

LIGO: Next Generation

Advanced LIGO should reach design sensitivity in 2020. Some further updates have been proposed for the detectors, taking aLIGO into the next generation of interferometric gravitational wave detectors.

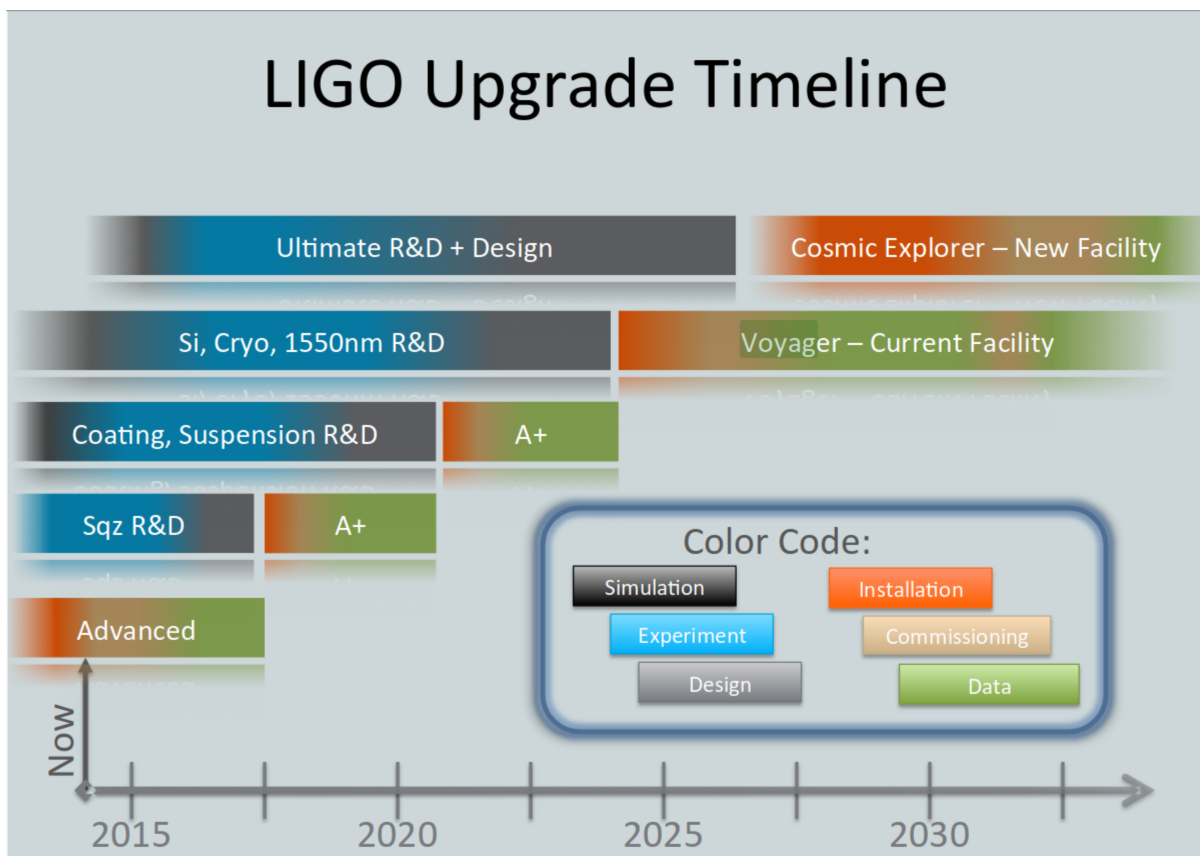


Figure 1.6: LIGO upgrade timeline. [53] Projected schedules are presented for three major potential detector epochs: A+, LIGO Voyager and LIGO Cosmic Explorer.

The two designs proposed for LIGO updates are LIGO Voyager and Cosmic Explorer. [53] These will follow another less extensive update, A+.

In the ideal scenario, A+ would bring the reach of the detectors to 340Mpc for binary neutron stars. The increased sensitivity would be reached through the implementation of two stages of

upgrades:

- Frequency dependent squeezing.
- Bigger masses, bigger laser beam sizes and better mirror coatings.

Using squeezed light, heavier test masses and reducing coating thermal noise could potentially double the reach of Advanced LIGO. [58]

LIGO Voyager is planned for 2025, and will follow the A+ update. LIGO Voyager will be a major upgrade of the current LIGO instruments, bringing its reach to 1100Mpc for binary neutron stars. After such an extensive upgrade, gravitational wave astronomy will be a well-established field, prompting more investment into new facilities. LIGO Cosmic Explorer is a planned design for such a facility. Cosmic Explorer will be a gravitational wave observatory with a binary neutron star reach beyond a redshift of 1. [53].

1.3 Detections

Gravitational waves can be detected directly, through directly measuring the distortion of space-time caused by their passing through a detector, or indirectly, through measuring the effects of gravitational waves on the orbits of compact binary systems. Gravitational Waves have been detected both indirectly and directly.

1.3.1 Indirect Detection

Gravitational radiation was first observed indirectly, in a binary pulsar system. The system had been previously discovered by Hulse and Taylor in 1975, a discovery that would later earn them the 1993 Nobel Prize in Physics. [59] This system consists of two neutron stars orbiting each other with a period of 7.75 hours, with one of them emitting radio pulses. [32] The indirect detection of gravitational radiation was made through the precise measurement of pulse arrival times of this binary pulsar, PSR 1913+16. The system was monitored from 1975 to 1981, and the delays in pulse arrival time were found to be consistent with orbital decay that matched predictions made by a loss of energy through gravitational radiation. [60]

The binary system was subsequently monitored for decades, through measurements of the timing of its radio pulses. Thirty years of observations still showed the decay of its orbit to be consistent with the predictions made by general relativity. The change in the orbital period of the binary pulsar agreed with the values predicted by energy loss through emission of gravitational radiation within 0.2%. [61]

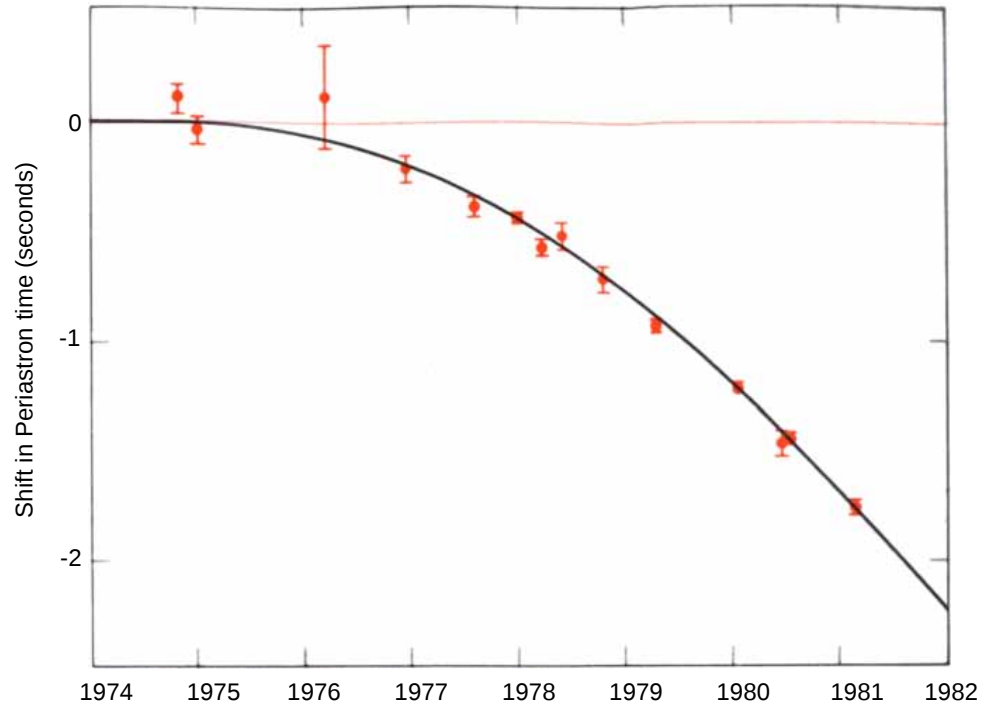


Figure 1.7: Shift in periastron time for PSR 1913+16, showing the decaying orbit due to gravitational radiation. The red dots are observations, while the black line is the prediction from GR. [60]

1.3.2 Direct Detection

At the time of writing there have been six confirmed direct detections of gravitational waves. All but one of these came from the merger of two black holes; the other detection being a binary neutron star coalescence.

The first direct detection of gravitational waves was made by the two detectors of the Advanced Laser Interferometer Gravitational-Wave Observatory (aLIGO) on the morning of 14th September 2015. The detection was a transient signal coming from two black holes of masses $30_{-4}^{+5}M_{\odot}$ and $29_{-4}^{+4}M_{\odot}$ at a distance of 440_{-180}^{+160} Mpc coalescing into a final black hole of mass $62_{-4}^{+4}M_{\odot}$ and effectively radiating $3.0_{-0.5}^{+0.5}M_{\odot}$ in gravitational waves. [1] This discovery was made after years of work by the scientific community, on the 100th anniversary of Albert Einstein's theory of general relativity.

This historical event was a breakthrough in more than one way; not only was this the first

direct detection of gravitational waves, it was also the first direct observation of a black hole, and the first observation of a binary system of two black holes orbiting each other. When observing only in the electromagnetic spectrum, black holes could only be observed through their effects on surrounding matter.

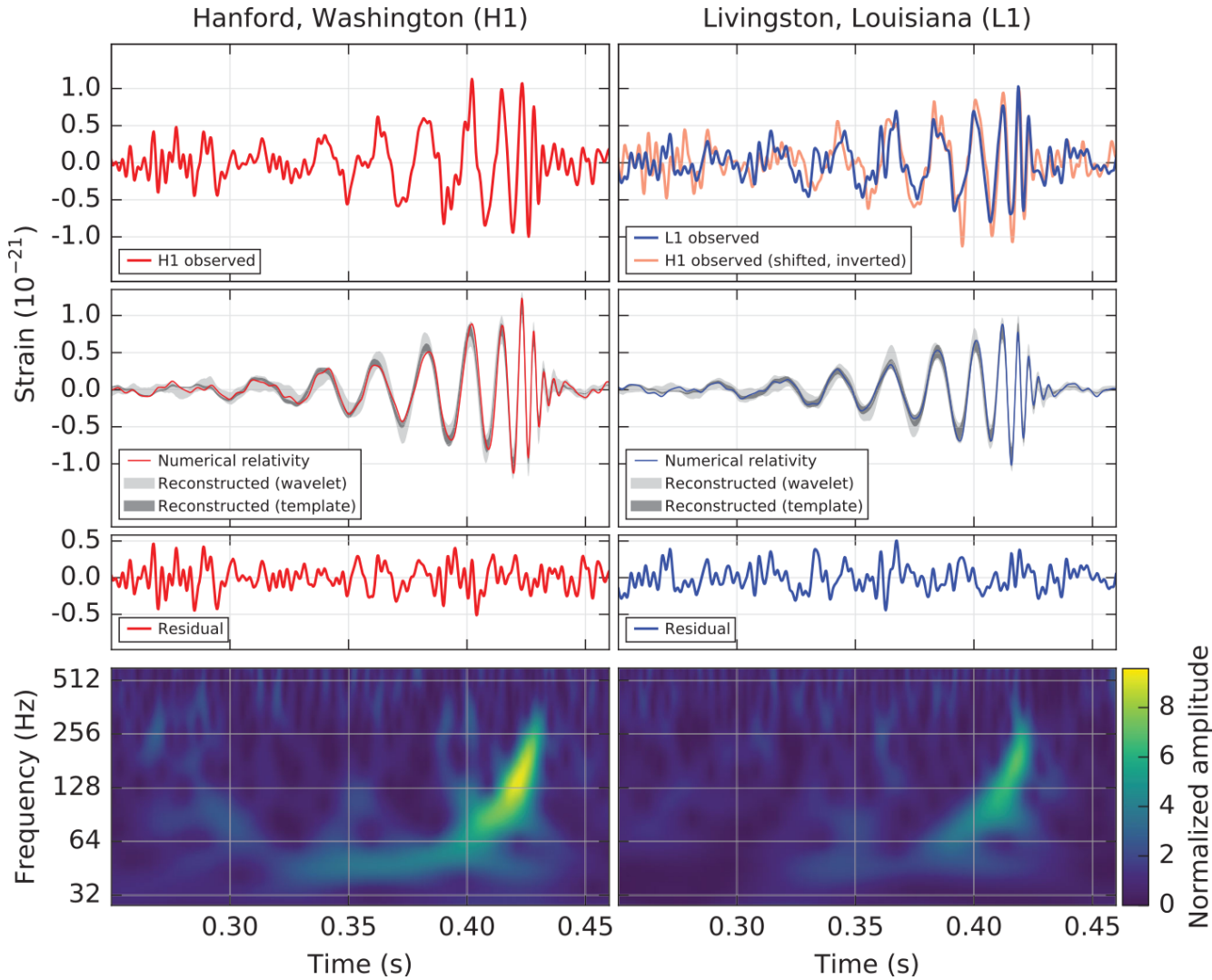


Figure 1.8: The measured signal at LIGO Hanford and LIGO Livingston for GW150914. [1] *Top row*: strain at LIGO Hanford and LIGO Livingston. *Second row*: projected strain in the 35-350 Hz band, with numerical relativity waveform. *Third row*: residuals. *Bottom row*: time frequency representation of the data.

Another event, GW151226, called the Boxing Day event, was detected as part of the first Advanced LIGO observing run. Once again, the signal was produced by the coalescence of two black holes. This time of masses of the original black holes were $14.2^{+8.3}_{-3.7}M_{\odot}$ and $7.5^{+2.3}_{-2.3}M_{\odot}$, coalescing into a final black hole with mass $20.8^{+6.1}_{-1.7}M_{\odot}$. [62] A further three binary black hole mergers were detected during the second aLIGO observing run.

The first detection of binary neutron stars coalescing was made during O2. Two neutron

stars, located at 40_{-14}^{+8} Mpc, merged, radiating gravitational waves and producing a short GRB and a kilonova. [39, 63]

1.3.3 Future Observing Runs and Detections

The second observing run for Advanced LIGO was recently completed, on 25th August 2017. The third observing run, O3, is planned for 2018-19, starting in Fall 2018. aLIGO will then be entering the late phase of its operation.

At design sensitivity, aLIGO is expected to detect binary black hole mergers ($30 M_{\odot}$) at a distance of up to 1640 Mpc, and binary neutron star mergers up to 190 Mpc. [64] The Virgo detector is similar to aLIGO, though less sensitive. Its role is however crucial in improving the localisation of gravitational wave events. Another detector, KAGRA, is currently under construction. At design sensitivity, it will detect BNS mergers up to 140Mpc and BBH mergers up to 1270Mpc.

	LIGO		Virgo		KAGRA	
PHASE	BNS Range(Mpc)	BBH Range(Mpc)	BNS Range(Mpc)	BBH Range(Mpc)	BNS Range(Mpc)	BBH Range(Mpc)
Early	40-80	415-775	20-65	220-615	8-25	80-250
Mid	80-120	775-1110	65-85	615-790	25-40	250-405
Late	120-170	1110-1490	65-115	610-1030	40-140	405-1270
Design	190	1640	125	1130	140	1270

Table 1.1: Detector sensitivities. [64] These are given for different phases of each detector, expressed as a range in Mpc for BNS and $30M_{\odot}$ BBH systems.

Table 1.1 presents plausible ranges of sensitivities for different phases of each detector. Values for binary black hole mergers are quoted for systems of two $30M_{\odot}$ black holes. The timelines for all phases are defined in table 1.2 for each detector.

PHASE	Advanced LIGO	Advanced Virgo	KAGRA
Opening	-	-	2018-19
Early	2015-16	2017	2019-20
Mid	2016-17	2018-19	2020-21
Late	2018-19	2020-21	2021-22
Design	2020	2021	2022

Table 1.2: Detector phases. [64] Each phase corresponds to a new observing run and improvement in sensitivity of the detector.

The search for gravitational waves is far from over; only one type of gravitational waves, compact binary coalescences, has been directly detected so far. The search for continuous, burst and stochastic sources is still ongoing.

In the future, with the help of space borne gravitational wave detectors like LISA, multi-band gravitational wave astronomy will be possible. With different sensitivities to certain frequencies, it'll be possible to detect objects evolving in time with both LISA and ground-based interferometric detectors. Figure 1.9 shows characteristic strains of compact binary coalescences, with the sensitivities of different detectors. Ever since the days of Jansky, and the gradual opening of

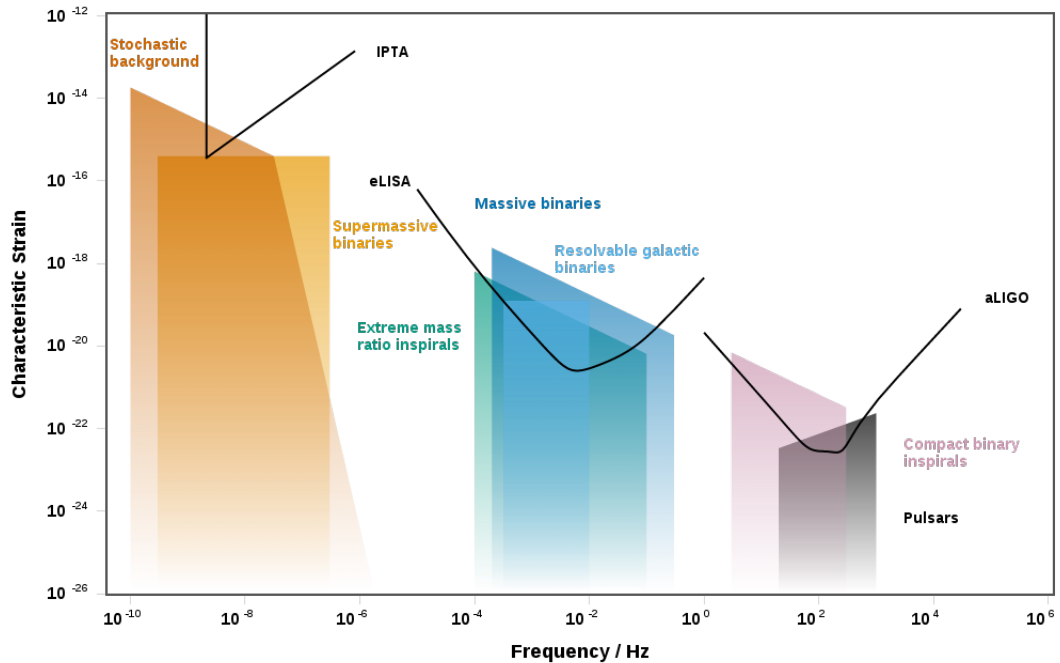


Figure 1.9: Characteristic strains of compact binary coalescences by frequency. [65] The solid black lines are detector sensitivities, and the colour boxes represent characteristic strains for different types of CBC.

new windows to the cosmos in the electromagnetic spectrum, many of the great advancements in astronomy, astrophysics and cosmology have been serendipitous discoveries. Likewise, we can expect the unexpected from further observations in the gravitational wave spectrum.

Chapter 2

Bayesian Data Analysis

Bayesian inference has a peculiar history. First developed by a reverend in the eighteenth century as a way to estimate the probability of a certain event occurring knowing only how many times that event had occurred in the past, it originally went largely unnoticed. The work was published posthumously, with amended and added material by Richard Price. [66] The ideas uncovered by Bayes' work were also rediscovered independently and given their mathematical form by Pierre Simon Laplace. [67] Bayesian inference went largely underappreciated for many years; only during the twentieth century did the theory resurface, after many successes in real life applications, from war decision making to plane searches.

This chapter is an introduction to Bayesian inference and probability theory, and its applications to the physical sciences, in particular astrophysics and cosmology.

2.1 Introduction

2.1.1 Probability Theory

Probability Theory can be regarded as an extension of logical reasoning. It is concerned with the *plausibility* of propositions. That is, probability is not concerned with strictly deductive reasoning, but plausible reasoning: how plausible a hypothesis is based on information, rather than a logical deduction based on the same information. [68]

The scientific method makes extensive use of probability theory. Figure 2.2 is a schematic representation of the scientific method; statistical inference relies on probability theory. There are two main approaches to probability theory: Bayesian and frequentist approaches, which are outlined in this chapter.

2.1.2 History of Bayes' theorem

When he developed the ideas that would later lead to Bayesian inference, Rev. Thomas Bayes was looking for a way to infer cause from effects. The question he asked himself was simple:

how could one obtain the probability of an event occurring, knowing only how many times it had previously occurred or not occurred?

Although it is called Bayesian inference, much of the work on the mathematical formalism and scientific applications of Bayes' theorem was done by Laplace. When Thomas Bayes first introduced his ideas about probability, he used a thought experiment: he was trying to predict where a ball would land on a table, based on where the ball had landed previously.

The core idea of Bayes' theory of probability is that we can update our initial belief with new data to obtain an improved belief.

Bayesian inference was met with much criticism; to some, the theory appeared to be guess work, with poorly justified priors. It was met with particular virulence in the 19th century, notably during the trial of Alfred Dreyfus, when mathematician Henri Poincaré used Bayesian reasoning to refute the accusations made against Dreyfus. [67]

However, Bayesian inference knew its biggest triumphs during the Second World War. Its resurgence started with the release of Harold Jeffreys' *The Theory of Probability* in 1939, during the last year of peace before the start of the war. His work developed a theory of scientific inference using Bayes' theorem. [67,69]

During the Second World War, the German naval forces used Enigma, an enciphering machine, to exchange crypted messages, with the encryption system changing daily. Alan Turing developed a Bayesian inference technique, which he named Banburismus, to crack the Enigma code. [67]

The superiority of Bayesian methods has since been demonstrated in many areas.

2.1.3 The Bayesian and Frequentist Approaches

Traditionally, probability theory has been approached from a frequentist point of view. The frequentist approach to probability relies on the outcome of a theoretically infinite number of identical experiments. [70] In comparison, the Bayesian approach features a more intuitive view of probability, where prior information on data and hypotheses is taken into account. For events that are very unlikely and unrepeatable, the Bayesian approach is clearly superior.

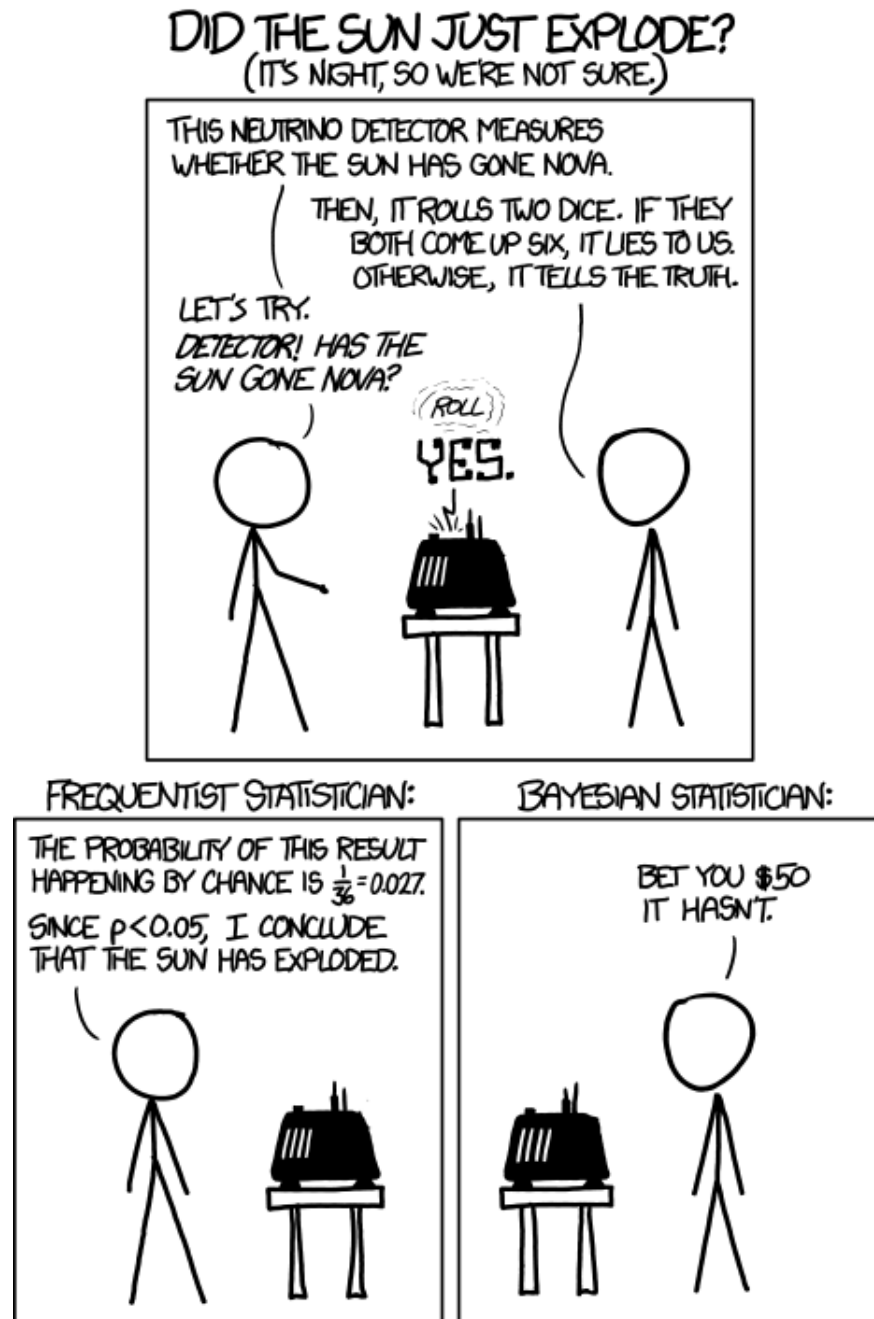


Figure 2.1: The frequentist approach and Bayesian approach illustrated by Randall Munroe. [71]

In Figure 2.1, an extreme comparison of frequentist and Bayesian approaches is humorously presented in the context of an unlikely astrophysical phenomenon.

2.1.4 The Role of Bayesian Inference in Physical Sciences

The effectiveness of Bayesian inference was historically demonstrated with triumphant success in the cracking of the Enigma code during the Second World War. However, the theory has many more applications, especially in the physical sciences. While initially met with some resistance

from the scientific community, in recent years, Bayesian methods have been increasingly used in the fields of physics and astronomy.

Bayesian inference has many advantages in astrophysics and cosmology, for the following reasons: [72]

- The increasing complexity of models means that the scientific returns of future surveys are limited by the sophistication and efficiency of the inference tools used.
- The "discovery zone" is between 3 and 4 σ : Bayesian inference could make the difference between claiming or missing a discovery.
- Some effects that are not really present do not need to be explained.
- Resources are limited, so optimal strategies need to be in place to maximise the scientific returns.
- Sometimes the data available cannot be improved.

Bayesian inference also offers more a more straightforward method of dealing with nuisance parameters, compared to frequentist methods. These parameters are parameters that are of less interest, but still need to be handled in the analysis. In Bayesian inference, this is done through marginalisation, which is detailed in section 2.2.3.

For Cosmology

Cosmology, like most fields relying on astronomical observations, has to deal with limited, complex and sometimes poor data. This makes Bayesian inference is an ideal statistical tool for modern cosmology.

The recent data explosion in cosmology meant that more refined and efficient statistical tools were required. For instance, maps of the CMB (see section 3.5.1) went from 10^3 pixels with COBE to 10^7 pixels with Planck. [72]

For Gravitational Wave Data Analysis

Bayesian inference plays a key role in the analysis of data coming from aLIGO. As discussed in chapter 1 the aLIGO interferometers are limited by noise. While improvements to the instruments can help reduce noise, Bayesian inference provides tools for maximising our ability to discriminate between noise and signals from astrophysical sources.

Discriminating between noise and astrophysical signals is not the only area of gravitational wave astronomy that benefits from the application of Bayesian methods. It is also useful in parameter estimation of the systems that produced the signals. Gravitational waves from a binary system have large parameter spaces, containing 9 to 17 dimensions. [73] Dealing with such

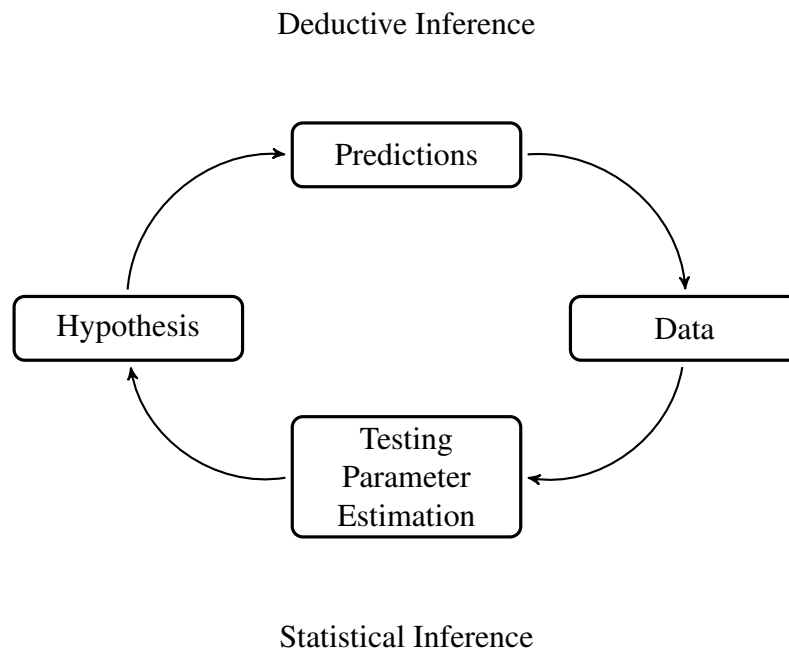


Figure 2.2: A schematic representation of the scientific method.

large parameter spaces requires sophisticated and efficient statistical tools, which are provided by Bayesian inference.

2.2 Basics of Bayesian Inference

Bayesian inference fundamentally differs from the more traditional frequentist approach in that it defines probability as a measure of our degree of belief. The frequentist approach, on the other hand, defines probability as the number of times a certain outcome happens in a number of trials, in the limit of an infinite number of trials. A good example of a frequentist probability is the probability of rolling a certain number on a 6-sided die: this comes up as $\frac{1}{6}$.

2.2.1 Notations

Bayesian inference makes use of a number of notations specific to probability theory. Some of this notation is defined in E.T. Jaynes. [68, 70]

- $p(A)$ is the probability of a proposition A being true. Going back to the dice example, given $A \equiv$ "The value of the die is 6", then $p(A) = \frac{1}{6}$.
- \bar{A} represents proposition A being false.
- AB , also written A, B , is the logical product of propositions A and B . It denotes A and B being both true (logical AND). Since the order of these statements does not matter, $AB = BA$.

- $p(A, B)$ represents the joint probability of A and B, with A, B the logical product of A and B.
- $A + B$ is the logical sum or disjunction of A and B. [68]. It denotes at least one of propositions A and B being true (logical OR).

2.2.2 Deriving Bayes' Theorem

Bayesian inference relies on the application of an equation called Bayes' Theorem, or Bayes' rule. This theorem can be derived from the basic rules of sum and product of probabilities. These are outlined below.

The Sum Rule

$$p(A|B) + p(\bar{A}|B) = 1, \quad (2.1)$$

in which $p(A|B)$ is the probability that A is true given B, and $p(\bar{A}|B)$ is the probability that A is not true given B. Given that there are only two possible outcomes (either A is true or isn't), and that the product $A\bar{A}$ is always false (the two propositions cannot be true at the same time) the sum of these probabilities must add up to 1. The two propositions governing the sum rule are of the Aristotelian logical type. [68]

$$A\bar{A} = 0, \quad (2.2)$$

$$A + \bar{A} = 1, \quad (2.3)$$

where 0 represents the proposition always being false, and 1 represents the proposition always being true (as used in Boolean algebra).

The Product Rule

$$p(A, B|C) = p(A|C)p(B|A, C) = p(B|C)p(A|B, C) \quad (2.4)$$

$p(A, B|C)$ is the probability of A and B being true given C. This is known as the joint probability of A and B. The product rule can be derived through extended logic. [74]

Bayes' Theorem

When combining these rules, we arrive at the expression of Bayes's theorem seen in equation 2.5.

$$p(H|D,I) = \frac{p(H|I)p(D|H,I)}{p(D|I)}, \quad (2.5)$$

where:

- $p(H|D,I)$ is the posterior,
- $p(H|I)$ is the prior,
- $p(D|H,I)$ is the likelihood,
- $p(D|I)$ is the marginal likelihood, or evidence.

2.2.3 Marginalisation

Marginalisation offers a way of dealing with nuisance parameters. If a distribution depends on parameters that are of little or no interest to us, these are called nuisance parameters.

In Bayesian inference, nuisance parameters are dealt with through marginalisation: that is, integrating through the entire parameter space for the nuisance parameters.

For example, for a probability $p(X)$ depending on a continuous parameter H :

$$p(X) = \int_H p(X,H)dH, \quad (2.6)$$

$$p(X) = \int_H p(X|H)p(H)dH. \quad (2.7)$$

Marginalisation can also be applied to the discrete case, with $p(X)$ depending on a parameter H that can take n values H_i :

$$p(X) = \sum_{i=1}^n p(X|H_i)p(H_i) \quad (2.8)$$

This is especially useful for the denominator, or marginal likelihood, of Bayes' theorem. Applying marginalisation to the marginal likelihood as defined in equation 2.5, in the discrete case with a hypothesis H_i :

$$p(D|I) = \sum_{i=1}^n p(D|H_i,I)p(H_i), \quad (2.9)$$

$$p(H_i|D,I) = \frac{p(H_i|I)p(D|H_i,I)}{\sum_{i=1}^n p(D|H_i,I)p(H_i)}. \quad (2.10)$$

2.3 Model Selection

There are two main problems addressed by Bayesian Data Analysis: model selection and parameter estimation. In a model selection problem, we are trying to find the best model that fits a set of observations.

While each model can contain parameters that accept a range of values, which are to be estimated through parameter estimation, competing models might contain a different number of parameters. Model selection problems help discriminate between two competing models and decide on which model is most probable given our current knowledge. Model selection tests competing models independent of the values of their parameters (all parameters are marginalised). [74]

Bayesian inference is a great tool for model selection in cosmology. [72] For example, testing the Λ CDM model is a model selection problem.

2.4 Parameter Estimation

Model selection is not the only problem that can be addressed using Bayesian inference. Within an accepted model, there will be a number of free parameters; we can use parameter estimation to constrain their values.

Within Bayesian statistics, the application of Bayes' theorem to a continuous hypothesis space is a parameter estimation problem. [74]

In parameter estimation, we are interested in the values of model parameters for a given model that is assumed to be true. While in model selection, we marginalised all parameters, in parameter estimations, we test different values of a parameter within a single model.

The previous section discussed the successes of Bayesian inference in the selection of cosmological models. Parameter estimation is also a problem in cosmology, and it benefits from a Bayesian approach. [72]

Chapter 3

Overview of Modern Cosmology

The word Cosmos is used to describe the entire universe that surrounds us. As such, cosmology, the study of the cosmos, is the study of the whole universe as a system, from its history to its evolution and the models and parameters that govern it.

Where astrophysics is concerned with the physical phenomena that govern objects and interactions within the universe, cosmology is concerned with the dynamical evolution of the universe as whole. Many fields of physics and astronomy tie into cosmology.

3.1 The Road to Precision Cosmology

For many thousands of years, it was assumed that our planet occupied a very special place in the universe.

The Ancient Greeks, in a cosmological model developed by Ptolemy, believed the Earth to be the centre of the universe, orbited by the Sun, Moon and planets, with static stars in the background; this assumption went unchallenged until the 1500s when Copernicus introduced the heliocentric model. Even then, Copernicus put our solar system at a very special place, with the Sun at the centre of the universe. [75]

Newton took us closer to our current view of the universe; he believed that other stars like our Sun, with orbiting planets around it, existed, in a static configuration.

The picture of the solar system as part of a galaxy came from the Herschels; however, once again, the theme of putting our solar system at a special place underlies this model, and our solar system was believed to be at the centre of the Milky Way. [75, 76]

Galaxies were first understood as "spiral nebulae". Shapley believed that our galaxy was one galaxy amongst others; however, he also believed us to be at the centre of the universe.

In 1952, at a meeting of the International Astronomical Union, Baade postulated that our galaxy was just one galaxy, and that the universe was much larger than previously believed, doubling the estimate previously made by Edwin Hubble, an astronomer who made significant contributions to cosmology, notably the constant that bears his name, as detailed in the following

sections. [75]

It was therefore a long road to modern cosmology; in the twentieth century, cosmology entered a new era of precision.

3.2 Cosmological Principle and Standard Cosmological Model

In order to study the universe as a single system, assumptions need to be made. The standard assumptions that underlie every aspect of modern cosmology are known under the name of cosmological principle, and underlie every aspect of cosmology. This principle can be easily summarised by the idea that the place we occupy in the universe is not, in any way, special. [75] This means that on large scales (typically larger than 300Mpc), the universe looks smooth. The particular properties assumed for the universe on large scales are homogeneity and isotropy. Homogeneity means that the universe looks the same at any point, while isotropy means that it looks the same in every direction.

The cosmological principle holds on large scales. Large scales can be defined observationally: galaxy redshift surveys such as the Sloan Digital Sky Survey can be used to probe the redshift distribution of galaxies in the universe. While structure is observed on smaller scales, such as filaments, voids and clusters, on large scales (> 300 Mpc) there is no distinguishable structure. Figure 3.1 shows a slice of a galaxy redshift map taken by the SDSS.

3.3 The Expanding Universe

Chapter 1 introduced the main concepts of Einstein's general relativity. The theory has some profound consequences for the universe as a whole. If we assume homogeneity and isotropy on large scales, Einstein's equations can be applied to the universe as a fluid with pressure p and mass density ρ . Assuming a static universe with a radius of curvature R gives these final equations; a full derivation is available in Peebles. [78]

$$\frac{4}{3}\pi G(\rho + 3p) = 0 \quad \frac{8}{3}\pi G\rho - \frac{1}{R^2} = 0 \quad (3.1)$$

These equations give $p = -\rho/3$, meaning that for a positive density, the pressure of the universe is negative, which is not possible for ordinary matter. With that in mind, Einstein modified his equations.

In general relativity, the energy-momentum tensor is the source for the gravitational field. This means there is a possibility for vacuum energy: the energy density of empty space. [11] Starting from Einstein's field equation:

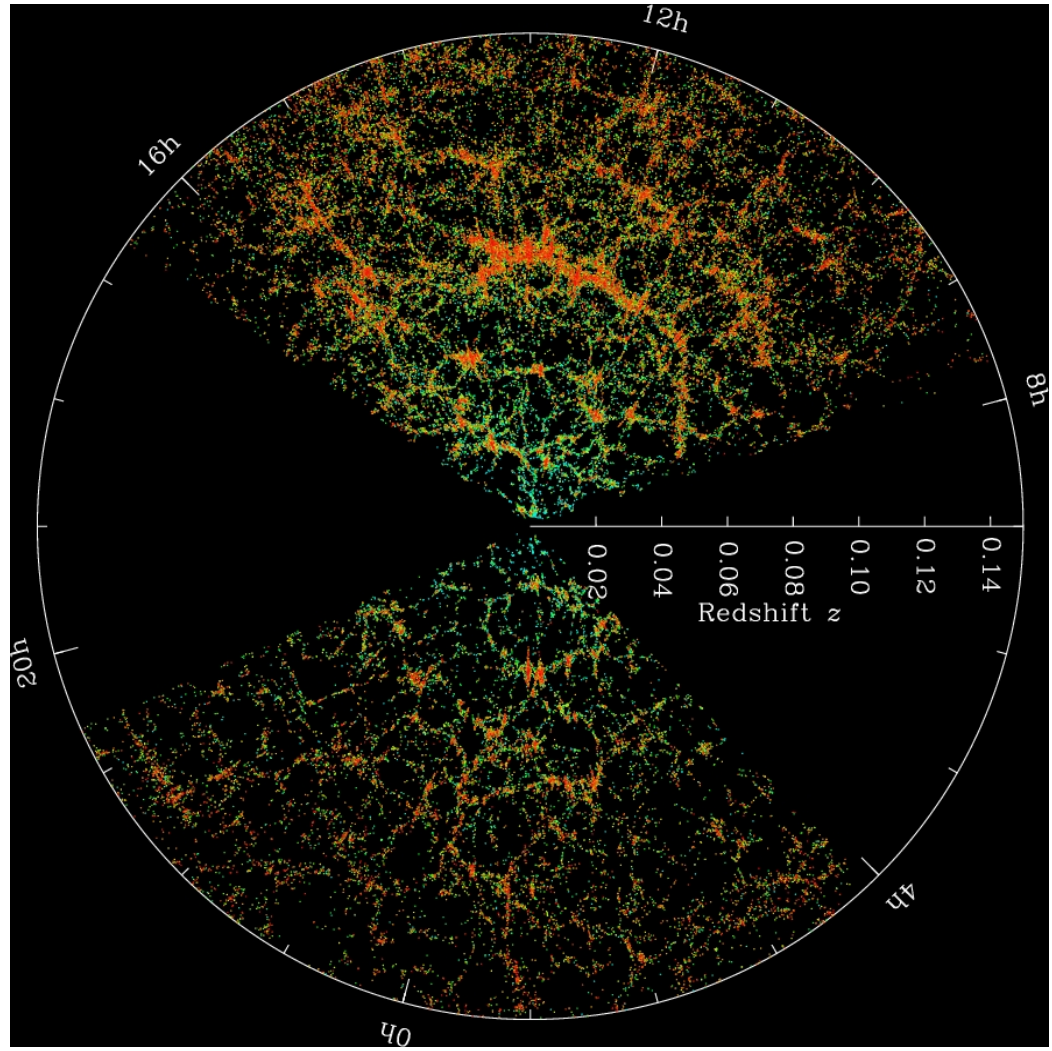


Figure 3.1: The Sloan Digital Sky Survey’s map of the universe. Each dot is a galaxy, and the colour its g-r colour. [77] From this map, some structure in the form of filaments and voids appears on smaller scales. However, on large scales, the distribution of galaxies is roughly uniform.

$$R_{\mu\nu} - \frac{1}{2}Rg_{\mu\nu} = 8\pi GT_{\mu\nu}, \quad (3.2)$$

where $R_{\mu\nu}$ is the Ricci curvature tensor, R is the scalar curvature, $g_{\mu\nu}$ is the metric tensor, G is Newton’s gravitational constant and $T_{\mu\nu}$ is the stress-energy tensor.

We can decompose the energy-momentum tensor $T_{\mu\nu}$ into two parts, one corresponding to ordinary matter, and one corresponding to the vacuum. This allows us to rewrite equation 3.2. Decomposing the energy-momentum tensor into matter and vacuum $T_{\mu\nu}^{(M)}$ and $T_{\mu\nu}^{(vac)} = -\rho_{vac}g_{\mu\nu}$ respectively

$$R_{\mu\nu} - \frac{1}{2}Rg_{\mu\nu} = 8\pi G(T_{\mu\nu}^{(M)} - \rho_{vac}g_{\mu\nu}). \quad (3.3)$$

A new term Λ , is then introduced to characterise the vacuum part associated with the energy-momentum tensor, with $\Lambda = 8\pi G\rho_{vac}$.

$$R_{\mu\nu} - \frac{1}{2}Rg_{\mu\nu} + \Lambda g_{\mu\nu} = 8\pi GT_{\mu\nu} \quad (3.4)$$

This gives a vacuum energy density

$$\rho_{vac} = \frac{\Lambda}{8\pi G}. \quad (3.5)$$

Einstein first introduced the cosmological constant Λ to his field equations in an effort to produce an equation that would describe a static universe. A static, finite universe was the accepted cosmological model for a very long time. However, any solution to Einstein's equations leading to a static universe would be highly unstable, meaning any small perturbation in the density of the universe would cause rapid collapse or expansion; the static mass distribution is gravitationally unstable, and large scale approximation of homogeneity could not last longer than the lifetime of a Sun-like star. [78]

Einstein's model of the universe therefore seemed to have little theoretical support. The idea of a static, finite universe was, in any case, soon to be completely overturned by observations.

A peculiar phenomenon arises if we look into the depths of our universe: everything seems to be moving away from us. Not only do astrophysical objects appear to be moving away from us, but the rate at which they are moving away accelerates with increasing distance. This phenomenon was first observed by Edwin Hubble in 1929. [79] The Hubble constant, H_0 , is named after him and is the constant of proportionality between the recession velocity of galaxies v and their distance to us r .

$$H_0 = \frac{v}{r} \quad (3.6)$$

At first glance, one could think that this observed recession of surrounding galaxies places us at a special place in the universe, as was theorised by the Ancient Greeks and many civilisations and scientists after them. However, this phenomenon would happen no matter where an observer is standing. This is because it isn't the galaxies themselves that are moving. If we imagine an expanding grid of coordinates, with each galaxy at a certain point, then their coordinates do not change; rather, the grid expands, and the space between each point expands with it. [75, 78]

While Edwin Hubble's observations of the recession speed of galaxies were the first observational evidence of the expansion of the universe, an expanding universe had been previously predicted by theory. Indeed, the discovery of the expansion of the universe was made through a mixture of theory and observations, with many contributors. [78] In 1922, Russian physicist Alexander Friedmann derived a set of equations that described the expansion of an isotropic and homogeneous universe, starting from Einstein's field equations. [80, 81] Fried-

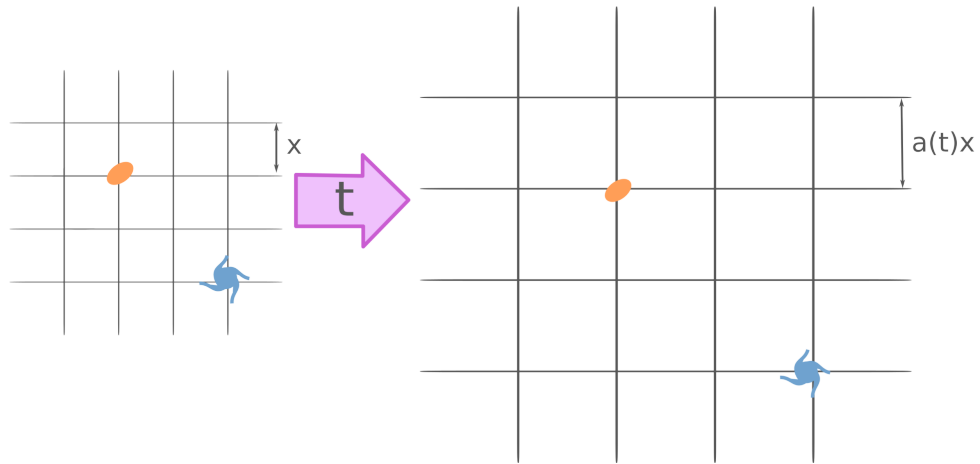


Figure 3.2: Expansion of coordinate grid, with $a(t)$ the scale factor of the universe.

mann's work, which pre-dates the first measurements of the rate of expansion of the universe, describes the time evolution of the universe for different values of a parameter k , the curvature of space. [80–82]

In Friedmann's equations, the evolution of the relative expansion is described by a newly introduced variable: the scale factor of the universe a . The scale factor a is a dimensionless number representing the relative expansion of the universe. It is a function of time, and defines the relationship between the proper separation of two objects at an arbitrary time t , $x(t)$, and the proper separation at present day x_0 .

$$a(t) = \frac{x(t)}{x_0} \quad (3.7)$$

The expansion of the universe means that the proper distance between galaxies with a large separation increases with time. [78] The large separation is required to observe the expansion, as gravitationally bound systems such as galaxy clusters do not expand. The Hubble parameter is defined in terms of the scale factor.

$$H \equiv \frac{\dot{a}(t)}{a(t)} \quad (3.8)$$

The Hubble parameter therefore evolves with time. The Hubble constant H_0 is the Hubble parameter measured at present time.

The relationship between the redshift and scale factor of the universe can be derived from the Friedmann-Lemaître-Robertson-Walker (FLRW) metric. In the metric, spatial coordinates are comoving; this means objects remain at fixed coordinates, with the expansion characterised

only by the scale factor $a(t)$. [75]

$$ds^2 = -c^2 dt^2 + a^2(t) \left[\frac{dr}{1-kr^2} + r^2(d\theta^2 + \sin^2\theta d\phi^2) \right] \quad (3.9)$$

where k is the curvature of the universe. For light propagation:

$$ds = 0. \quad (3.10)$$

For a radially propagating ray, travelling from $r = 0$ to $r = r_0$, that means $d\theta = d\phi = 0$. Setting this and $ds = 0$ in equation 3.9:

$$\frac{cdt}{a(t)} = \frac{dr}{\sqrt{1-kr^2}}. \quad (3.11)$$

To derive the time taken for the light to travel from $r = 0$ to $r = r_0$, we integrate equation 3.11.

$$\int_{t_e}^{t_r} \frac{cdt}{a(t)} = \int_0^{r_0} \frac{dr}{\sqrt{1-kr^2}}, \quad (3.12)$$

where t_e is the time at emission and t_r the time at reception.

Now imagining a light ray being emitted from $r = 0$ and received at $r = r_0$ shortly after the first light ray. Since the galaxies are comoving and therefore in the same coordinates, the emission and reception times would, respectively, be $t_e + dt_e$ and $t_r + dt_r$.

$$\int_{t_e+dt_e}^{t_r+dt_r} \frac{cdt}{a(t)} = \int_0^{r_0} \frac{dr}{\sqrt{1-kr^2}} \quad (3.13)$$

The left-hand sides of equation 3.12 and equation 3.13 are equal, allowing us to write:

$$\int_{t_e}^{t_r} \frac{cdt}{a(t)} = \int_{t_e+dt_e}^{t_r+dt_r} \frac{cdt}{a(t)}. \quad (3.14)$$

Now, since the areas under the curve determined by $\frac{c}{a(t)}$ are the same from t_e to t_r and $t_e + dt_e$ and $t_r + dt_r$, and the area from $t_e + dt_e$ to t_r is common to both, we can conclude that the area from t_e to $t_e + dt_e$ is equal to the area from t_r to $t_r + dt_r$. This allows us to write:

$$\int_{t_e}^{t_e+dt_e} \frac{cdt}{a(t)} = \int_{t_r}^{t_r+dt_r} \frac{cdt}{a(t)}. \quad (3.15)$$

The slices are narrow, which means we can approximate the area under the curve to a rect-

angle, making it simply width times height. We obtain

$$\frac{dt_r}{a(t_r)} = \frac{dt_e}{a(t_e)}. \quad (3.16)$$

Now, assuming an expanding universe, $a(t_r) > a(t_e)$ for any t_e . Therefore $dt_r > dt_e$; the time interval increases with the expansion of the universe.

Now imagining each light ray is actually a crest of a wavelength, then $\lambda \propto dt \propto a(t)$, giving

$$\frac{\lambda_r}{\lambda_e} = \frac{a(t_r)}{a(t_e)}. \quad (3.17)$$

For an observer on earth, $t_r = t_0$. The redshift is defined in equation 3.18.

$$\frac{a(t_0)}{a(t_e)} \equiv 1 + z \quad (3.18)$$

3.3.1 The Accelerating Universe

While the universe had been known to be expanding for a longer time, the discovery by Riess et al. and Perlmutter et al. that this rate of expansion was accelerating was a surprise to the scientific community. [83,84] Up until 1998, cosmologists believed the expansion of the universe to be decelerating due to gravity. They tried to measure this deceleration, quantifying it as the deceleration parameter q_0 . [85]

The 1998 paper presents evidence for a non-zero cosmological constant; Einstein's cosmological constant was considered a "blunder" after Edwin Hubble observed that the universe was in fact expanding. However, Λ is now necessary to explain the acceleration of this expansion. Observations of high-redshift Type Ia supernovae have shown luminosity distances 10% to 15% larger than expected in a $\Lambda = 0$ universe. [84]

The discovery has some profound implications for the fate and nature of the universe. This means the universe will keep expanding, rather than the expansion slowing down as was previously thought. It also heralded the start of theoretical work on dark energy, which is responsible for the accelerating expansion of the universe.

3.4 Measuring the Hubble Constant

In 1929, Edwin Hubble discovered a relationship between the radial velocity and distance to nearby galaxies (which he called extra-galactic nebulae). [79] This relation introduced the constant of proportionality that bears his name, the Hubble constant.

$$H_0 = \frac{v}{r}, \quad (3.19)$$

where v is the radial velocity and r the distance.

For small redshifts, $v = cz$, and we can approximate the proper distance between galaxies r to the luminosity distance D_L . This gives:

$$D_L = \frac{cz}{H_0}. \quad (3.20)$$

Its value was originally measured to be $H_0 = 500 \text{ km s}^{-1} \text{ Mpc}^{-1}$, as measured by Edwin Hubble, after whom the constant is named. In 1958, cosmologist Allan Sandage highlighted some issues in the calibrations used for previous estimates of the Hubble constant. He gave the first reasonable value of the Hubble constant, at $H_0 = 75 \text{ km s}^{-1} \text{ Mpc}^{-1}$, which is close to the accepted values of today. [86]

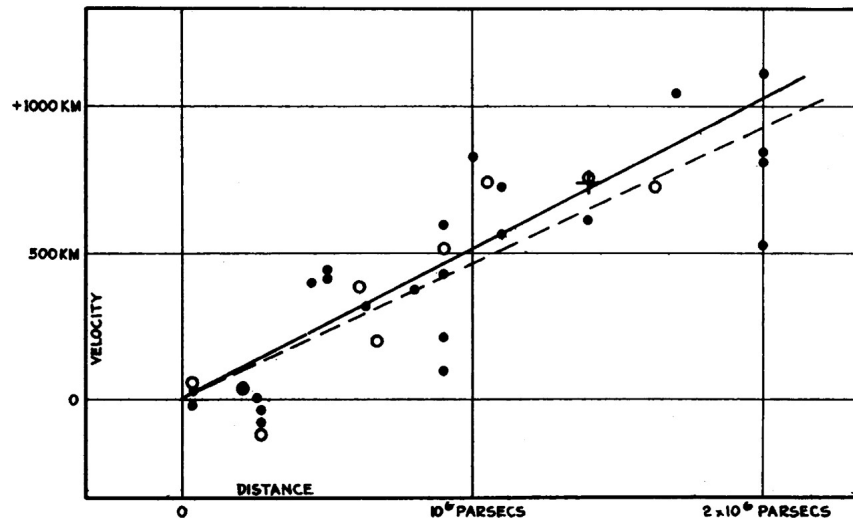


Figure 3.3: Edwin Hubble's original plot of the redshift-luminosity distance relationship. [79]

The recession speed of a galaxy cannot be directly measured, but it can be measured through its redshift. When galaxies are moving away from us, or when the space between the galaxies and us is expanding, their characteristic absorption and emission lines are shifted towards the red end of the electromagnetic spectrum. Conversely, if a galaxy is moving towards us, these lines are shifted towards the blue end of the spectrum, and we talk about blueshift. [75]

This technique for measuring the velocity of a galaxy was first used by 1912 by Silpher, when he used measurements of the redshift of Andromeda to determine the velocity at which our neighbour galaxy was moving towards us. [87]

More specifically, the redshift z of an object is defined as the fractional Doppler shift of its emitted light due to radial motion. [88] The cosmological redshift is the part of an object's

redshift that is due to the expansion of the universe. In cosmology, it is used as a distance marker. However, it should be noted that this is not quite true; since the rate of expansion of the universe evolves with time, so does the redshift. However, this is a very small change, and is small compared to the changes in redshift due to the change in peculiar velocity of either the source or the observer. [89]

There are several methods for measuring the Hubble constant, which are detailed in subsequent sections. Methods for measuring the Hubble constant can be either indirect (largely model-dependent) or direct (model-independent). For direct methods, we need to be able to measure distances to > 100 Mpc. [90] For indirect methods, such as the ones employed by the Planck Collaboration, the Λ CDM model is usually assumed.

3.4.1 The Hubble Flow

To measure the Hubble constant, we need to measure the velocity of the Hubble flow. The equation that describes the Hubble flow relates an object's recession speed to its distance.

$$v_H = H_0 d, \quad (3.21)$$

where the recession velocity v_H is the velocity of the Hubble flow, which characterises the rate of expansion of the universe.

The redshift of galaxies helps us measure the velocity of the Hubble flow. However, in order to have:

$$v_H = cz, \quad (3.22)$$

we need to only measure the cosmological redshift. However, the Hubble flow is not the only contributor to an object's redshift.

3.4.2 Peculiar Velocities

The redshift of a galaxy offers a measure of the velocity of the object. There is a difference between the observed redshift of a galaxy and its cosmological redshift, which is the part of the redshift associated with the expansion of the universe. This difference comes from the peculiar velocities of galaxies. [88]

While on large scales, galaxies are receding away from us due to the Hubble flow, locally, objects still interact if they're gravitationally bound. Due to gravitational interactions, local galaxies move with seemingly random velocities, adding an extra component to their measured radial speed that is not due to the expansion of the universe.

The effect is most noticeable in very nearby objects, since the recession velocity is proportional to the galaxy's distance, and at sufficiently small luminosity distances we can have

$$v_{pec} \gg v_H. [91,92]$$

3.4.3 Cosmography

At low redshift, and assuming that peculiar velocities are either negligible or have been corrected for, the assumption made in equation 3.20 holds. We assume that $v = cz$, with v the velocity of the Hubble flow. This is a non-relativistic approximation, and only holds true for small redshifts. At higher redshifts, more complex equations need to be used to measure the velocity of the Hubble flow. These equations depend on the geometry and matter content of the universe. [88]

Cosmography equations can be derived starting from Friedmann's equations. Starting from Poisson's equation for gravitational acceleration:

$$\nabla \cdot \mathbf{g} = -4\pi G(\rho + 3p), \quad (3.23)$$

and considering the gravitational acceleration at the surface of a sphere, it can be shown that [78,81]

$$\frac{\ddot{a}}{a} = -\frac{4}{3}\pi G(\rho + 3p). \quad (3.24)$$

If we add the cosmological constant

$$\frac{\ddot{a}}{a} = -\frac{4}{3}\pi G(\rho + 3p) + \frac{\Lambda}{3}. \quad (3.25)$$

For redshifts less than 1000, the universe is matter-dominated. This means that the pressure p is small compared to the matter density ρ . From energy conservation, it can be shown that the density varies as $\rho \propto a(t)^{-3}$. We can now rewrite the Hubble parameter in terms of the density parameters of the universe. [78]

$$H^2 = \left(\frac{\dot{a}}{a}\right)^2 = \frac{8}{3}\pi G\rho + \frac{kc^2}{a^2} + \frac{\Lambda}{3}, \quad (3.26)$$

where kc^2 is a constant of integration, related to the curvature k of the universe.

$$H^2 = \left(\frac{\dot{a}}{a}\right)^2 = \left(\frac{\dot{z}}{1+z}\right)^2 = H_0^2[\Omega_M(1+z)^3 + \Omega_k(1+z)^2 + \Omega_\Lambda] \quad (3.27)$$

Ω_M is the matter density parameter, Ω_k the spatial curvature density parameter and Ω_Λ the vacuum density parameter. They are defined as follows:

$$\Omega_M = \frac{8\pi G\rho_0}{3H_0^2}, \quad (3.28)$$

where ρ_0 is the matter density of the universe at present time,

$$\Omega_k = -\frac{kc^2}{a^2 H_0^2}, \quad (3.29)$$

$$\Omega_\Lambda = \frac{\Lambda}{3H_0^2}, \quad (3.30)$$

and since at $H = H_0$ we have $a = 1$:

$$\Omega + \Omega_k + \Omega_\Lambda = 1. \quad (3.31)$$

We can define the function [88]

$$E(z) \equiv \sqrt{\Omega_M(1+z)^3 + \Omega_k(1+z)^2 + \Omega_\Lambda}. \quad (3.32)$$

The Hubble constant evolves with time, with the subscript 0 indicating present time. For an observer measuring the Hubble constant at a redshift z , its value is

$$H(z) = H_0 E(z). \quad (3.33)$$

The line of sight comoving distance is the distance between two nearby objects which remains constant if they are both moving with the Hubble flow.

$$D_C = D_H \int_0^z \frac{dz}{E(z)}, \quad (3.34)$$

with D_H the Hubble distance as defined in equation 3.35.

$$D_H = \frac{c}{H_0} \quad (3.35)$$

The luminosity distance is determined in terms of the transverse comoving distance D_M .

$$D_L = (1+z)D_M \quad (3.36)$$

D_M is the transverse comoving distance. It is equivalent to the proper motion distance, and is related to the line of sight comoving distance in the following way:

$$D_M = \begin{cases} D_H \frac{1}{\sqrt{\Omega_k}} \sinh[\sqrt{\Omega_k} \frac{D_C}{D_H}] & \text{for } \Omega_k > 0, \\ D_C & \text{for } \Omega_k = 0, \\ D_H \frac{1}{\sqrt{|\Omega_k|}} \sin[\sqrt{|\Omega_k|} \frac{D_C}{D_H}] & \text{for } \Omega_k < 0. \end{cases} \quad (3.37)$$

These equations are defined for any curvature k (open, flat or closed universe). However, we now know that observations are consistent with models with $\Omega_k = 0$, meaning that we are living in a flat universe. [93]

3.5 Methods for Measuring the Hubble Constant

3.5.1 The Cosmic Microwave Background

In 1964, a faint radiation filling the sky in all directions was observed using the Holmdel Horn Antenna at the Crawford Hill Laboratory. The discovery, reported in 1965, was of what we call the cosmic microwave background radiation (CMBR). [94] This radiation is of a black-body form with a present day temperature:

$$T_0 = 2.725 \pm 0.001K. \quad (3.38)$$

The CMB is radiation which has travelled and cooled down since the epoch of recombination. [75] On large angular scales, it contains the imprints or primordial gravitational potential fluctuations [95, 96]

The Planck mission is the successor to the WMAP and COBE satellites, a third-generation space mission designed to probe the anisotropies in the cosmic microwave background. [93]

Planck measurements of the CMB can be used to obtain a measurement for H_0 . The measurement is made from the temperature fluctuations in the CMB. To make this measurement, the Λ CDM model needs to be assumed. Irregularities in the cosmic microwave background are called anisotropies.

The cosmological principle, which states that the universe is homogeneous and isotropic, is not exact; small irregularities are expected. The small irregularities that are present in the cosmic microwave background radiation are called anisotropies. Those differences in temperature in the cosmic microwave background are extremely small, of the order of $\frac{\Delta T}{T} 10^{-5}$. [75] This makes CMB anisotropies hard to detect, and it took until 1992 for the COBE mission to measure them. [95]

The expansion history of the universe is encoded into the CMB, meaning that we can use it to measure the Hubble constant; baryon acoustic oscillations can be used to measure the expansion of the universe. [97] The acoustic peaks in the CMB power spectrum are determined by the physics of recombination. The expansion history of the universe determines the relationship between that intrinsic physical scale and its angular size as a function of redshift.

The angular power spectrum of the universe, seen in figure 3.5 as measured by WMAP, was found to be consistent with an inflationary, spatially flat Λ CDM model specified by 6 parameters. [98–100]

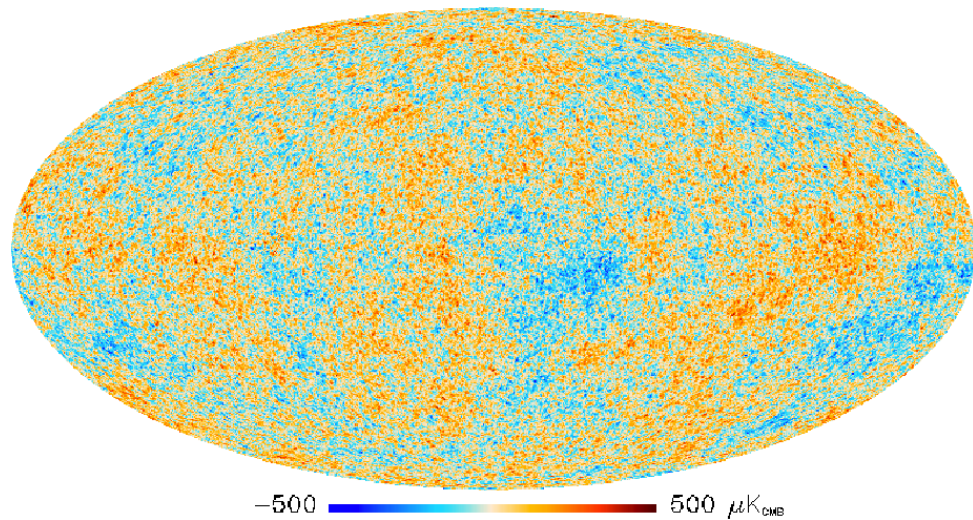


Figure 3.4: Map of the CMB from 2013 Planck results. [100] This map estimates the CMB over 97% of the sky. The angular resolution is $5'$. The associated colour is the temperature of each pixel, which shows temperature anisotropies in the CMB.

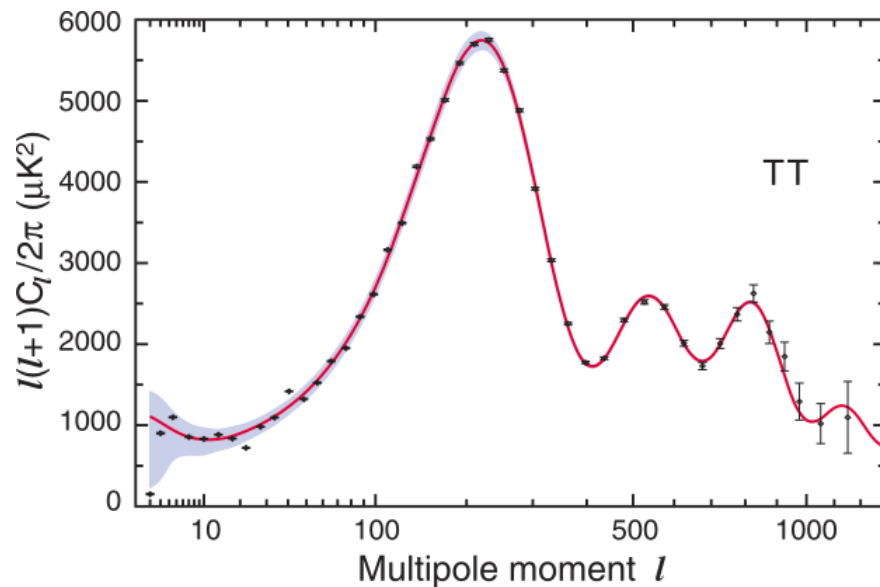


Figure 3.5: Angular power spectrum from 9 year WMAP results with best fit from Λ CDM. [99]

3.5.2 Standard Candles

In order to make a local measurement of the Hubble constant, it is necessary to be able to determine the distance to astrophysical objects. This is not a straightforward calculation for very distant objects; while there is a relationship between luminosity and distance, we need a reference for how bright an object should be.

Measuring distances in astronomy is not a straightforward problem. In the electromagnetic spectrum, astronomers have to rely on the cosmic distance ladder: a succession of different methods of measuring distances to far-out objects, each rung of the ladder defined by how close

the objects are. For objects that are closer by, the parallax method can be used. [101] The parallax method is a direct measurement of distance to nearby (on astronomical scales!) celestial objects. The GAIA mission, which is the successor to ESA's HIPPARCOS mission, is cataloguing a billion stars. [102]

However, for more distant objects, as are needed in the determination of the Hubble constant, indirect methods of measuring and calibrating distances are needed.

In general, for objects that are further out, we measure the luminosity distance D_L , a quantity that relates an object's observed flux F to its intrinsic luminosity L . [103]

$$D_L = \sqrt{\frac{L}{4\pi F}} \quad (3.39)$$

Therefore, if we know the absolute luminosity of an observed object, we can infer its distance.

Standard candles are astrophysical objects with a characteristic light curve, meaning they can be used to determine relative distances between two standard candles. As seen in equation 3.39, if we know an object's intrinsic luminosity and observe its flux, a distance can be obtained.

However, measuring precise distances in astronomy is still not an easy task, and even standard candles are subject to many systematics and other sources of error.

Cepheid Variable Stars

Cepheids are variable stars that have a high luminosity and pulsate radially. This variability means that they are easy to identify and classify. [104]

In 1908, astronomer Henrietta Swann Leavitt made observations of over a thousand variable stars in the Magellanic Clouds. [105] From these observations, it was found that the luminosity of these stars was related to their pulsation period: their luminosity increased with the period or their pulsation. [106, 107] This relationship, called the Cepheid period-luminosity relationship, or Leavitt Law, is both a powerful and reliable tool for measuring distances to nearby galaxies. [103]

Type Ia Supernovae

While they are powerful distance calibrators, Cepheids do not allow us to probe far enough into the smooth Hubble flow to get a measurement of the Hubble constant. Type Ia supernovae are brighter objects than Cepheids, meaning greater distances can be probed, well into the smooth Hubble flow. [108] They are extremely luminous point sources, making them ideal standard candles for measuring extragalactic distances. [109]

Type Ia supernovae result from the thermonuclear explosions of white dwarfs composed of carbon and oxygen. [110] Since all Type Ia Supernovae are the result of the same physical

mechanism, meaning they have very characteristic light curves and can be used as a distance indicator.

3.6 Discrepancies in Measurements of the Hubble Constant

The need for an independent measurement of the Hubble constant comes from discrepancies in measurements using different methods. Since its first estimation at $H_0 = 500 \text{ km s}^{-1} \text{ Mpc}^{-1}$, the value of the Hubble constant has been refined.

The first precision measurement was made by the Hubble telescope, named after the constant it sought to measure. Since that first measurement, the value for the Hubble constant has been refined and measured with different instruments and using the different methods described previously.

The Hubble Space Telescope (HST) Key Project was a mission designed to measure the Hubble constant. It used Cepheid and Type Ia supernovae to measure distances to galaxies. This first result gave a combined value of $H_0 = 72 \pm 8 \text{ km s}^{-1} \text{ Mpc}^{-1}$. [111]

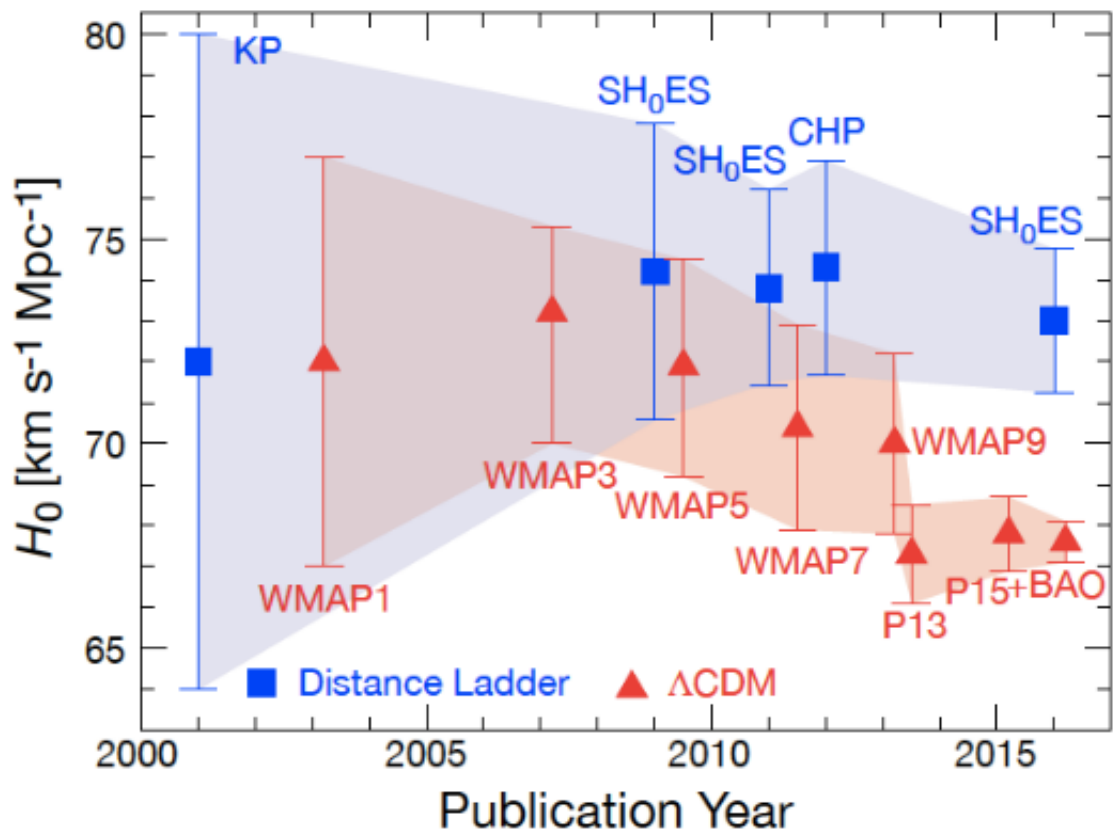


Figure 3.6: Discrepancies in current measurements of the Hubble constant. The data points in blue are from model-independent measurements in the local universe, while red data points are results from model-dependent measurements that assume the Λ CDM model. [108]

Even today, with refined measurements and in the era of precision cosmology, there is still much uncertainty about the value of the Hubble constant. Local measurements and CMB measurements provide information about the two ends of the visible expansion history of the universe, and can therefore be used as a test of the standard cosmological model. [112] There is currently a tension of 3.4σ between measurements of the Hubble constant using different methods; namely, there is a discrepancy between local measurements of the Hubble constant and model-dependent measurements inferred from the CMB. [90]

Results from the Planck collaboration give a value of $H_0 = 67.8 \pm 0.9 \text{ km s}^{-1} \text{ Mpc}^{-1}$ as of 2015. [93] Recent results from Type Ia supernovae give a value of $H_0 = 73.24 \pm 1.74 \text{ km s}^{-1} \text{ Mpc}^{-1}$. [112] Results from measurements using strong lensing give a value of $H_0 = 71.9^{+2.4}_{-3.0} \text{ km s}^{-1} \text{ Mpc}^{-1}$. [113]

Should these discrepancies persist, it could indicate that new physics are at play. [108] This is a still unresolved problem in cosmology; the discrepancy could indicate unknown systematic errors in the Planck analysis, or it could indicate the presence of physics beyond the standard model. [112]

Chapter 4

Methods for measuring the Hubble Constant using Standard Sirens

A discussion of current tensions in the results from different methods of measuring of the Hubble constant was presented in the previous chapter. These discrepancies highlight a need for a new, independent way to obtain a value for the rate of expansion of the universe. This chapter will discuss another method, independent of traditional electromagnetic methods, of measuring the Hubble constant. This method makes use of gravitational wave signals from compact binary coalescences, which are also known as standard sirens. [3]

This chapter presents an overview of standard sirens, and methods for obtaining the redshift corresponding to the binary merger’s host galaxy. Statistical methods are discussed in-depth and a Bayesian formalism is derived for measuring the Hubble constant using gravitational wave signals from compact binary coalescences and a magnitude-limited electromagnetic galaxy catalogue.

4.1 Standard Sirens

4.1.1 Theory

As previously mentioned in section 3.5.2, obtaining distances to celestial objects well into the smooth Hubble flow is not a straightforward problem in astronomy, and we need to rely on indirect measurements that are subject to many astrophysical systematics. This problem is specific to electromagnetic observations; in the gravitational wave spectrum, absolute distances can be obtained from observations. While distance estimates from gravitational wave signals are not perfect, and have large errors (up to 40%), they nonetheless present an advantage in that they are not subject to the same systematic errors as the electromagnetic distance scale.

When gravitational waves are observed due to energy loss and shrinking of orbits in a compact binary system, a luminosity distance to the source can be directly determined. [114] This

is what makes compact binary coalescences standard sirens: during their inspiral phase, as they orbit closer and closer to each other until eventually merging, their orbits decay through the emission of gravitational radiation. These standard sirens are similar to standard candles in the electromagnetic spectrum, in that they yield a luminosity distance to an astrophysical object. However, gravitational wave standard sirens, unlike standard candles like Cepheid variables and Type Ia Supernovae, do not depend on the knowledge of other rungs on the cosmic distance ladder; they are self-calibrating, making them a powerful tool for cosmography. [115] Standard sirens are not subject to the same astrophysical systematics (extinction, etc.) as standard candles. Furthermore, they do not rely on a cosmological distance ladder, being absolutely calibrated by general relativity; the only calibration present is the assumption that general relativity describes the waveform. [115] They are also tools for cosmology, as the amplitude of gravitational waves is proportional to the inverse of the distance (see equation 1.8), while the amplitude of electromagnetic waves follows an inverse square law.

The inspiral phase of compact binary coalescences is well modelled, making parameter estimation possible from the waveform, which is how a luminosity distance can be obtained. Thanks to recent breakthroughs in the field of numerical relativity (NR), distance estimation from the whole CBC waveform is now possible. [34–37]

As discussed in section 1.1.4, there are three types of compact binary coalescences that we know of: black hole - black hole (BBH), black hole - neutron star (BH-NS) and neutron star - neutron star (BNS). While we might expect, or have indeed observed in the case of the binary neutron star merger GW170817, an electromagnetic counterpart from a BNS or BH-NS system merging, no such counterpart is expected from BBH coalescences.

In his 1986 paper, Schutz proposed that the coalescences of neutron stars in binary systems could be useful standard sirens for measuring the Hubble constant. [114] In the original paper, the measurement of the Hubble constant is proposed without an electromagnetic counterpart.

For a binary neutron star system located at a distance $D_L = 100r_{100}$ Mpc, emitting gravitational waves at a frequency of $100f_{100}$ Hz:

$$r_{100} = 7.8f_{100}^{-2}(\langle h_{23} \rangle \tau)^{-1}, \quad (4.1)$$

where $\langle h_{23} \rangle = \langle h \rangle * 10^{23}$, and $\langle h \rangle$ is the root mean square amplitude, or strain, of the gravitational waves, averaged over all detector and source orientations. [114]

From this equation, we can see that the luminosity distance of the system is dependent on the strain h , the parameter measured by gravitational wave detectors.

This result is less straightforward than it would seem, as the equation yields a value for the strain averaged over all orientations, while inferring h from observations by a network of gravitational wave detector will depend on the position, orientation and distance of the binary system. [114]

There are two parameters needed to measure the Hubble constant: redshift and luminosity

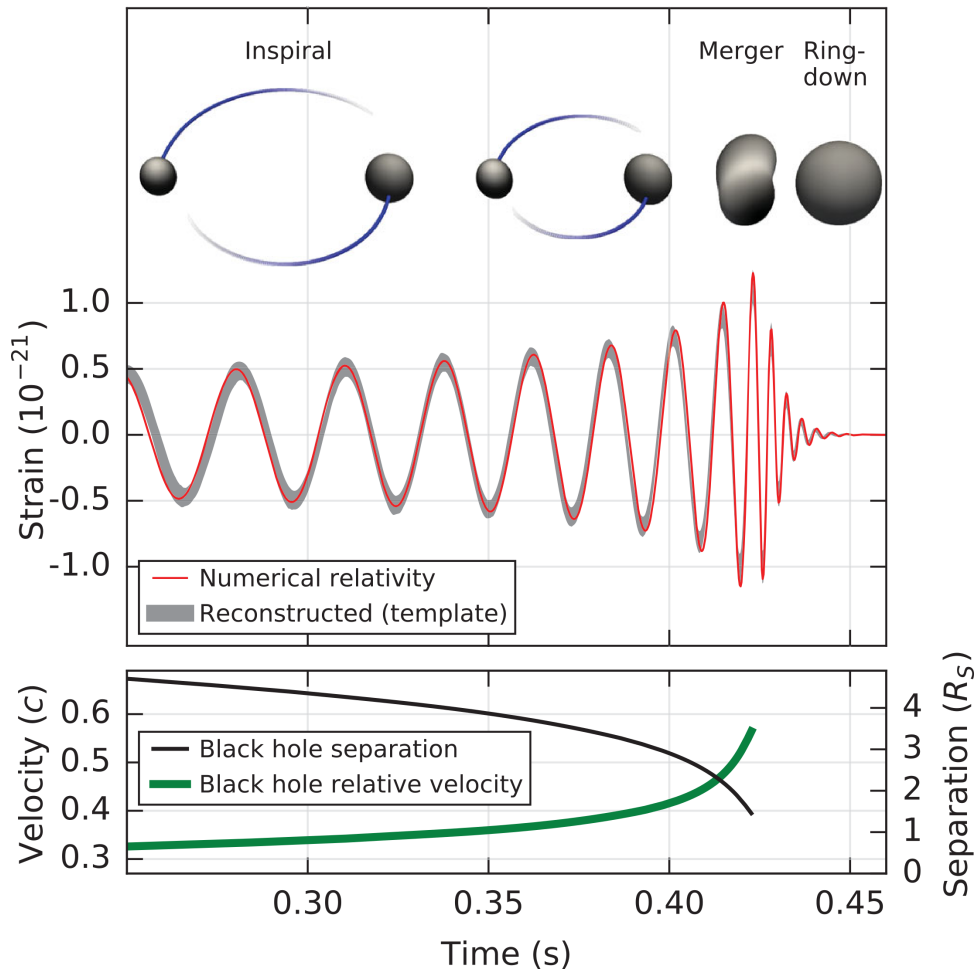


Figure 4.1: Juxtaposition of the reconstructed signal for GW150914 and the signal obtained from numerical relativity. [1] This shows how well observations agree with NR predictions.

distance. While the analysis of gravitational wave signals from CBCs yields a luminosity distance, a redshift cannot be obtained directly from the data, as it is degenerate with the mass of the system. [114] The chirp mass \mathcal{M} and redshift z of the system are combined into the redshifted chirp mass \mathcal{M}_z , and a system with, for example, a chirp mass \mathcal{M} and a redshift $z = 2$ will look identical to a system with a chirp mass $3\mathcal{M}$ and no redshift. [3, 116].

$$\mathcal{M}_z = (1+z) \frac{(m_1 m_2)^{3/5}}{(m_1 + m_2)^{1/5}} \quad (4.2)$$

In the case of binary neutron stars, even when no electromagnetic counterpart is present, a redshift can be assigned to the system by assuming a sufficiently narrow mass distribution for neutron stars. This gives an estimate of the intrinsic mass of the components of the system. This information, combined with the redshifted mass parameter encoded in the waveform, leads to a narrow distribution of possible redshifts for the system. [117] However, the redshift obtained from assigning a narrow mass distribution to neutron stars would be due to the total velocity of the system, which would include any peculiar velocity of the binary neutron star within its host

galaxy; in order to measure the Hubble constant, we need the redshift of the host galaxy in the smooth Hubble flow.

While binary neutron stars and BH-NS systems can have associated electromagnetic counterparts, this is not the case for binary black hole coalescences. And, unlike neutron stars, black holes do not have a narrow mass distribution from which a redshift could be obtained. [118] The range of masses of binary black holes measured by LIGO can be seen in Figure 4.2.

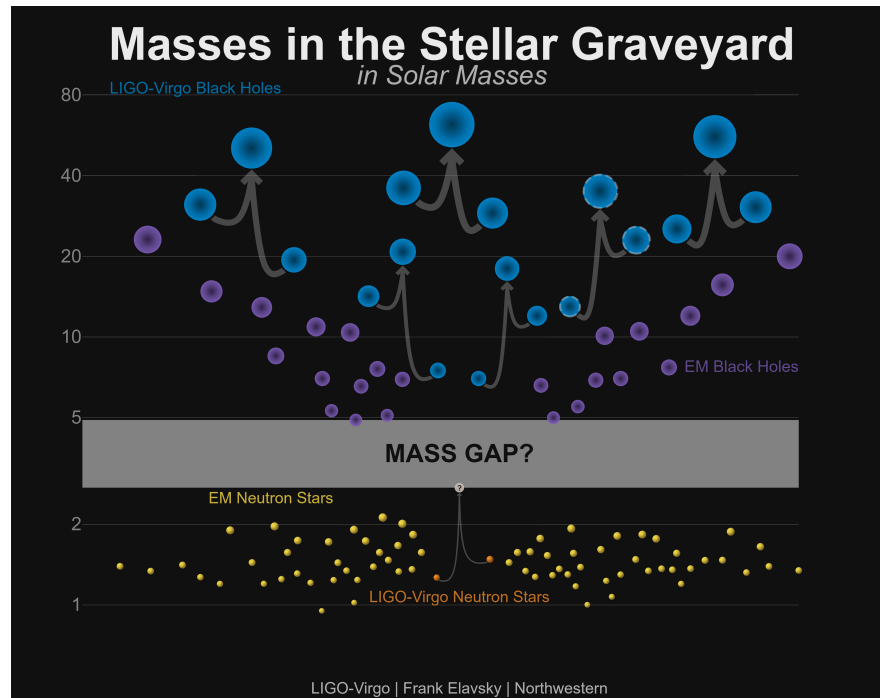


Figure 4.2: Masses in the stellar graveyard. [119] This is a representation of the range of masses of neutron stars and stellar mass black holes, measured in the EM spectrum or by LIGO-Virgo.

4.1.2 Previous Work

Since Schutz proposed the use of standard sirens in 1986, different prospects for constraining the value of the Hubble parameter using compact binary coalescences have been investigated.

As mentioned in the previous section, there are two main approaches to measuring the Hubble constant using standard sirens:

- A multi-messenger astronomy (MMA) approach, relying on the observation of an electromagnetic counterpart to the gravitational wave signal to get a host galaxy and associated redshift.
- A statistical approach, in which there is no electromagnetic counterpart, and the most probable host galaxy, and associated redshift, must be identified from the gravitational wave data only, based on its localisation and distance measurement.

Del Pozzo presented work on the statistical method in 2012. In this work, a network of second generation gravitational wave detectors is considered, and GW sources are only considered up to $z = 0.1$, or $D_L = 460\text{Mpc}$ in a ΛCDM model. [120] Using this method, a measurement for the Hubble constant is obtained at 4 – 5% accuracy at 95% confidence, with a few tens of observations. The work presented in this project differs in that it considers all GW sources and an incomplete EM catalogue.

Taylor and Gair investigated prospects for cosmology using binary neutron stars in the Einstein Telescope era. With estimated detection rates of up to thousands a year, ET is ideal for cosmology using standard sirens. [121]

Taylor, Gair and Mandel also released work on the prospects for constraining the Hubble constant with advanced gravitational wave detectors, using only GW observations. [117] This work relied on the narrowness of the mass distribution of neutron stars to get around the mass-redshift degeneracy. However, BBH have a much wider mass distribution.

Some extensive work has been done on the multi-messenger method of measuring the Hubble constant with standard sirens, along with other aspects of cosmology such as probing dark energy. [116, 122, 123] Previous work by Holz and Hughes in 2005 has investigated supermassive BBH coalescences as standard sirens, but relying on an independent localisation of the binary in the electromagnetic spectrum, making such standard sirens rare. [116]

We now know that short gamma ray bursts are associated with BNS. [39] From previous work by Nissanke et al., an estimated 30 GW-GRB events are needed to reach a 1% precision in a standard siren measurement of the Hubble constant. [115]

Work on MMA standard siren measurements of the Hubble constant was also applied to the first standard siren measurement of the Hubble constant. [124]

4.2 Electromagnetic Galaxy Catalogues

We want to constrain the Hubble constant using the statistical method described previously. To this end, we use gravitational wave signals from compact binary coalescences and an EM catalogue of galaxies that provides us with values for the redshift and apparent magnitude of each galaxy in the catalogue. The measured apparent magnitude, m , and redshift, z , are taken to be delta functions, and the measured SNR $\hat{\rho}$ is drawn from a non-central chi-squared distribution with two degrees of freedom, centred around the true value of the SNR.

4.2.1 Current Galaxy Catalogues for the EM follow-up of Gravitational Waves

Since we are measuring the Hubble constant with a statistical approach, and do not rely on coincident electromagnetic observations, it is necessary to have access to a galaxy catalogue in

order to identify a redshift for the source.

The most promising galaxy catalogue for the electromagnetic follow-up for gravitational wave events is the GLADE catalogue, a galaxy catalogue constructed from several surveys specifically for this purpose. The catalogue used prior to GLADE was GWGC (Gravitational Wave Galaxy Catalogue), a catalogue which is complete to 40Mpc. With advanced detector sensitivities, a catalogue that is more complete at larger distances is needed.

The GLADE (Galaxy List for the Advanced Detector Era) catalogue is constructed from four different galaxy catalogues, and contains close to 2 million galaxies, each of which have a B -band magnitude and a distance estimated from the redshift and an assumed H_0 . The catalogue is complete to 73Mpc and reaches half completeness around 300Mpc, with slowly decreasing completeness. [125]

4.2.2 Comparison of Simulated Galaxy Catalogue to Real Galaxy Catalogues

We use a simulated galaxy catalogue for the electromagnetic counterparts to the gravitational wave signals. The catalogue is assumed to be a full-sky catalogue, which is similar to the type of catalogue that would currently be used for the electromagnetic follow-up of gravitational wave signals, such as the GLADE catalogue. [125]

Each gravitational wave event is assumed to be coming from a different area of the sky; as such, a new list of galaxies is generated for each event.

The catalogue contains two parameters: the apparent magnitude and the redshift of each galaxy. This somewhat replicates the parameters measured by GLADE, where the most important parameters are the B -band magnitude and the redshift. Since the catalogue is a compilation of several galaxy catalogues, not all galaxies have the same measured parameters. However, we assume access to a catalogue where an apparent magnitude and a redshift would be available for each galaxy in the field. In the simulated catalogue, the redshift z is assumed to be the cosmological redshift (we therefore assume negligible peculiar velocities), and no particular band is assumed for the apparent magnitude m .

The apparent magnitude and redshift are taken to be delta functions, with no measurement error. This is again an approximation; however, in a real galaxy catalogue, these errors would be small. [126] This is especially true of spectroscopic redshift measurements, which would have negligible errors. Conversely, for photometric redshifts, which are measured using multi-band photometry and are more common in galaxy catalogues, errors on z would be larger. [127]

The galaxy number density is taken as simply a constant number of galaxies per unit Mpc^{-3} . The distribution is taken to be uniform in volume, which is an approximation. This is an approximation, as the distribution should be uniform in co-moving volume. At high redshifts, the number density of galaxies would also drop. [128] However, at redshift $z < 1$, this is a reasonable

approximation. At these redshifts, the number density is close to 0.01Mpc^{-3} . [128, 129]

The uniformity of the distribution itself is also an approximation, as in a real galaxy survey, features like clustering would appear. This can for example be seen in figure 3.1, where filaments, clusters and voids are visible features of the galaxy redshift distribution.

The catalogue is set up to be magnitude-limited, with a limiting magnitude of $m_{th} = 20$. GLADE is characterised by completeness: the completeness of a galaxy catalogue is defined by how many of the existing galaxies in the field are included within the catalogue at a certain distance. Half-completeness is the distance at which 50% of the galaxies are in the catalogue. The completeness is estimated in comparison to other galaxy catalogues, meaning it can be greater than 100%. [130] In the case of real catalogues like GLADE, half-completeness is reached at 300Mpc. [125] While the simulated catalogue is defined in terms of limiting magnitude, from figure 5.7 it can be seen that half-completeness is reached at the same order of magnitude for distances in Mpc.

Localisation information is not modelled in the catalogue. Instead, what is simulated is the same localisation area for every gravitational wave event, as the focus is more on the impact of the apparent magnitude selection effects than on the localisation of the host galaxy itself. In real standard siren measurements of the Hubble constant, localisation is a very important parameter, as it defines how many potential host galaxies would be in the field. [39, 122]

4.3 Identifying the Host Galaxy

The most straightforward way to obtain a redshift for a GW event is if there is an electromagnetic counterpart to the signal. In the case of two neutron stars coalescing, we expect to get an optical and radio electromagnetic counterpart with a characteristic light curve. This counterpart is called a kilonova, an afterglow with a characteristic timescale of one week. [131] Their emission is believed to be fairly isotropic. [132]

The coalescence of two neutron stars is also associated with the emission of short gamma ray bursts, with short GRBs also associated with kilonovae. [63, 133, 134] However, these are beamed and short-lived, making kilonovae a potentially better prospect for identifying an EM counterpart. The gravitational wave observation of GW170817 was associated with a short GRB, GRB 170817 A, but future BNS events might not have a GRB counterpart. [63] In the case of binary black holes, we do not expect an EM counterpart, so the redshift needs to be determined through statistical methods. There is therefore a lot of interest to finding the host galaxy of a GW event using statistical methods

We want to match the gravitational wave signal to its potential host galaxy; this means testing out a calculated distance measurement (using the Hubble law and galaxy's redshift) for each galaxy in the field for each gravitational wave event and for a wide range of values of the Hubble constants.

4.4 Events Outside the Galaxy Catalogue

Standard siren measurements of the Hubble constant rely on finding a way to obtain an associated redshift. In this project, this is done through using statistical methods to identify the host galaxy from a catalogue. Theoretically, one could choose to only consider events that are within the reach of the electromagnetic galaxy catalogue. However, galaxy catalogues measure the redshift and the apparent magnitude of galaxies; associated distance measurements are usually made through the use of the Hubble law. In the absence of constraints on the Hubble constant, it is therefore impossible to know the reach of the galaxy catalogue in terms of luminosity distance, as the catalogue is limited by the apparent magnitude m , which is a function of luminosity distance D_L and absolute magnitude M .

$$M - m = 5 \log_{10} D_L - 5 \quad (4.3)$$

Since we're assuming a broad, uniform prior on the Hubble constant, we do not know a priori if the host galaxy from which the gravitational wave signal originates is within the galaxy catalogue; all we can do is assign a probability of the host galaxy being within the galaxy catalogue given a Hubble constant.

4.5 Bayesian Inference

Measuring the Hubble constant is a parameter estimation problem: we are trying to determine the value of a variable given a certain model. In this case, the model we are assuming that the universe is expanding, and that the luminosity distance and redshift of objects are related through the Hubble law.

$$D_L = \frac{cz}{H_0} \quad (4.4)$$

This is a local approximation. At higher redshifts, more complex cosmography equations would be required. [88] These are outlined in section 3.4.3. However, the above equation is used for simplicity, as the main aim of the experiment is to characterise selection effects; the focus here is not to measure the geometry of the universe, but to demonstrate the impact of selection effects due to an incomplete galaxy catalogue on a standard siren measurement of the Hubble constant.

In measuring the Hubble constant, we are trying to find, based on an accepted model, the most plausible value, or range of values, that would match observational evidence.

We consider the case where we have two sets of data: one is a set of luminosity distances obtained from gravitational wave signals. The other set is an electromagnetic catalogue of galaxies, containing the apparent magnitude and redshift of each galaxy.

The focus of this method is on correcting the biases introduced by the inferior reach of electromagnetic catalogues compared to the reach of aLIGO, especially in the case of BBH standard sirens. There are therefore four main components that we require to evaluate for the Bayesian formalism we apply to this problem:

- The probability that the data given the host galaxy is within the galaxy catalogue
- The probability that the data given the host galaxy is outwith the galaxy catalogue
- The probability of the host galaxy being in the catalogue given a Hubble constant
- The probability of the host galaxy being outside the catalogue given a Hubble constant

All of the Bayesian formalism for this problem is derived from these four elements and equation 4.5. This equation is a direct application of Bayes's theorem, and represents the probability of a certain value of the Hubble constant given our data $\hat{\rho}$.

$$p(H_0|\hat{\rho}, I) = \frac{p(\hat{\rho}|H_0, I)p(H_0|I)}{p(\hat{\rho}|I)} \quad (4.5)$$

4.6 Choice of Priors

There are two parts to the problem: one is the derivation of the Bayesian formalism, which is expressing the presented problem in a mathematical form by applying Bayes' theorem to it. The other part is choosing priors on the variables we are considering in the equations.

There are several variables used in this problem, each of which is attributed a prior.

- The Hubble constant H_0 . A prior is applied to characterise our prior knowledge of the value of the parameter.
- The measured signal-to-noise ratios from the gravitational wave signals, $\hat{\rho}$
- The measured apparent magnitude of each galaxy in the electromagnetic catalogue, m .
- The measured redshift of each galaxy in the electromagnetic catalogue, z .
- The distribution of absolute magnitudes M .
- The distribution of redshifts z .

4.6.1 Prior on H_0

In order to avoid biases and make a truly independent measurement of the Hubble constant, a broad, uniform prior (a "top hat") is used for $p(H_0)$.

While past measurements of the Hubble constant have reached values of up to $500 \text{ kms}^{-1}\text{Mpc}^{-1}$, in recent years, measurements have broadly been between values of $60 \text{ kms}^{-1}\text{Mpc}^{-1}$ and $80 \text{ kms}^{-1}\text{Mpc}^{-1}$. [79, 108] Therefore, a flat prior from $40 \text{ kms}^{-1}\text{Mpc}^{-1}$ to $120 \text{ kms}^{-1}\text{Mpc}^{-1}$ is very conservative.

Since the Hubble constant is a scale factor, a Jeffreys prior might be preferred. However, a uniform prior is used for simplicity, and to match the choice of prior in the 2017 standard siren measurement of the Hubble constant. [124]

The prior that we adopt on the Hubble constant is a top hat function in the range $40 \text{ kms}^{-1}\text{Mpc}^{-1}$ to $120 \text{ kms}^{-1}\text{Mpc}^{-1}$. Instead of testing a continuous variable space, we test a discrete values of H_0 , with a bin width of $0.1 \text{ kms}^{-1}\text{Mpc}^{-1}$. This is to maximise the efficiency of the code.

4.6.2 Priors for the Electromagnetic Data

Prior on the Measured Redshift and Apparent Magnitude

The measured redshift and apparent magnitude are assumed to have no errors, therefore are being treated as delta functions.

Prior on the Redshift Distribution of Galaxies

The distribution of galaxies is assumed to be uniform in volume. All galaxies are assumed to be the same, and the number density, in counts per Mpc^3 , is fixed at 0.006Mpc^{-3} .

More details on the generation of galaxies for the electromagnetic catalogue are presented in section 4.2.2.

Prior on the Absolute Magnitude Distribution of Galaxies

The luminosity distribution of galaxies is normally described by the Schechter luminosity function. [126] However, the Schechter function is poorly constrained for very faint galaxies, and the luminosity distribution can be approximated to a Gaussian. The absolute magnitude is a function of the luminosity.

$$M = -2.5 \log_{10} \frac{L}{L_{\odot}} + 4.72 \quad (4.6)$$

For simplicity, the distribution of absolute magnitudes of the galaxies is therefore approximated to a Gaussian distribution centred around a value $M^*(H_0)$, as defined in equation 4.7 and with $\sigma = 1.4$. [135] Assuming that all galaxies are the same, this is a reasonable approximation;

for example, it was observed in 1997 that bright galaxies, such as type E, type S0, and spiral galaxies, have Gaussian-like luminosity functions. [136]

The value of M^* is defined in equation 4.7, using typical values for spiral galaxies. [135] It is important to note that this value, and therefore the distribution of galactic absolute magnitudes, depends on H_0 .

$$M^* = -16.8 + 5 \log_{10}(h), \quad (4.7)$$

where h is defined in the following way

$$H_0 = 100h \text{ kms}^{-1} \text{Mpc}^{-1}, \quad (4.8)$$

and the absolute magnitude distribution function $\Phi(M)$ is defined by:

$$\Phi(M) = \frac{1}{\sqrt{2\pi\sigma^2}} e^{-\frac{M-M^*}{2\sigma^2}}. \quad (4.9)$$

To obtain an apparent magnitude, one of the two parameters present in the galaxy catalogue (along with redshift), we use the luminosity distance relationship (see equation 3.20) and the distance modulus, in equation 4.10.

$$M - m = 5 \log_{10} D_L - 5, \quad (4.10)$$

where M is the absolute magnitude, m the apparent magnitude and D_L the luminosity distance. These two equations give the absolute magnitude of the galaxy M as a function of the Hubble constant H_0 , the redshift z and the apparent magnitude m :

$$M(m, z, H_0) = m + 5 - 5 \log_{10} \left(\frac{cz}{H_0} \right). \quad (4.11)$$

4.6.3 Priors for the Gravitational Wave Data

The SNR distribution is simplified as all systems are assumed to have the same parameters (and therefore the same emission strength) and the distribution of galaxies is uniform in volume.

Since gravitational waves are not subject to astrophysical processes such as absorption by the interstellar medium (ISM), we consider the distribution of SNRs for gravitational wave signals to depend solely on the emission strength and distance to the source. [33] In the case we are considering, all emission strengths are equal, making the distribution of SNRs depend only on the distribution of luminosity distances, which is uniform in volume. This simplified model ignores parameters such as the inclination angle of the binaries and the choice of network of gravitational wave detectors. In a real standard siren measurement of the Hubble constant, the degeneracy between the luminosity distance and the inclination of the binary is a major source

of uncertainty. [124]

The mass distribution of the binaries is also ignored. There are therefore two emission strengths we are considering in this model: one for binary neutron star mergers, and one for binary black hole mergers, assuming each black hole to have a mass of $30M_{\odot}$.

For each event, the measured SNR is drawn from a non-central chi-squared distribution where the non-centrality parameter is the real SNR.

$$\rho(D_L) = \frac{\rho_{th} D_L}{D_{L_{th}}} \quad (4.12)$$

Here $\rho(D_L)$ is the true SNR of a source at luminosity distance D_L , ρ_{th} is the threshold SNR for detection of GW, and $D_{L_{th}}$ is the luminosity distance at which $\rho(D_{L_{th}}) = \rho_{th}$. This is defined by the range of the detectors. The threshold SNR for detection of gravitational waves is always taken to be $\rho_{th} = 8$.

Several scenarios are considered for a network of second generation gravitational wave detectors, ranging from mid-aLIGO sensitivities (O2) to design sensitivity.

Period	BBH range (Mpc)	BNS range (Mpc)
Early	415 - 775	40 - 80
Mid	775 - 1110	80 - 120
Late	1110 - 1490	120 - 170
Design	1640	190

Table 4.2: Sensitivity range for aLIGO. [64] These are given for different detector phases, for binary neutron star coalescences and $30M_{\odot}$ binary black hole coalescences.

Every event is assumed to have the same localisation area, which is again a simplification, as we do not consider any angular co-ordinate information in this project. Normally, the localisation would be better for closer events.

4.7 Derivation of Bayesian formalism

Having now assigned a prior to each variable, some Bayesian formalism can now be derived to address the problem.

The problem of measuring the Hubble constant using standard sirens and a limited, incomplete electromagnetic galaxy catalogue is, as are most problems involving incomplete data, best handled with a Bayesian approach. We want to derive some Bayesian formalism for this problem. As a parameter estimation problem, what we want to obtain is the posterior distribution on values of H_0 given some data \hat{p} .

The main equation is the following:

$$p(H_0|\hat{\rho}, I) = \frac{p(\hat{\rho}|H_0, I)p(H_0|I)}{p(\hat{\rho}|I)}, \quad (4.13)$$

with H_0 the Hubble constant, $\hat{\rho}$ the data (measured SNR of each event) and I the background information.

The prior on the Hubble constant, $p(H_0|I)$, is taken to be broad and uniform.

The EM catalogue available would be smaller than the span of potential GW detections. To account for this, the first equation is broken down into four terms which will be calculated independently.

G and \bar{G} represent the following propositions:

- G = the host galaxy is within the galaxy catalogue.
- \bar{G} = the host galaxy is outside the galaxy catalogue.

Note that $G + \bar{G} = 1$. Marginalising over G and \bar{G}

$$p(\hat{\rho}|H_0, I) = \sum_{X=G, \bar{G}} p(\hat{\rho}, X|H_0, I), \quad (4.14)$$

where $X = G$ or \bar{G} .

$$p(\hat{\rho}|H_0, I) = p(\hat{\rho}|G, H_0, I)p(G|H_0, I) + p(\hat{\rho}|\bar{G}, H_0, I)p(\bar{G}|H_0, I) \quad (4.15)$$

Finally, the probability of the data given detection and a Hubble constant:

$$p(\hat{\rho}|H_0, D, I) = p(\hat{\rho}|G, H_0, D, I)p(G|H_0, D, I) + p(\hat{\rho}|\bar{G}, H_0, D, I)p(\bar{G}|H_0, D, I), \quad (4.16)$$

where D is the detection of GW (in this case we always assume there is a detection).

4.7.1 Probability of the Data Given the Host Galaxy is Within the Galaxy Catalogue: $p(\hat{\rho}|G, H_0, D, I)$

This is the probability of the data given that the GW signal came from a galaxy within the EM catalogue, H_0 and the background information. This is marginalised over all z , m and M .

$$p(\hat{\rho}|G, H_0, D, I) = \int_{-\infty}^{\infty} \int_{-\infty}^{\infty} \int_0^{\infty} p(\hat{\rho}, z, m, M|G, H_0, D, I) dz dM dm \quad (4.17)$$

$$p(\hat{\rho}|G, H_0, D, I) = \int_{-\infty}^{\infty} \int_{-\infty}^{\infty} \int_0^{\infty} p(\hat{\rho}|z, m, M, G, H_0, D, I) p(z, m, M|G, H_0, D, I) dz dM dm \quad (4.18)$$

Now ρ depends on D_L , and therefore only on H_0 and z , according to equation 3.20.

$$p(\hat{\rho}|z, m, M, G, H_0, D, I) = p(\hat{\rho}|z, G, H_0, D, I) = p(\hat{\rho}|\rho(z, H_0), D, I) \quad (4.19)$$

This is the probability of the observed SNR, $\hat{\rho}$ given a "true" SNR for a luminosity distance, $\rho(D_L) = \rho(z, H_0)$, as defined in equation 4.12. The probability of $\hat{\rho}^2$ is a non-central chi-squared distribution with non-centrality parameter $\rho^2(z, H_0)$.

$$p(\hat{\rho}|\rho(z, H_0), D, I) = p_{\chi^2}[\hat{\rho}^2, \rho^2(z, H_0)] \quad (4.20)$$

Using Bayes's theorem for the second part of the equation:

$$p(z, m, M|G, H_0, D, I) = \frac{p(D|z, m, M, G, H_0, I)p(z, m, M|G, H_0, I)}{p(D|G, H_0, I)}. \quad (4.21)$$

The probability of a signal being detected depends only on the SNR. The SNR is a function of the luminosity distance, which itself is a function of the redshift and Hubble constant. We can therefore rewrite:

$$p(D|z, m, M, G, H_0, I) = p(D|z, H_0, G, I). \quad (4.22)$$

Now marginalising $p(D|G, H_0, I)$ over all z , M and m :

$$p(D|G, H_0, I) = \int_{-\infty}^{\infty} \int_{-\infty}^{\infty} \int_0^{\infty} p(D, z, m, M|H_0, G, I) dz dM dm, \quad (4.23)$$

$$p(D|G, H_0, I) = \int_{-\infty}^{\infty} \int_{-\infty}^{\infty} \int_0^{\infty} p(D|z, H_0, G, I) p(z, m, M|G, H_0, I) dz dM dm. \quad (4.24)$$

Rewriting equation 4.21:

$$p(z, m, M|G, H_0, D, I) = \frac{p(D|z, H_0, G, I) p(z, m, M|G, H_0)}{\int_{-\infty}^{\infty} \int_{-\infty}^{\infty} \int_0^{\infty} p(D|z, H_0, G, I) p(z, m, M|G, H_0, I) dz dM dm}. \quad (4.25)$$

Since the host galaxy is in the catalogue in this case, z and m are defined as delta functions, as they are measurements with no error on them. The probability of z is therefore a delta function at each z_j corresponding to galaxy j . The same is the case for apparent magnitude m_j . There is a unique value of M for given m , z , and H_0 , so $p(M|G, H_0, I)$ also becomes a delta function, and we define $M_j = M(z_j, m_j, H_0)$.

$$p(z, m, M|G, H_0, I) = p(z, m|G, H_0, M, I) p(M|G, H_0, I) = \delta(z - z_j; m - m_j; M - M_j) \quad (4.26)$$

$p(D|z, m, M, G, H_0, I)$ is only a function of D_L , and therefore $\rho(z, H_0)$. Given that we have G , it is only evaluated at discrete values z_j , so:

$$p(D|z, m, M, G, H_0, I) = p(D|z, H_0, G, I) = p(D|z_j, H_0, I) = \mathcal{S}_{\chi^2} \left[\rho_{th}^2, \rho^2(z_j, H_0) \right]. \quad (4.27)$$

The probability of each galaxy j producing a detectable signal is the survival function of the chi-squared distribution with non-centrality parameter $\rho^2(z_j, H_0)$ evaluated at ρ_{th} . Here \mathcal{S} is the survival function, defined as the probability of a continuous random variable X with cumulative distribution function (CDF) $F(t)$.

$$\mathcal{S}(x) = P(X > x) = \int_x^\infty f(u) du = 1 - F(x) \quad (4.28)$$

In this case the survival function $\mathcal{S}_{\chi^2}(\rho_{th}^2 | \rho^2(z_j, H_0))$ represents the probability of $\hat{\rho}$ given a non-central chi-squared distribution with non-centrality parameter $\rho(z_j, H_0)$.

Given discrete values of z_j , we can also rewrite equation 4.20.

$$p(\hat{\rho}|z, H_0, G, D, I) = p(\hat{\rho}|z_j, H_0, D, I) = p_{\chi^2} \left[\hat{\rho}^2, \rho^2(z_j, H_0) \right] \quad (4.29)$$

Finally, this gives us the final expression for $p(\hat{\rho}|G, H_0, I)$.

$$p(\hat{\rho}|G, H_0, D, I) = \sum_{j=1}^N p_{\chi^2} \left[\hat{\rho}^2, \rho^2(z_j, H_0) \right] \frac{\mathcal{S}_{\chi^2}[\rho_{th}^2, \rho^2(z_j, H_0)]}{\sum_{j=1}^N \mathcal{S}_{\chi^2}[\rho_{th}^2, \rho^2(z_j, H_0)]} \quad (4.30)$$

4.7.2 Probability of the Host Galaxy Being in the EM Catalogue Given a Hubble Constant : $p(G|H_0, D, I)$

The next term in the equation is the probability of the host galaxy being in the catalogue, given detection of gravitational waves and a Hubble constant.

First, we marginalise over m, M and z .

$$\begin{aligned} p(G|H_0, D, I) &= \int_{-\infty}^{\infty} \int_{-\infty}^{\infty} \int_0^{\infty} p(G, z, m, M|H_0, D, I) dz dM dm \\ &= \int_{-\infty}^{\infty} \int_{-\infty}^{\infty} \int_0^{\infty} p(G|H_0, z, m, M, D, I) p(z, m, M|H_0, D, I) dz dM dm \end{aligned} \quad (4.31)$$

Since the galaxy catalogue is magnitude-limited, the probability of the host galaxy being in the catalogue depends only on the galaxy's measured apparent magnitude. We can therefore rewrite $p(G|H_0, z, m, M, D, I)$:

$$p(G|H_0, z, m, M, D, I) = p(G|m, I). \quad (4.32)$$

The catalogue is magnitude-limited with a hard cut on the threshold magnitude m_{th} , so this is a Heaviside step function $\mathcal{H}(x)$. The term becomes:

$$\begin{aligned} p(G|H_0, D, I) &= \int_{-\infty}^{\infty} \int_{-\infty}^{\infty} \int_0^{\infty} \mathcal{H}(m_{th} - m) p(z, m, M|H_0, D, I) dz dM dm \\ &= \int_{-\infty}^{m_{th}} \int_{-\infty}^{\infty} \int_0^{\infty} p(z, m, M|H_0, D, I) dz dM dm. \end{aligned} \quad (4.33)$$

Now the probability of z , m and M given a Hubble constant and GW detection must equal 1 when marginalised over all possible values, since the host galaxy must have some m , M and z for a given H_0 . We therefore have:

$$\int_{-\infty}^{\infty} \int_{-\infty}^{\infty} \int_0^{\infty} p(z, m, M|H_0, D, I) dz dM dm = 1. \quad (4.34)$$

Therefore, a normalisation constant, $C(H_0)$, is needed to get $p(z, m, M|H_0, D, I)$. This normalisation constant only depends on H_0 . The term becomes:

$$p(z, m, M|H_0, D, I) = C(H_0) p(D|H_0, z, m, M, I) p(z, m, M|H_0, I), \quad (4.35)$$

$$p(z, m, M|H_0, I) = p(z, M|H_0, I) p(m|z, M, H_0, I). \quad (4.36)$$

$p(m|H_0, I)$ is not known, but both $p(z|H_0)$ and $p(M|H_0, I)$ are known and independent of each other. Given a value for redshift, absolute magnitude, and the Hubble constant, there is only one value for the apparent magnitude, so $p(m|z, M, H_0, I)$ becomes a delta function.

Since the distribution of redshifts is uniform in volume, the probability of a redshift z is simply proportional to its squared value.

$$p(z|H_0, I) \propto z^2 \quad (4.37)$$

The probability of an absolute magnitude $p(M|H_0, I)$ is proportional to the distribution of absolute magnitudes.

$$p(M|H_0, I) \propto \Phi(M), \quad (4.38)$$

where $\Phi(M)$ is the Gaussian distribution on galaxy absolute magnitudes, as defined previously in equations 4.9 and 4.7. Unlike with the redshift, this is dependent on the Hubble constant H_0 .

Now the probability of detection depends only on the measured SNR, which depends on D_L . $p(D|H_0, z, m, M, I)$ is therefore only dependent on z and H_0 , and is defined by the non-central chi-square distribution with non-centrality parameter $\rho(z, H_0)$.

$$p(D|H_0, z, m, M, I) = p(D|H_0, z, I) = \int_{\rho_{th}}^{\infty} p(\hat{\rho}|\rho(z, H_0), I) d\hat{\rho} = \mathcal{S}_{\chi^2}(\rho_{th}^2, \rho^2(H_0, z)), \quad (4.39)$$

where $\hat{\rho}$ is the x-coordinate of χ^2_2 with non-centrality parameter $\rho(z, H_0)$. With each term defined, we have an expression for the normalisation constant $C(H_0)$.

$$\frac{1}{C(H_0)} = \int_{-\infty}^{\infty} \int_{-\infty}^{\infty} \int_0^{\infty} \int_{\rho_{th}}^{\infty} p(\hat{\rho}|\rho(z, H_0), I) p(M|H_0, m, z, I) p(z, m|H_0, I) d\hat{\rho} dz dM dm \quad (4.40)$$

And finally, the term for the probability of the host galaxy being within the galaxy catalogue for a given value of the Hubble constant becomes:

$$p(G|H_0, D, I) = \int_{-\infty}^{m_{th}} \int_{-\infty}^{\infty} \int_0^{\infty} \int_{\rho_{th}}^{\infty} \frac{p(\hat{\rho}|\rho(z, H_0), I) p(M|H_0, m, z, I) p(z, m|H_0, I)}{\int_{-\infty}^{\infty} \int_{-\infty}^{\infty} \int_0^{\infty} \int_{\rho_{th}}^{\infty} p(\hat{\rho}|\rho(z, H_0), I) p(M|H_0, m, z, I) p(z, m|H_0, I) d\hat{\rho} dz dM dm} d\hat{\rho} dz dM dm. \quad (4.41)$$

The final expression for $p(G|H_0, D, I)$ is:

$$p(G|H_0, D, I) = \int_{-\infty}^{m_{th}} \int_0^{\infty} \frac{\mathcal{S}_{\chi^2_2}[\rho_{th}^2, \rho^2(z, H_0)] z^2 \Phi[M(H_0, m, z)]}{\int_{-\infty}^{\infty} \int_0^{\infty} \mathcal{S}_{\chi^2_2}[\rho_{th}^2, \rho^2(z, H_0)] z^2 \Phi[M(H_0, m, z)] dz dm} dz dm. \quad (4.42)$$

4.7.3 Probability of the Data Given the Host galaxy is Outwith the Galaxy Catalogue : $p(\hat{\rho}|\bar{G}, H_0, D, I)$

This is the probability of the data given that the gravitational wave signal came from a galaxy outwith the electromagnetic galaxy catalogue. First, this probability is marginalised over all m , z and M .

$$p(\hat{\rho}|\bar{G}, H_0, D, I) = \int_{-\infty}^{\infty} \int_{-\infty}^{\infty} \int_0^{\infty} p(\hat{\rho}|\bar{G}, z, m, M, H_0, D, I) p(z, m, M|\bar{G}, H_0, D, I) dz dM dm \quad (4.43)$$

Now, the joint probability of z , m and M given a Hubble constant, detection and the host galaxy not being in the galaxy catalogue has to be 1 when marginalised over all values of z , m and M .

$$\int_{-\infty}^{\infty} \int_{-\infty}^{\infty} \int_0^{\infty} p(z, m, M|\bar{G}, H_0, D, I) dz dM dm = 1 \quad (4.44)$$

We therefore need a normalisation constant, $K(H_0)$. This term therefore becomes

$$p(z, m, M|\bar{G}, H_0, D, I) = K(H_0) p(\bar{G}|z, m, M, H_0, D, I) p(z, m, M|H_0, D, I). \quad (4.45)$$

Whether the host galaxy is within the galaxy catalogue or not depends only on the galaxy's apparent magnitude. Therefore

$$p(\bar{G}|z, m, M, H_0, D, I) = p(\bar{G}|m, I), \quad (4.46)$$

which is a Heaviside step function. We now have:

$$p(z, m, M | \bar{G}, H_0, D, I) = K(H_0) \mathcal{H}(m - m_{th}) p(z, m, M | H_0, D, I), \quad (4.47)$$

$$\begin{aligned} \frac{1}{K(H_0)} &= \int_{-\infty}^{\infty} \int_{-\infty}^{\infty} \int_0^{\infty} \mathcal{H}(m - m_{th}) p(z, m, M | H_0, D, I) dm dM dz \\ &= \int_{m_{th}}^{\infty} \int_{-\infty}^{\infty} \int_0^{\infty} p(z, m, M | H_0, D, I) dz dM dm. \end{aligned} \quad (4.48)$$

Now $p(z, m, M | H_0, D, I)$ is already known.

$$\frac{1}{K(H_0)} = \int_{m_{th}}^{\infty} \int_0^{\infty} \mathcal{S}_{\chi^2}[\rho_{th}^2, \rho^2(z, H_0)] z^2 \Phi[M(H_0, m, z)] dz dm \quad (4.49)$$

Now deriving an expression for the second half of the equation, $p(\hat{\rho} | \bar{G}, z, m, M, H_0, D, I)$:

$$p(\hat{\rho} | \bar{G}, z, m, M, H_0, D, I) = p_{\chi^2}(\hat{\rho}^2, \rho^2(z, H_0)). \quad (4.50)$$

The final expression for $p(\hat{\rho} | \bar{G}, H_0, D, I)$ is:

$$p(\hat{\rho} | \bar{G}, H_0, D, I) = \int_{m_{th}}^{\infty} \int_0^{\infty} \frac{p_{\chi^2}[\hat{\rho}^2, \rho^2(z, H_0)] \mathcal{S}_{\chi^2}[\rho_{th}^2, \rho^2(z, H_0)] z^2 \Phi[M(H_0, m, z)]}{\int_{m_{th}}^{\infty} \int_0^{\infty} \mathcal{S}_{\chi^2}[\rho_{th}^2, \rho^2(z, H_0)] z^2 \Phi[M(H_0, m, z)] dz dm} dz dm. \quad (4.51)$$

4.7.4 Probability of the Host Galaxy Being Outwith the EM Catalogue Given a Hubble Constant :: $p(\bar{G} | H_0, D, I)$

The final term is the probability of the host galaxy being in the catalogue given detection and a Hubble constant. Since:

$$p(\bar{G} | H_0, D, I) + p(G | H_0, D, I) = 1, \quad (4.52)$$

and we have already determined $p(G | H_0, D, I)$ in section 4.7.2, this term simply becomes:

$$p(\bar{G} | H_0, D, I) = 1 - p(G | H_0, D, I). \quad (4.53)$$

Chapter 5

Results

Using the method described in the previous chapter, results are obtained for several observing scenarios. These scenarios correspond to two types of compact binary coalescences: binary black hole mergers and binary neutron star mergers. Typical aLIGO sensitivities are considered, for different phases of the detector.

5.1 Parameters

The toy model developed for this project depends on several parameters, some of which vary and some of which are fixed. These parameters are the following:

- The galaxy density, in number per Mpc^{-3} . A fixed number was taken for this, assuming all galaxies to be the same (Milky Way type galaxies). It is fixed at 0.006Mpc^{-3} .
- The localisation of the GW event, in square degrees. This affects the number of potential host galaxies in the field for each event. Since the catalogue does not contain any localisation information, effectively, all this does is reduce the number density of galaxies. This was taken to be 10 square degrees for all events.
- The threshold on the apparent magnitude of the galaxy that is detectable by the EM telescope (related to the completeness of the catalogue). This was fixed at $m = 20$. Future telescopes, such as the LSST, could however perform deeper searches, up for an r-magnitude $m_r = 27.5$. [137]
- The reach of the gravitational wave detector. Keeping the threshold SNR for detection at $\rho_{th} = 8$, this depends on the detector sensitivity and the systems considered (BBH or BNS).
- The number of detected gravitational wave events.

Each gravitational wave event is modelled as coming from a different area of the sky; in order to model this, a new "universe" of host galaxies is generated for each new event. The gravitational wave event is generated by selecting a random galaxy, obtaining an SNR from the non-central chi-squared distribution, and accepting the first event with $\rho > \rho_{th}$.

The code was first tested on a coarse array of H_0 values, with a bin width of $1 \text{ kms}^{-1}\text{Mpc}^{-1}$, for testing purposes. It was then run again with finer sampling; each value of H_0 was tested discretely with a bin width of $0.1 \text{ kms}^{-1}\text{Mpc}^{-1}$, rather than as a continuous variable; this makes the problem more straightforward to deal with and the code faster to run. The code was run on the Raven Supercomputing Cluster, which is part of ARCCA (Advanced Research Computing at Cardiff). It is available in Appendix A.

5.2 Binary Black Hole Merger Scenario

We run the code with signal-to-noise ratios and associated luminosity distances typical to binary black hole mergers. This particular scenario would normally require that we use a statistical approach in order to find the host galaxy, as we do not expect an EM counterpart for vacuum binary black holes. [23] In this scenario, it is important to take into account biases due to the incompleteness of galaxy catalogues; as the detectors can probe greater distances for these events, and the galaxy density is taken to be uniform in volume, it is more likely that the host galaxy will not be within the electromagnetic galaxy catalogue.

The binary black hole mergers are assumed to all be identical, varying only in luminosity distance. The typical aLIGO sensitivities are for $30M_{\odot}$ black holes.

We use values that are typical for two coalescing black holes of $30M_{\odot}$ detected by Advanced LIGO for the luminosity distance at the threshold SNR for detection of gravitational waves.

Results are presented for different detector sensitivities and number of events, with the 90% and 68% intervals of confidence for each posterior on H_0 .

Number of events	BBH range (Mpc)	$\hat{\rho} > 150$ removed?	H_0 (90% confidence interval)
500	900	No	$68.9^{+0.4}_{-0.4} \text{ kms}^{-1}\text{Mpc}^{-1}$
1000	900	No	$68.8^{+0.5}_{-0.3} \text{ kms}^{-1}\text{Mpc}^{-1}$
2000	900	No	$70.0^{+0.3}_{-0.4} \text{ kms}^{-1}\text{Mpc}^{-1}$
3000	900	No	$70.0^{+0.3}_{-0.3} \text{ kms}^{-1}\text{Mpc}^{-1}$
2000	900	Yes	$70.8^{+0.8}_{-1.0} \text{ kms}^{-1}\text{Mpc}^{-1}$
3000	900	Yes	$70.6^{+0.8}_{-0.9} \text{ kms}^{-1}\text{Mpc}^{-1}$
3000	1300	No	$69.9^{+0.4}_{-0.4} \text{ kms}^{-1}\text{Mpc}^{-1}$

Table 5.2: Final results for BBH observing scenarios.

At typical sensitivities for binary black hole mergers, final posteriors tend to be dominated by very high SNR events; this demonstrates that at least some events coming from a galaxy within the EM galaxy catalogue are necessary to make a measurement of the Hubble constant.

While lower SNR events do not provide much information on their own, they nonetheless narrow down the final posterior, which would be helpful in making standard siren measurements of the Hubble constant competitive with EM methods.

Even at design sensitivity, with a sufficient number of events, a measurement can be obtained for the Hubble constant. This is demonstrated in results with a coarse sampling of H_0 . In the results with finer sampling, there is only one very high SNR event ($\rho > 300$, all others $\rho < 100$), making it insufficient to make the final combined posterior converge towards the true value of the Hubble constant.

At design sensitivity for aLIGO ($D_L(\rho_{th}) = 1640\text{Mpc}$), the final posterior obtained from 2000 events is dominated by one very high SNR event. However, the result is noticeably improved by the combined posterior.

In the following plots, each colour curve represents a single posterior from one event, while the dashed black curve is the combined posterior from all events. The thin dashed red line is the true value for H_0 .

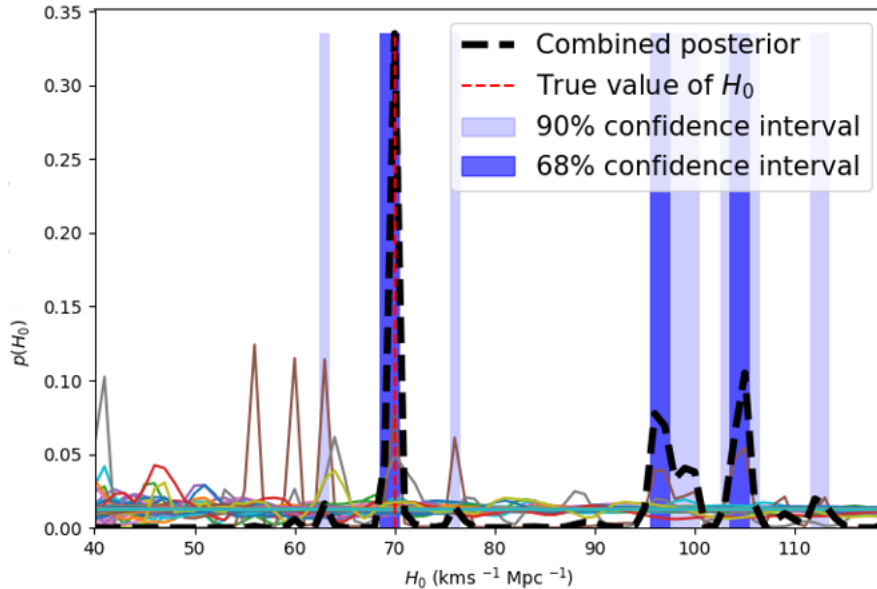


Figure 5.1: Results for 2000 events at $D_L(\rho_{th}) = 1640\text{Mpc}$, with a H_0 bin width of $1 \text{ kms}^{-1}\text{Mpc}^{-1}$. Results show strong support for the true value of the Hubble constant $H_0 = 70.0 \text{ kms}^{-1}\text{Mpc}^{-1}$ but do not fully constrain that results, since the results also support other values of H_0 .

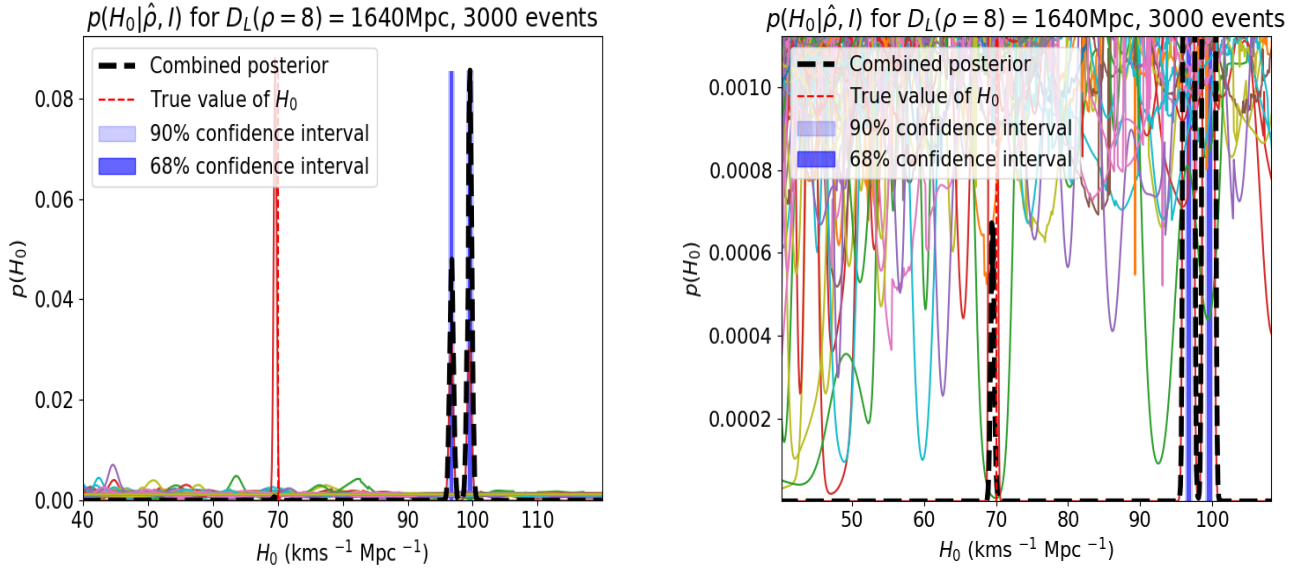


Figure 5.2: Results for 3000 events, $D_L(\rho_{th}) = 1640\text{Mpc}$, with a H_0 bin width of $0.1\text{ kms}^{-1}\text{Mpc}^{-1}$. The second and third plot are the zoomed-in combined posterior. This is dominated by one high SNR event.

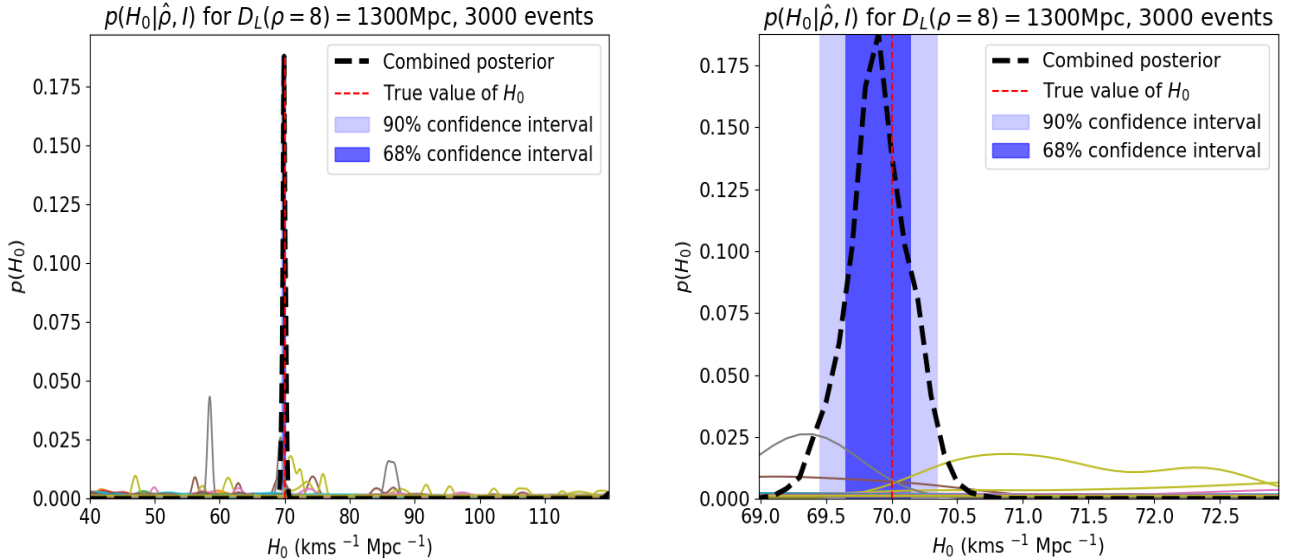


Figure 5.3: Results for 3000 events, $D_L(\rho_{th}) = 1300\text{Mpc}$. The results converge towards the true value of the Hubble constant.

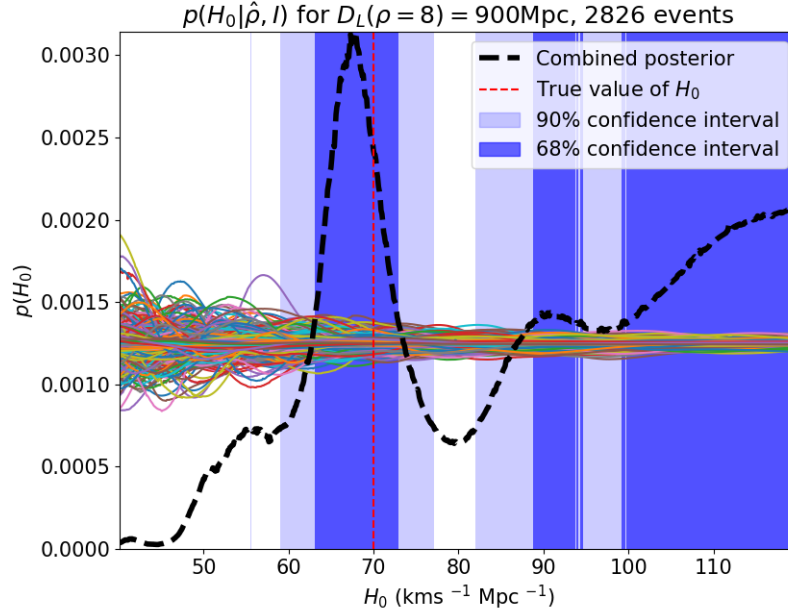


Figure 5.4: Results for events with $\hat{\rho} < 20$ at $D_L(\rho_{th}) = 900\text{Mpc}$. There is strong support for the true value of H_0 , but it is not tightly constrained, especially at high values of H_0 .

Figure 5.2 presents a zoomed-in combined posterior on H_0 . This is dominated by one loud event, and shows that there is some support for three values of the Hubble constant (one of them being the true value $H_0 = 70.0 \text{ kms}^{-1}\text{Mpc}^{-1}$, but the combined posterior does not have enough support for it to be within any of the confidence intervals presented). This means there is a host galaxy that matches this high SNR GW event for three values of the Hubble constant. Figure 5.1 shows results for similar parameters, using a larger bin width for the values of the Hubble constant. The results are similarly dominated by one loud event, with support for several values of the Hubble constant.

Figure 5.3 shows result for O3 sensitivity, with $D_L(\rho_{th}) = 1300\text{Mpc}$. The results clearly converge towards the true value of the Hubble constant.

In figure 5.4, results are presented when combining only events with $\hat{\rho} < 20$. This emphasises the importance of loud events. However, even low SNR events already constrain the Hubble constant for lower values.

5.3 Binary Neutron Star Merger Scenario

We run the code with signal-to-noise ratios and associated luminosity distances that are typical to binary neutron star mergers. Like with the binary black hole models, three different observing scenarios were considered, up to aLIGO design sensitivity at $D_L(\rho_{th}) = 190\text{Mpc}$. While EM counterparts can be expected from the coalescence of two neutron stars, it is still interest-

ing to investigate the prospects for measuring the Hubble constant using statistical methods in those scenarios. While GW170817 benefited from good localisation due to being very nearby, some events might be further and poorly localised, or there could be no detection of an EM counterpart.

The results are presented in a similar fashion to the BBH results, with each thin colour line being the posterior for an individual event and the thick black dashed line being the combined posterior.

Number of events	BNS range (Mpc)	H_0 (90% confidence interval)
50	190	$74.0^{+3.1}_{-3.6} \text{ kms}^{-1} \text{ Mpc}^{-1}$
100	190	$72.2^{+2.1}_{-2.2} \text{ kms}^{-1} \text{ Mpc}^{-1}$
200	190	$72.7^{+1.9}_{-2.1} \text{ kms}^{-1} \text{ Mpc}^{-1}$
500	190	$71.1^{+1.0}_{-0.9} \text{ kms}^{-1} \text{ Mpc}^{-1}$
1000	190	$70.3^{+0.5}_{-0.6} \text{ kms}^{-1} \text{ Mpc}^{-1}$
1500	190	$70.1^{+0.5}_{-0.4} \text{ kms}^{-1} \text{ Mpc}^{-1}$
2000	190	$70.2^{+0.4}_{-0.4} \text{ kms}^{-1} \text{ Mpc}^{-1}$
2000	100	$70.2^{+0.2}_{-0.3} \text{ kms}^{-1} \text{ Mpc}^{-1}$
2000	150	$70.3^{+0.3}_{-0.3} \text{ kms}^{-1} \text{ Mpc}^{-1}$

Table 5.4: Final results for BNS observing scenarios.

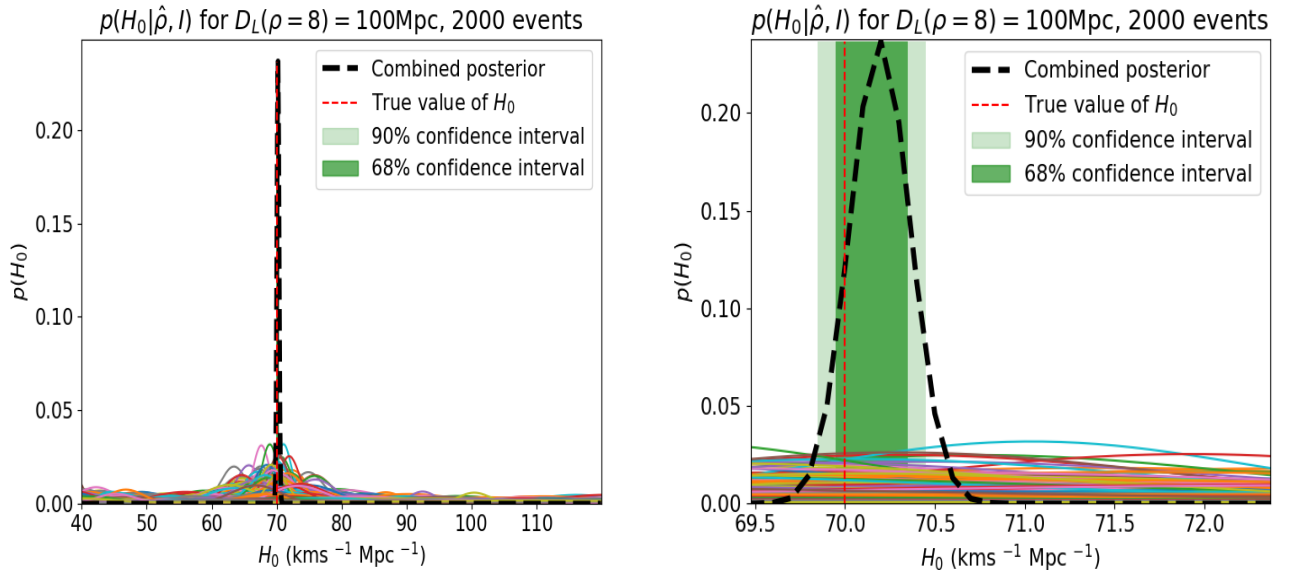


Figure 5.5: Results for 2000 events, $D_L(\rho_{th}) = 100 \text{ Mpc}$. A slight bias towards higher values of H_0 is present in the final result, but there is still strong support for the true value of H_0 , which is within the 90% confidence interval.

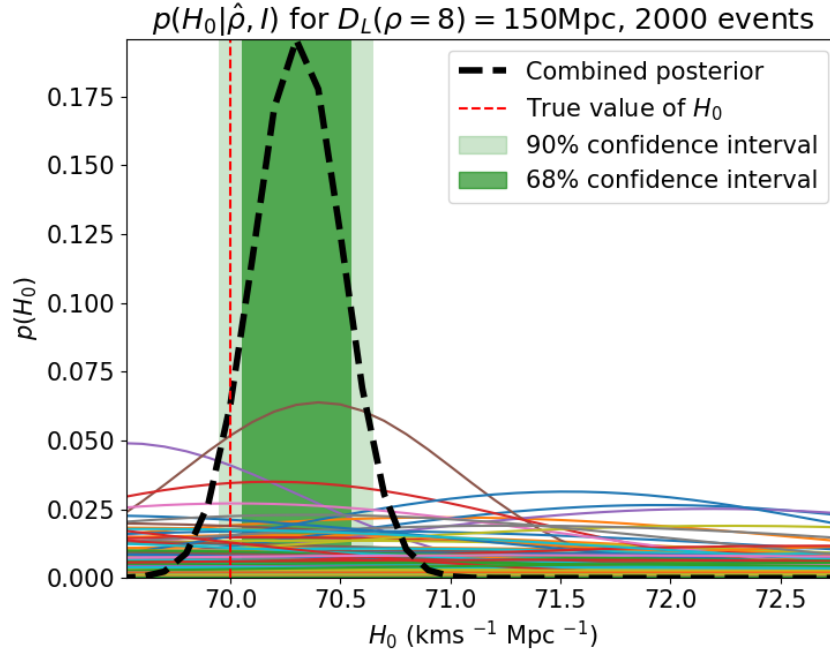


Figure 5.6: Results for 2000 events, $D_L(\rho_{th}) = 150\text{Mpc}$, zoomed-in posterior. A slight bias towards higher values of H_0 is present in the final result.

As seen in figures 5.5 and 5.6, a bias is seen towards higher Hubble constants for lower aLIGO sensitivity (here, BNS sensitivities for O3 and below). This is due to numerical limitations of the code at such low threshold luminosity distances. Those limitations are discussed in more depth at the end of this chapter. However, the focus of this project is on deeper searches (at design sensitivity, $D_{Lth} = 190\text{Mpc}$ for BNS), since O2 did not yield such a large number of events.

5.4 Probability of the Host Being in the Galaxy Catalogue

The probability of the host galaxy being in the galaxy catalogue depends on the threshold distance for detection of gravitational wave signals and on the limiting apparent magnitude of the electromagnetic survey.

Figure 5.7 is one example of the distribution of luminosity distances and apparent magnitude for our simulated universe. This is for a BBH scenario, meaning galaxies are modelled to a further distance. From this figure, it is clear that for any observing scenario for BBH, there are fewer galaxies within the EM galaxy catalogue than outwith.

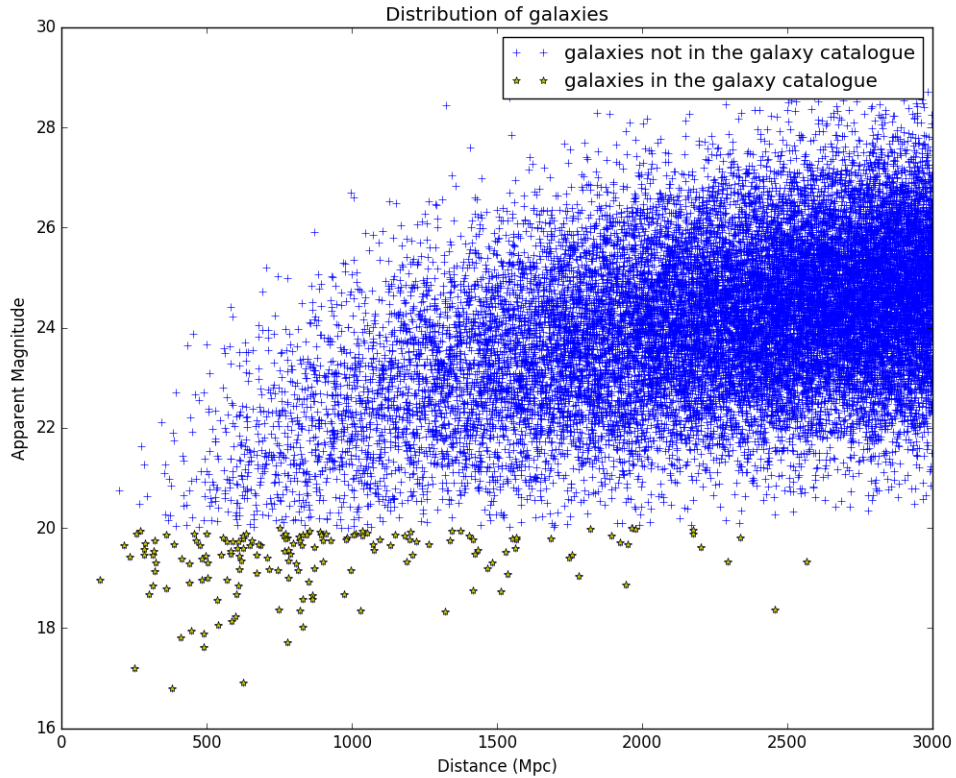


Figure 5.7: Typical distribution of apparent magnitude and luminosity distance (for $H_0 = 70 \text{ km s}^{-1} \text{ Mpc}^{-1}$) of galaxies. For typical BBH aLIGO sensitivity ranges, the majority of galaxies in the field are not within the galaxy catalogue.

The probability of the host being within or outwith the galaxy catalogue is derived in chapter 4. There is a hard cut on the limiting magnitude of the EM galaxy catalogue, making the probability of a galaxy being within the catalogue only dependent on its apparent magnitude m . Over all galaxies, the probability of the host associated to a GW event being brighter than the limiting apparent magnitude depends on the distance threshold for GW detection and the absolute magnitude distribution of galaxies. Translating the limiting apparent magnitude of the EM catalogue into a limiting distance depends on the value of H_0 . The higher the value of H_0 , the fainter the galaxy for a given distance and absolute magnitude, making it less likely to be within the catalogue.

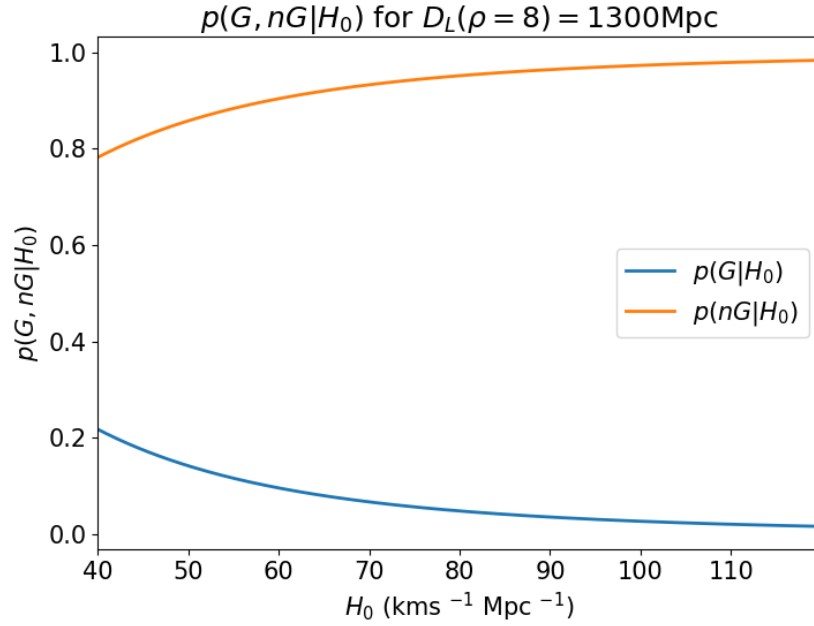


Figure 5.8: $p(G|H_0, D, I)$ and $p(\bar{G}|H_0, D, I)$ for $D_L(\rho_{th}) = 1300\text{Mpc}$. This plot shows that for typical BBH ranges, the host galaxy is less likely to be inside the galaxy catalogue, for all values of H_0 considered.

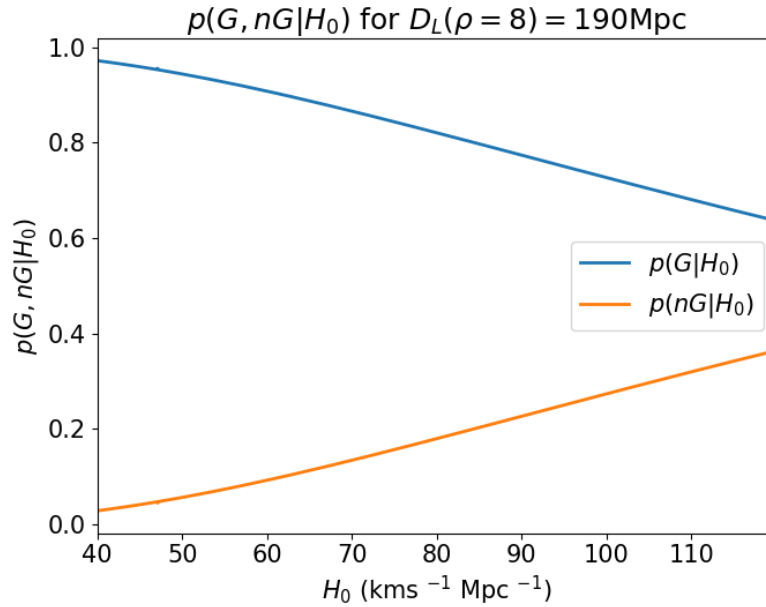


Figure 5.9: $p(G|H_0, D, I)$ and $p(\bar{G}|H_0, D, I)$ for $D_L(\rho_{th}) = 190\text{Mpc}$. This plot shows that for typical BBH ranges, the host galaxy is more likely to be inside the galaxy catalogue, for all values of H_0 considered.

For the BNS observing scenarios, even low SNR events would be relatively close to us. At design sensitivity, the reach of the Advanced LIGO detectors is $D_L = 190\text{Mpc}$ for binary neutron

stars. In this scenario, it is therefore much more likely to find the host galaxy within the EM catalogue; the GLADE catalogue, for example, is half-complete at $D_L = 300\text{Mpc}$. For BBH observing scenarios, the reach of aLIGO at design sensitivity is $D_L = 1640\text{Mpc}$, meaning only loud events would potentially come from host galaxies within the galaxy catalogue. Results for $p(G|H_0, D, I)$ and $p(\bar{G}|H_0, D, I)$ are presented for two observing scenarios, a BBH one in figure 5.8, and a BNS one in figure 5.9.

5.5 Posterior with no Bias Corrections

The code was run without any corrections to account for the incompleteness of the EM galaxy catalogue, for both BBH and BNS observing scenarios. The results highlight the importance of correcting for the bias this introduces.

Figures 5.10 and 5.11 are final results for H_0 in a BNS observing scenario and a BBH observing scenario. Figures 5.12 and 5.14 are results when only taking into the first half of equation 4.16: only potential host galaxies within the EM galaxy catalogue are considered, but a correction is applied to account for the incompleteness of the catalogue. Figures 5.13 and 5.15 are results assuming a complete galaxy catalogue.

These results highlight the need to correct for the incompleteness of the EM catalogue; especially in the case of the BBH scenario, the result is significantly skewed when the bias is not corrected for.

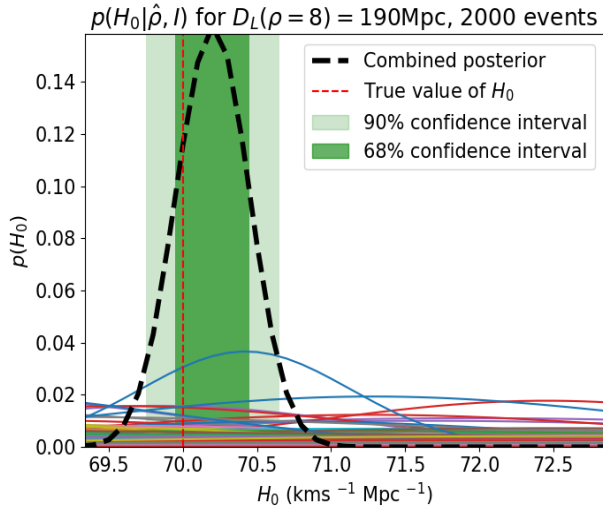


Figure 5.10: $p(H_0|\hat{\rho}, I)$ for $D_L(\rho_{th}) = 190\text{Mpc}$.

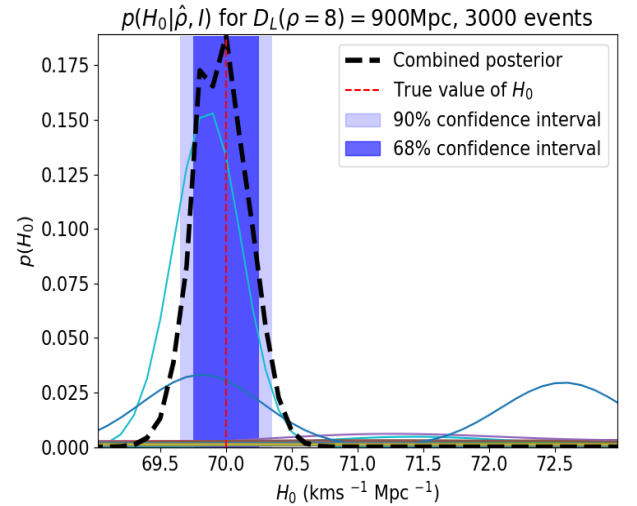


Figure 5.11: $p(H_0|\hat{\rho}, I)$ for $D_L(\rho_{th}) = 900\text{Mpc}$.

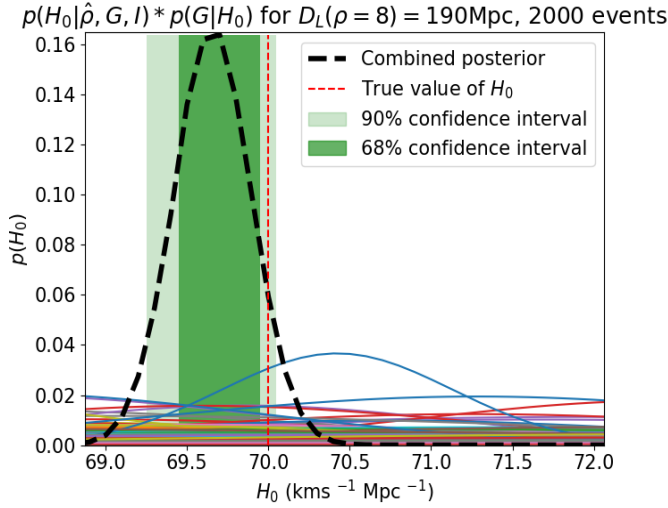


Figure 5.12: $p(H_0|G, \hat{\rho}, I) * p(G|H_0, I)$ for $D_L(\rho_{th}) = 190\text{Mpc}$.

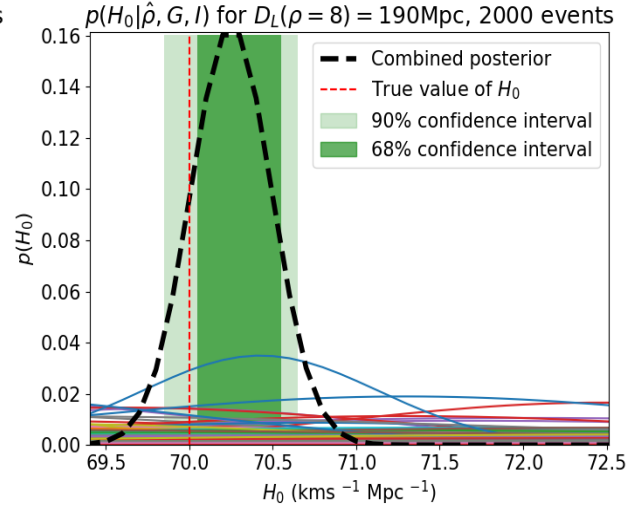


Figure 5.13: $p(H_0|G, \hat{\rho}, I)$ for $D_L(\rho_{th}) = 190\text{Mpc}$.

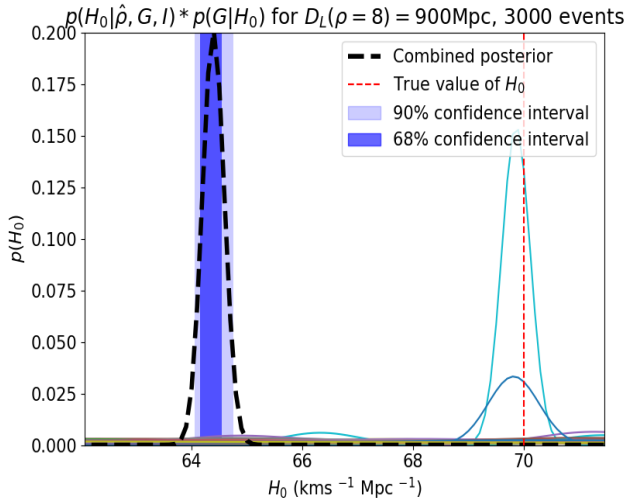


Figure 5.14: $p(H_0|G, \hat{\rho}, I) * p(G|H_0, I)$ for $D_L(\rho_{th}) = 900\text{Mpc}$.

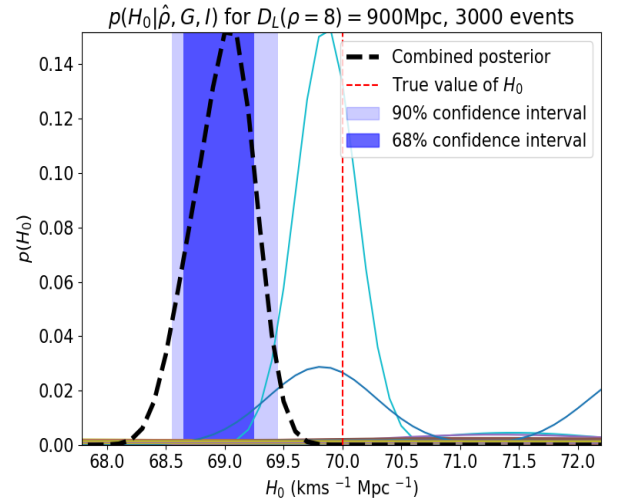


Figure 5.15: $p(H_0|G, \hat{\rho}, I)$ for $D_L(\rho_{th}) = 900\text{Mpc}$.

5.6 Interpretation of Results

Results were obtained for a wide range of observing scenarios. Six different aLIGO sensitivities were tested, corresponding to different phases of the Advanced LIGO detectors and different types of compact binary coalescences.

Even at design or late phase sensitivity for the binary black hole scenario, a measurement could potentially be obtained for the Hubble constant. While dominated by one loud event, the combined posterior from all events is significantly narrower, meaning a more precise measurement is obtained from many events. However, this experiment demonstrates that without a host galaxy, not a lot of information can be obtained from low SNR events alone; they only serve to narrow down the posterior dominated by events originating from a galaxy within the electromagnetic catalogue.

Work by Holz and Chen showed that the distribution of SNRs depend only on the detection threshold, and characterises the loudest events. After 4 detections, half the time the loudest event will have $\rho = 22$, going up to $\rho = 47$ for 40 detections. [33]. We can therefore reasonably expect several loud events during a real observing run.

The code is run for a very large number of events. For binary black holes, conservative estimates place the astrophysical rate of coalescences at $2 - 600 \text{ Gpc}^{-3} \text{ yr}^{-1}$, while the latest estimates place the rate of binary neutron star coalescences at $1540^{+3200}_{-1220} \text{ Gpc}^{-3} \text{ yr}^{-1}$. [39, 138] Detection rates for BBH by Advanced LIGO at design sensitivity are of $5.1 - 99 \text{ yr}^{-1}$. [139] It is therefore very unlikely to detect such a large number of events with second generation gravitational wave detectors.

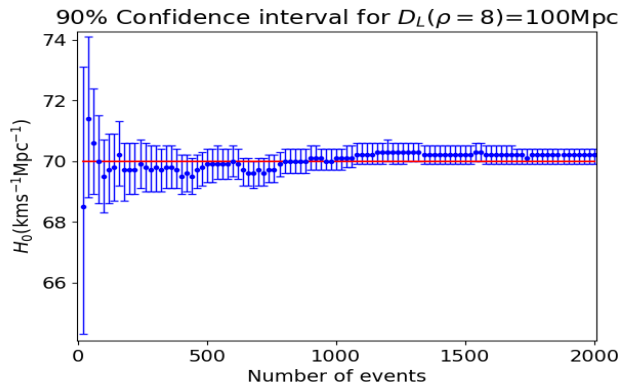


Figure 5.16: 90% confidence intervals derived from the posterior on H_0 , $D_L(\rho_{th}) = 100 \text{ Mpc}$. This shows the evolution of the width of the 90% confidence interval for different numbers of events making up the combined posterior.

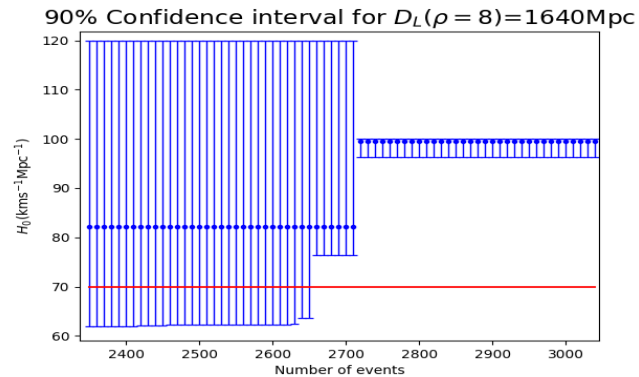


Figure 5.17: 90% confidence intervals derived from the posterior on H_0 , $D_L(\rho_{th}) = 1640 \text{ Mpc}$. This shows the evolution of the width of the 90% confidence interval for different numbers of events making up the combined posterior.

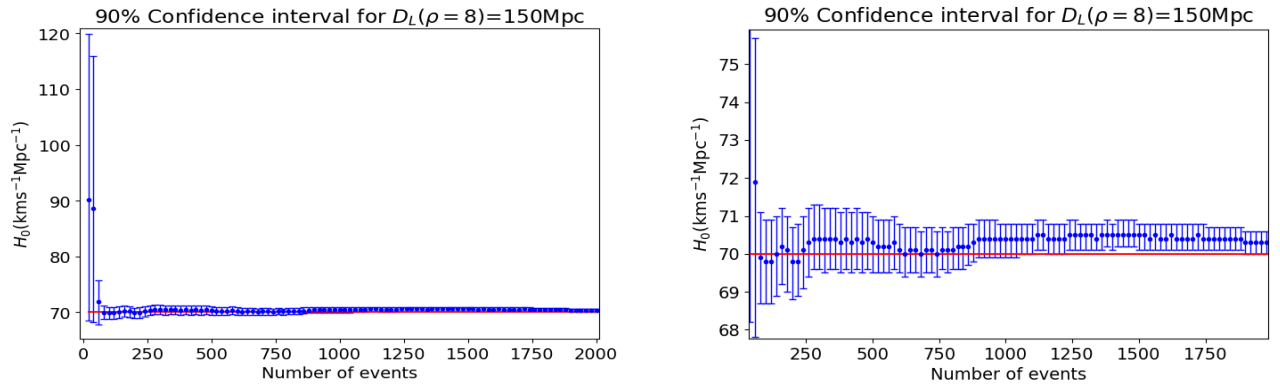


Figure 5.18: 90% confidence intervals derived from the posterior on H_0 for $D_L(\rho_{th}) = 150\text{Mpc}$.

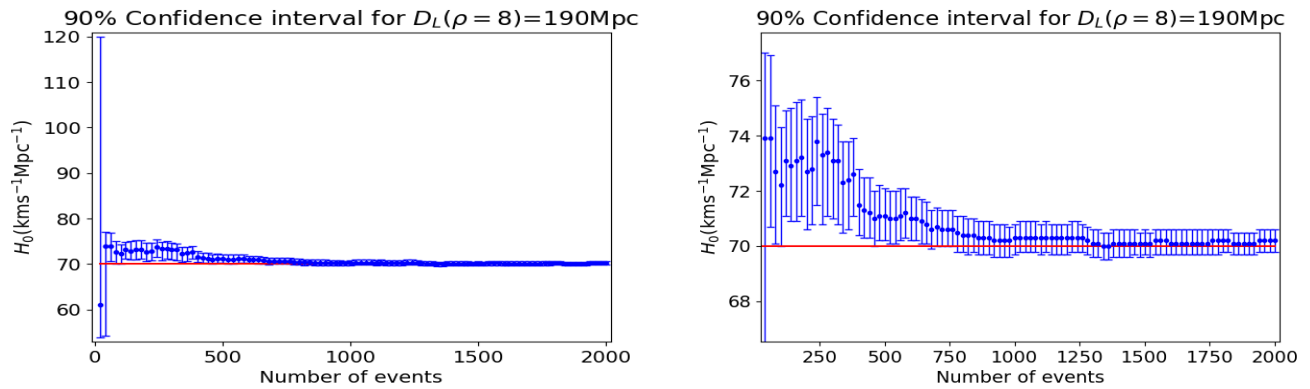


Figure 5.19: 90% confidence intervals derived from the posterior on H_0 for $D_L(\rho_{th}) = 190\text{Mpc}$.

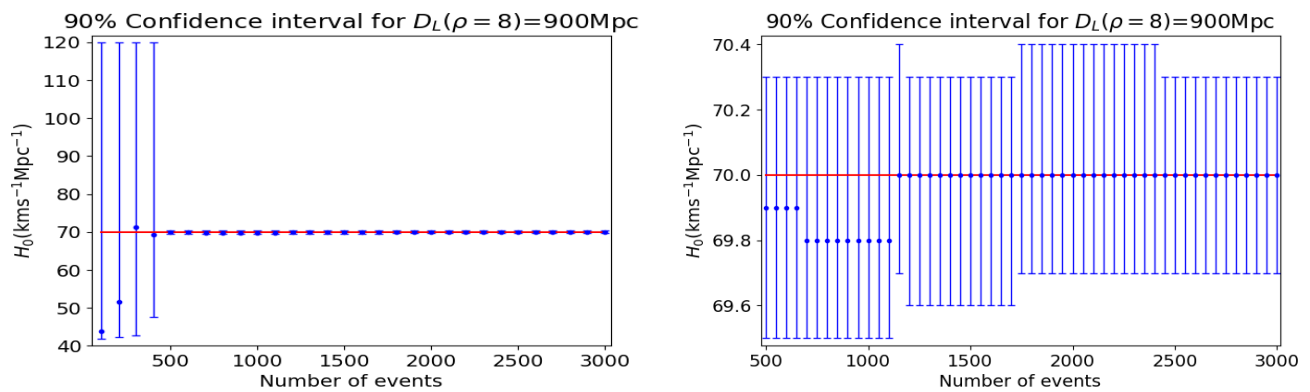


Figure 5.20: 90% confidence intervals derived from the posterior on H_0 for $D_L(\rho_{th}) = 900\text{Mpc}$.

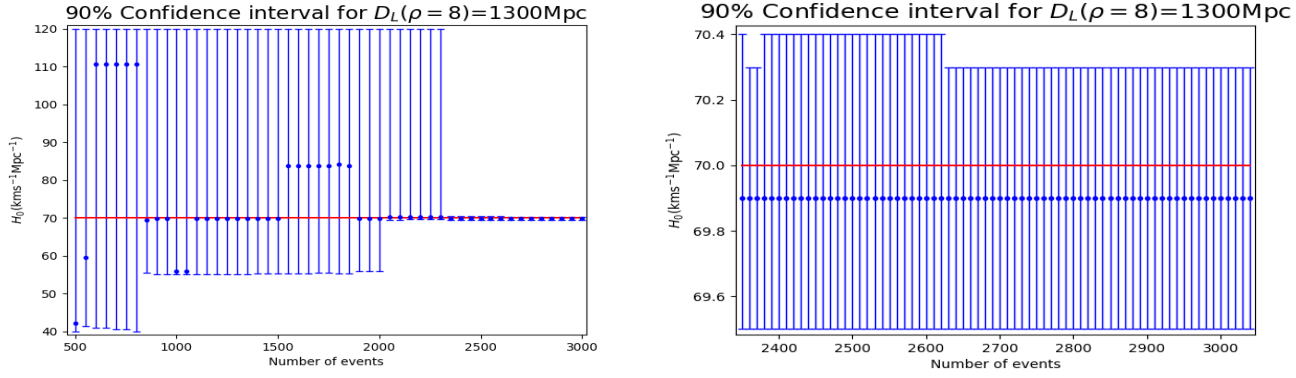


Figure 5.21: Confidence intervals derived from the posterior on H_0 , $D_L(\rho_{th}) = 1300\text{Mpc}$.

The plots in figures 5.16 to 5.21 show the evolution of the width of the posterior on H_0 with added individual GW events. Note that for low number of events, the 90% region of confidence is not the whole area; rather, it encompasses several discrete areas in that range, and the widest range possible is presented.

The results also demonstrate the importance of the golden binaries described by Chen and Holz. [116] Most of the constraints on H_0 are obtained from single events. However, the posterior is narrowed down by added events.

5.7 Limitations of the Model

There are some limitations to the code. Despite efforts in debugging, some numerical noise remains in the case where the threshold on the maximum detectable luminosity distance for gravitational wave events, $D_L(\rho_{th})$ is low (BNS O2 sensitivities). This bias is still present even with a large number of GW events ($N=2000$), making the final posterior on H_0 consistently slightly skewed towards higher values. This bias is more obvious when using a coarse sampling on H_0 .

A bias can be observed in the computation of one of the integration constant, $K(H_0)$, with

$$\frac{1}{K(H_0)} = \int_{m_{cut}}^{\infty} \int_{-\infty}^{\infty} \int_0^{\infty} p(z, m, M | H_0, D, I) dz dM dm. \quad (5.1)$$

As seen in figure 5.22, some numerical noise can be found in $K(H_0)$ for low $D_L(\rho_{th})$. This is most likely an issue with the survival function of the non-central chi-square distribution. This function was re-written as the scipy built-in function was too noisy; however, this new function could still contain noise. A specialised integrator could potentially fix this issue.

$\frac{1}{K(H_0)}$ is a term that appears in the computation of $p(H_0 | \bar{G})$. From the two figures 5.22 and 5.23, it can be seen that at lower $D_L(\rho_{th})$, the values of $1/K(H_0)$ are lower than would be

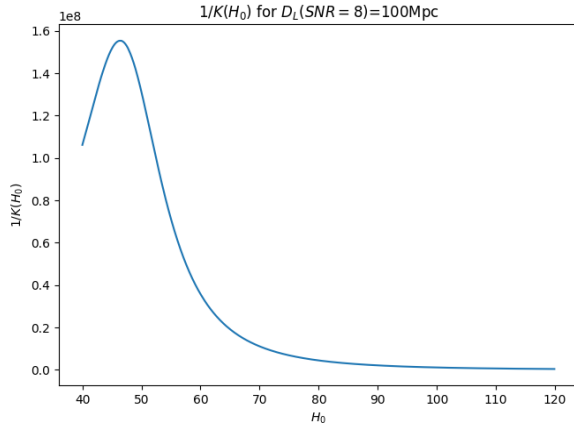


Figure 5.22: $\frac{1}{K(H_0)}$ for $D_L(\rho_{th}) = 100\text{Mpc}$.

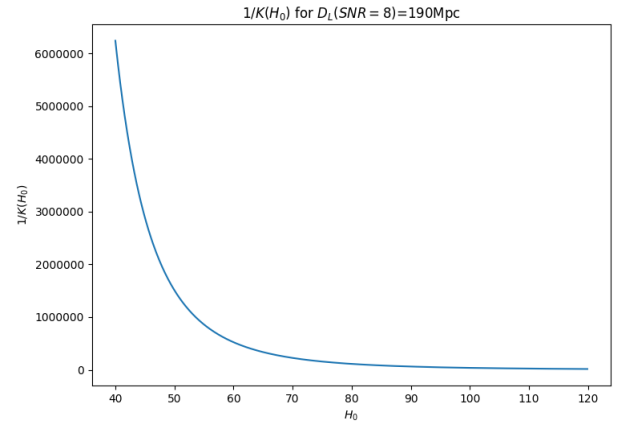


Figure 5.23: $\frac{1}{K(H_0)}$ for $D_L(\rho_{th}) = 190\text{Mpc}$.

expected. This would therefore introduce a slight bias towards higher Hubble constants, which is what is observed.

However, O2 has now been completed, with O3 under preparation, making the analysis for these sensitivities redundant: such a large number of binary neutron star mergers would not be expected.

As mentioned previously, the model used only focuses on one of the biases encountered in standard siren measurements of the Hubble constant.

Some numerical noise can also be observed in the posteriors for individual events with the finer sampling of H_0 ; this is also an issue that would require a purpose-built integrator. The noise is more prominent for high $D_L(\rho_{th})$, as seen in figure 5.24.

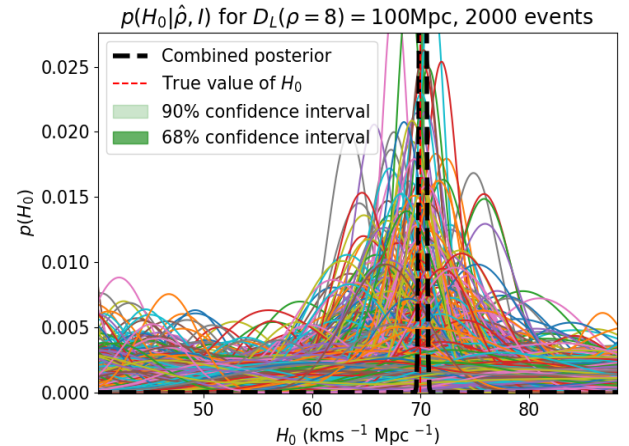
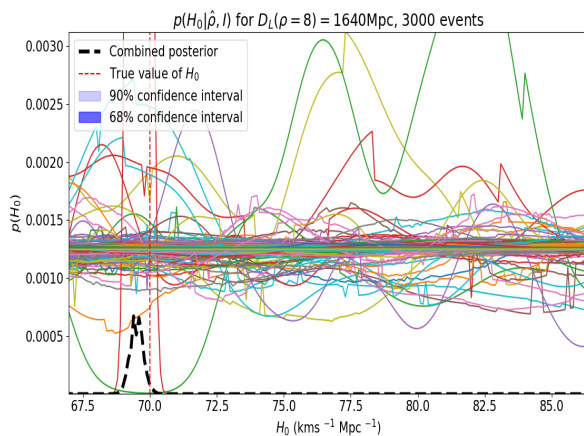


Figure 5.24: Noisy individual posteriors, with comparatively smooth posteriors at low $D_L(\rho_{th})$.

However, overall, results tend to converge towards the true value of the Hubble constant, with achieved precisions that are competitive with traditional EM methods, demonstrating that

statistical methods are a powerful tool in standard siren cosmology.

Chapter 6

Conclusions and Future Work

This chapter presents some conclusions drawn from this work, and discusses future work and issues to address in this field.

6.1 Conclusions and Insights from the Toy Model Experiment

This experiment primarily focused on the effects of an incomplete, magnitude-limited electromagnetic galaxy catalogue on a standard siren measurement of the Hubble constant. It presented a simplified version of ways to use Bayesian inference to measure the Hubble constant with standard sirens using statistical methods.

Previous work has investigated prospects for statistical measurements of the Hubble constant. This work differs both in its treatment of biases, and in its use of a broad, flat prior on H_0 . The main focus was to highlight the biases that come from the incompleteness, and inferior reach, of any electromagnetic galaxy catalogue. As we reach design sensitivity for the Advanced LIGO detectors, this bias could become an important one.

Previous research has been done by Chen and Holz on "golden events": events with a localisation volume that is small enough to easily find the host galaxy. [122] A small number of golden binaries per year is expected to be detected by future network of gravitational waves. In this experiment, it was found that much of the information about H_0 could be obtained from a single high SNR event, which is in line with this work. Especially in the case of binary black holes, not much information is obtained solely from binaries that do not have an EM counterpart within the galaxy catalogue. However, it was also demonstrated that we can obtain tighter constraints on the measurements by combining these golden binaries with many other low SNR events.

This work demonstrates the importance of the golden events described by Holz in any Standard Siren measurement of the Hubble constant. [122] The toy model was tested on very high number of events; such a large number of detections is unlikely to be reached before the advent of third generation detectors, which will have improved sensitivity and localisation.

6.2 Towards a Precise Measurement of the Hubble Constant Using Standard Sirens

This toy model experiment demonstrates that standard sirens are a viable and interesting way of measuring the Hubble constant. Results were obtained for a range of detector sensitivities; and while often dominating by a few loud events, low SNR events still allow for tighter constraints on the Hubble constant.

The recent results from GW170817 confirmed that standard sirens are a promising method for measuring the Hubble constant, and results have been obtained from only one event with an EM counterpart, despite the large errors on the luminosity distance. With improved sky localisation from Virgo, events with no EM counterparts could also be promising standard sirens, and we can expect a better measurement of the Hubble constant as we detect more compact binary coalescences.

However, even with rather poor localisation and many galaxies in the field, it is possible to make a measurement of the Hubble constant using statistical methods. This is an interesting method to explore for future observing runs, as binary coalescence detections are expected at a greater rate with increasing sensitivities.

The first gravitational wave standard siren measurement of the Hubble constant benefited from its excellent localisation and coincident electromagnetic phenomena. However, not all detections will be one of these so-called "golden binaries", and as sensitivities and ranges of the detectors increase, so does the need for taking into account selection effects when looking for the host galaxy of the merger.

With further research in the field, it might become easier to identify the host galaxy of compact binary coalescences. For example, with a good understanding of black hole populations in relation to types of galaxies, it would be possible to weigh the probability of each galaxy being the host. In this project, each galaxy was assumed to be the same, which would not be true in the context of a true measurement. Extensive efforts are currently being put into research on the statistical method of measuring the Hubble constant with standard sirens, accounting for many parameters such as localisation, galaxy luminosity, and spin and orientation of the binaries. Localisation, especially, would be of crucial importance in the use of gravitational waves as standard sirens.

6.3 Cosmology Using Multi-Messenger Astronomy

On 17th August 2017, a neutron star merger was detected by aLIGO for the first time. [39] Alongside these observations, multiple observations in the electromagnetic spectrum were made. While the loudness of the event made for easier localisation of the host galaxy, the multi-messenger observations confirmed the location of the host, and provided a redshift.

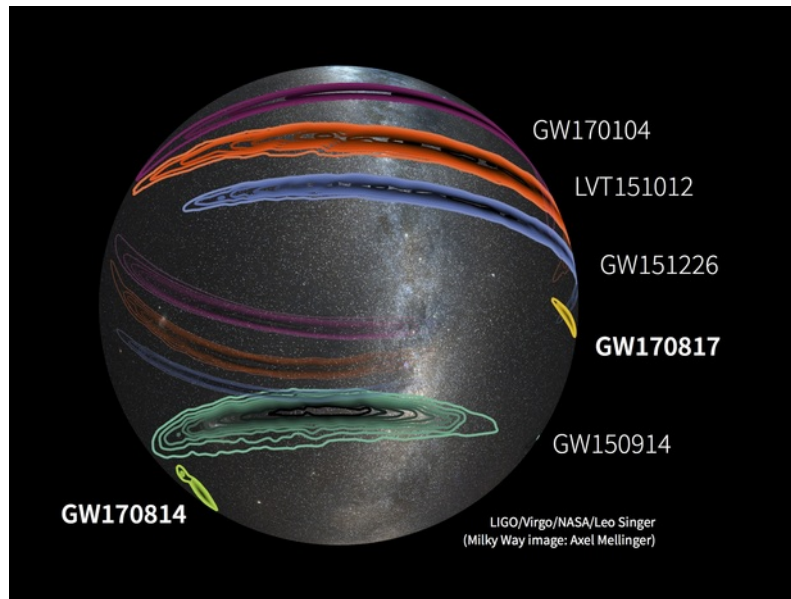


Figure 6.1: Sky localisations of gravitational wave signals detected by LIGO-VIRGO. [140]

Multi-messenger astronomy will not only help us measure the Hubble constant, it will give us new insights into cosmology.

6.3.1 Cosmology with Third Generation Gravitational Wave Detectors

This experiment focused on measuring the Hubble constant using second generation gravitational wave detectors. When third generation detectors like the Einstein Telescope come online, gravitational wave astronomers will be able to probe the universe to a reach similar to that of electromagnetic searches. Targeting a factor of 10 improvement over advanced detectors, the improvement on the rate of detection would be 1000. [57] Previous work has demonstrated that with 10^5 BNS detected by ET, constraints on cosmological parameters could match the ones from future forecasted measurements by CMB+BAO+SNIa. [121]

6.4 GW170817 and the First Gravitational Wave Standard Siren Measurement of the Hubble Constant

On 17th August 2017, the aLIGO detectors and several EM telescopes made observations of a neutron star merger in the gravitational wave spectrum and in several bands of the electromagnetic spectrum.

A short gamma ray burst, GRB 170817 A, was observed independently by the Fermi GMB (Gamma-ray Burst Monitor) and INTEGRAL (INTErnational Gamma Ray Astrophysics Laboratory) 1.7s after gravitational waves were detected from the merger. The source of this gamma ray burst was coincident with the location of GW170817, turning out to be originating from galaxy

NGC 4993. [141–143] With a probability of simultaneous detections occurring by chance being only 5.0×10^{-8} , these multi-messenger observations confirmed neutron star mergers as progenitors of short gamma ray bursts. [141] An associated redshift was obtained from these observations, allowing astronomers to use GW170817 as a standard siren. [124] This measurement is limited by the degeneracy between the inclination angle and luminosity distance of the binary, leading to large errors on the distance estimate from the gravitational wave data.

The current measurement has large errors, but as demonstrated in this project, several events could narrow down the posterior on H_0 . The current standard siren measurement agrees with both the local and the model-dependent CMB-inferred measurement. This could however change during upcoming observing runs, as more detections are made. Eventually, the standard siren measurement of the Hubble constant could discriminate between previously made measurements, giving more insight into whether the discrepancies come from new, unknown early universe physics, or from systematic errors.

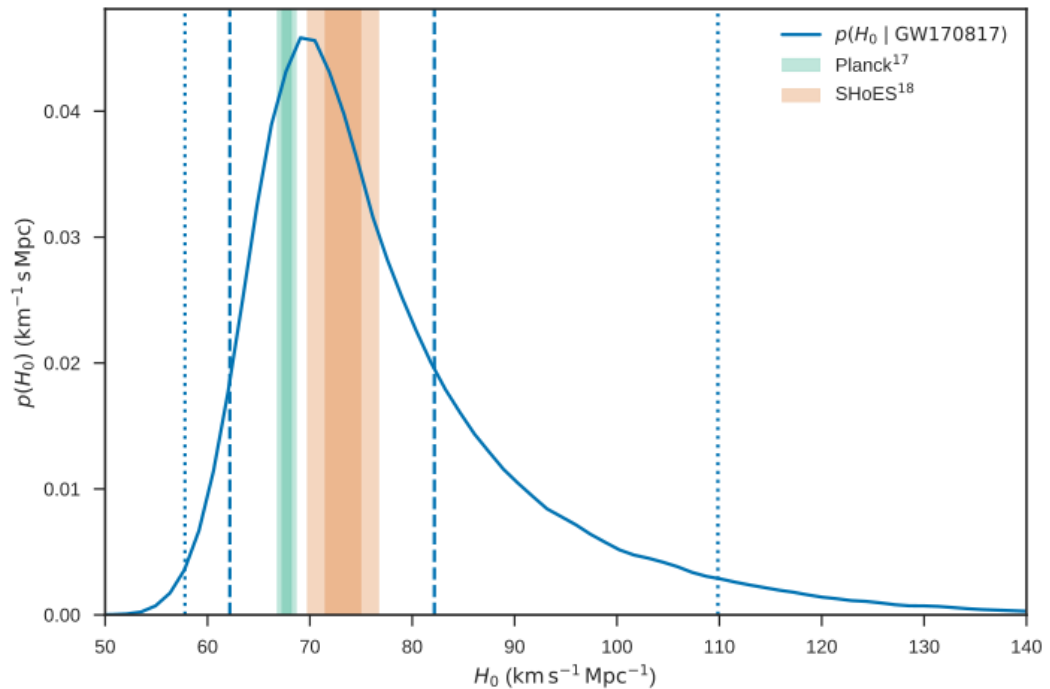


Figure 6.2: A standard siren measurement of H_0 using GW170817 and its associated EM counterparts. The 68.3% and 95.4% minimum credible intervals for the standard siren measurement are indicated by the dashed and dotted blue lines, while the Planck and SHoES credible intervals are in green and orange, respectively. [124]

Figure 6.3 shows a similar plot to Figure 3.6, presenting some key results from measurements of the Hubble constant since the first precise measurement by the Hubble Key Project in 2001. This plot is updated with the new result from the standard siren measurement of the Hubble constant. For now, this measurement is not competitive with EM methods, but with the success of current gravitational wave detectors and the third generation of detectors under study,

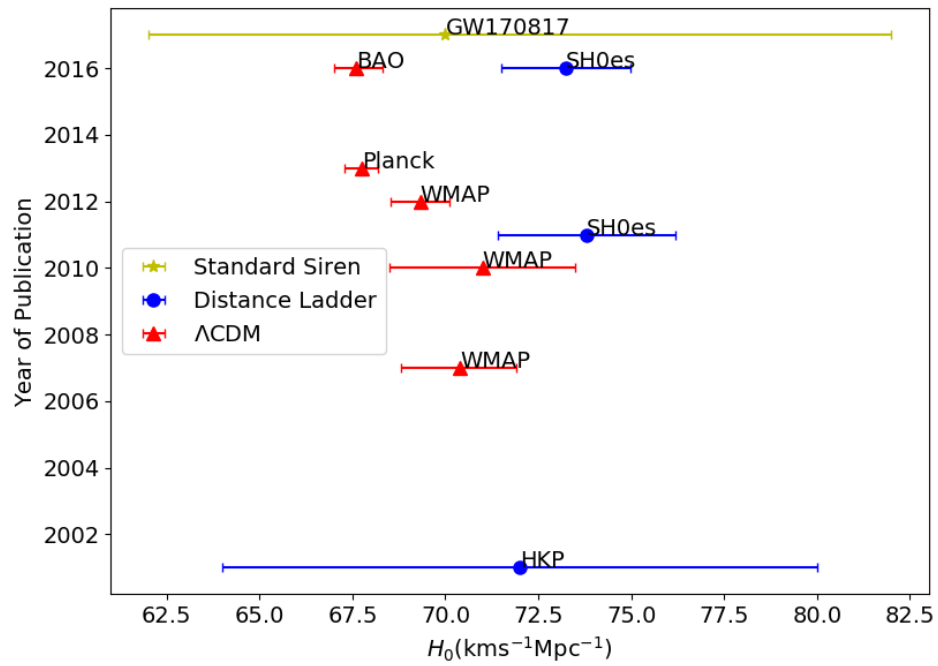


Figure 6.3: Timeline of measurements of the Hubble constant using different methods, updated with the new measurement from GW170817.

considerable improvements to this measurement are to be expected. The future of cosmology using standard sirens seems, with or without the "lights off", very bright!

Appendix A

Code

```
#!/usr/bin/env python

import numpy as np
from scipy.integrate import quad
from scipy.integrate import dblquad
from scipy.stats import ncx2, norm
from scipy.special import iv
from scipy.interpolate import splev, splrep
import argparse

def parser():
    """Parses command line arguments"""
    parser = argparse.ArgumentParser(prog='gaussmpc.py',
        description='simulates_hubble_constant_measurements_
        using_gw_observations')
    # arguments for reading in a data file
    parser.add_argument('SNRDL', 'snrdl', type=int, default
        =190, help='Threshold_luminosity_distance_for_GW_
        detection')
    parser.add_argument('v', 'label', type=int, default
        =100, help='A_label_for_this_simulation')
    parser.add_argument('Dens', 'ngal', type=float, default
        =0.006, help='Galaxy_density_in_number_per_unit_Mpc^3')
    return parser.parse_args()

args = parser()
```

```

def sigm(X, lim , sigma):
    return 1/(1+np.exp( (X lim)/sigma))

def marcumq1(a, b, reltol):

    # check consistent length vectors unless one or more is of
    # length 1
    a = np.array(a)
    b = np.array(b)
    if a.size>1 and b.size>1 and a.size!=b.size:
        print 'ERROR: input vectors to marcumq1 are
              inconsistent sizes. Exiting'
        exit(1)

    arg = a*b
    x = a/b
    frac = x
    s = iv(0, arg)
    diff = 2.0*s*reltol

    k = 1
    while (np.sum(diff>reltol*s)):
        diff = frac*iv(k, arg)
        s += diff
        frac *= x
        k += 1
    temp = np.exp( 0.5*(a*a + b*b))*s
    idx = np.argwhere(np.isnan(temp) + np.isinf(temp))
    temp[idx] = 1.0
    return temp

"""
GENERATING DATA
"""

```

```

SNRDL = args.snrdl #Distance in Mpc at SNR = 8
Dens = args.ngal*(10.0/41253.0) #galaxy density per unit Mpc,
    multiplied by fraction of sky
dlsnr = 8

h0true = 70.0 #true value of Hubble constant, for generating
    distances
dh0 = 0.1 #width of hubble bins
h0min = 40
h0max = 120
h0 = np.arange(h0min,h0max, dh0) #Array of Hubble constant
    values we want to test
c = 300000.0 #set up speed of light in km/s
htrue = h0true/100.0
h_array = h0/100.0

reltol = 1e 6 # Marcum q function tolerance

def lumdist(z,h):
    return (c*z)/h

def M_star(h):
    return 16.8+5*np.log10(h)

def red(h, snr):
    return (dlsnr*(SNRDL/snr))*h/c #Returns redshift as
    function of SNR, H0

def redm(m,M,h):
    return h/(10**6*c)*10**(1.0+0.2*(m M)) #Returns redshift
    as function of m, M, H0

def rho(h, z):
    return (dlsnr*(SNRDL/z))*h/c #Returns SNR as function of
    redshift, H0

def app_m(h,M,z):

```

```

        return M5+5*np.log10(c*z*10**6/h)
#apparent magnitude

def abs_m(h,m,z):
    return m+5.5*np.log10(c*z*10**6/h)
#absolute magnitude

def pG_H0(h,M,z):
    temp = ncx2.sf(SNRth**2,2,rho(h,z)**2) * z**2 * norm.
        pdf(M,loc=M_star(h/100.0),scale=sigma)
    return temp

def pRho_nG(h,M,v,z):
    temp = ncx2.pdf(SNR[v]**2,2,rho(h,z)**2) * K_H0(h,M,z)
    return temp

def K_H0(h,M,z):
    temp = QM_acc(rho(h,z)) * z**2 * norm.pdf(M,loc=M_star(
        h/100.0),scale=sigma)
    return temp

def luminosity(m,d):
    """
    returns the luminosity of a source given an apparent
        magnitude and a distance in Mpc
    """
    return 10**((0.4*(m-5.0*(np.log10(1e6*d)-1.0)))

Mstar = M_star(htrue)

m_th = 20 #Threshold on the apparent magnitude
sigma = 1.4 #sigma of Gaussian

SNRth = 8 #Threshold on the SNR

Ztruemax = 0.1*np.ceil(0.5+3*red(h0true,SNRth)/0.1) # "True"
        maximum redshift

```

```

Zmax = Ztruemax #Maximum redshift
DLmax = lumdist(Zmax, h0true)
DLtruemax = lumdist(Ztruemax, h0true)
Hosts = int(round((4/3)*np.pi*Dens*DLtruemax**3)) #number of
        host galaxies

seed = 0
if seed>0:
    np.random.seed(seed)

print("Event_%s_up_to_a_redshift_of_%f,_%s_host_galaxies" % (
    args.label, red(h0true, SNRth), Hosts))
print("True_max._redshift_is_%f" % Ztruemax)
print("Infinity_taken_at_redshift_%f" % Zmax)

SNR_ar = np.linspace(1,150,150)
marc_q = marcumq1(SNR_ar, SNRth, reltol)*(1+sigm(SNR_ar,5,0.05)
    )+ncx2.sf(SNRth**2,2.0,SNR_ar**2)*(sigm(SNR_ar,5,0.05))
int_Qm = splrep(SNR_ar, marc_q)

def sigm(X, lim, sigma):
    return 1/(1+np.exp((X-lim)/sigma))

def QM_acc(X):
    return splev(X, int_Qm)

"""
STATS
"""

```

```

def KH0(h):
    kh0 = dblquad(lambda z,M:K_H0(h,M,z), 28, 10, lambda M:redm
        (m_th,M,h), lambda M: Zmax,epsabs = 1.49e 9, epsrel =
        1.49e 9)
    return 1/kh0[0]

def pgh0(h):
    #p(G|H0)
    ch0 = dblquad(lambda z,M:pG_H0(h,M,z), 26, 12, lambda M:0,
        lambda M: Zmax,epsabs = 1.49e 9, epsrel = 1.49e 9)
    pg = dblquad(lambda z,M:pG_H0(h,M,z), 26, 12, lambda M:0,
        lambda M: redm(m_th,M,h),epsabs = 1.49e 9, epsrel = 1.49
        e 9)
    return pg[0]/ch0[0]

def psnrng(SNR,h,j):
    pSNRnG = dblquad(lambda z,M: ncx2.pdf(SNR**2,2,rho(h,z)**2)
        * QM_acc(rho(h,z)) * z**2 * norm.pdf(M,loc=M_star
        (h/100.0),scale=sigma), 26, 12, lambda M:redm(m_th,M,h)
        , lambda M: Zmax,epsabs = 1.49e 9, epsrel = 1.49e 9)
    return pSNRnG[0]*Kh[j]

Kh = np.array([KH0(hubble) for j,hubble in enumerate(h0)])
#Generating all integration constants for H0 array
pGh0 = np.array([pgh0(hubble) for j,hubble in enumerate(h0)]) #
    P(G|H0,D,I)
pnGh0 = 1.00 - pGh0 #P(nG|H0,D,I)

def Prho():
    #Main function, returns posterior for individual event
    redshifts = Ztruemax*(np.random.uniform(0,1,Hosts))

```

```

    *(1.0/3.0) #Generating redshifts
absmags = np.random.normal(Mstar, sigma, Hosts) #random M
    here
magnitudes = np.array([app_m(h0true, abmag, reds) for abmag,
    reds in zip(absmags, redshifts)])
catalog = redshifts[magnitudes < m_th]
mags = magnitudes[magnitudes < m_th]

def pdet(h):
#probability ncx2.pdf(SNR[v]**2,2,rho(h,z)**2) of galaxy j
    producing a detectable signal p(D|G,m,M,H0,z,I) (
    unchanged)
    snr = rho(h, catalog)
    temp = ncx2.sf( SNRth**2, 2, snr**2)
    return temp / np.sum(temp)

def psnrG(SNR, h, j):
#p(rho |G, H0, D, I)
    snr = rho(h, catalog)
    psnrG = ncx2.pdf( SNR**2, 2, snr**2 )
    if len(snr) == 0:
        psnrG = 0
    else:
        psnrG = psnrG * pdet(h)
    return np.sum(psnrG)

DL = (c*redshifts)/h0true #Luminosity distance

SNRtrue = dlsnr*(SNRDL/DL) #True SNR

#Rejection sampling

N = 1
l = 0
while l in xrange(N):
    k = np.random.randint(0, len(SNRtrue))

```

```

    snr = SNRtrue[k]
    SNRsq = ncx2.rvs(2, snr**2)
    snr2 = np.sqrt(SNRsq)
    if snr2 >= SNRth:
        SNR = snr2
        l +=1

pSNRG = np.array([psnrg(SNR, hubble, j) for j, hubble in
    enumerate(h0)])
pSNRnG = np.array([psnrng(SNR, hubble, j) for j, hubble in
    enumerate(h0)])
np.savetxt("{}_SNRDL_{}_G".format(args.label, SNRDL), pSNRG)
np.savetxt("{}_SNRDL_{}_nG".format(args.label, SNRDL),
    pSNRnG)
info = np.array([SNR, catalog.size])
np.savetxt("{}_INFO".format(args.label), info)
value = pSNRG*pGh0+pSNRnG*pnGh0
np.savetxt("{}_SNRDL_{}".format(args.label, SNRDL), value)

```

Prho()

Bibliography

- [1] LIGO Scientific Collaboration, Virgo Collaboration, B. P. Abbott, R. Abbott, T. D. Abbott, M. R. Abernathy, F. Acernese, K. Ackley, C. Adams, T. Adams, P. Addesso, R. X. Adhikari, *et al.*, “Observation of Gravitational Waves from a Binary Black Hole Merger,” *Phys. Rev. Lett.* **116** (Feb, 2016) 061102.
<https://link.aps.org/doi/10.1103/PhysRevLett.116.061102>.
- [2] K. G. Jansky, “Radio Waves from Outside the Solar System,” **132** (July, 1933) 66.
- [3] B. S. Sathyaprakash and B. F. Schutz, “Physics, Astrophysics and Cosmology with Gravitational Waves,” *Living Reviews in Relativity* **12** (Mar., 2009) 2,
[arXiv:0903.0338](https://arxiv.org/abs/0903.0338) [gr-qc].
- [4] *Quarterly Calendar*, vol. 3. The University of Chicago, August, 1894.
- [5] J. C. Maxwell, “VII. A dynamical theory of the electromagnetic field,” *Phil. Trans. R. Soc. Lond.* **155** (1865) 459–512.
- [6] A. Einstein, *Sidelights on Relativity*. Methuen Co, London, 1922.
- [7] A. Einstein, “Zur Elektrodynamik bewegter Körper,” *Annalen der Physik* **322** no. 10, (1905) 891–921. <http://dx.doi.org/10.1002/andp.19053221004>.
- [8] A. Einstein, “Die Feldgleichungen der Gravitation,” *Sitzungsberichte der Königlich Preußischen Akademie der Wissenschaften (Berlin)*, Seite 844-847. (1915) .
- [9] J. A. Wheeler, *A Journey into Gravity and Spacetime*. Scientific American Library, New York, 1990.
- [10] A. Einstein, “Über das Relativitätsprinzip und die aus demselben gezogenen Folgerungen,” *Jahrbuch der Radioaktivität und Elektronik* **4** (1908) .
- [11] S. M. Carroll, *Spacetime and Geometry - An Introduction to General Relativity*. Addison Wesley, San Francisco, 2004.
- [12] A. Einstein, “Die Grundlage der allgemeinen Relativitätstheorie,” *Annalen der Physik* **354** (1916) 769–822.

- [13] F. W. Dyson, A. S. Eddington, and C. Davidson, “A Determination of the Deflection of Light by the Sun’s Gravitational Field, from Observations Made at the Total Eclipse of May 29, 1919,” *Philosophical Transactions of the Royal Society of London Series A* **220** (1920) 291–333.
- [14] D. Kennefick, “Testing Relativity from the 1919 Eclipse - A Question of Bias,” *Physics Today* **62** (2009) 37–42.
- [15] A. Einstein, “Approximative Integration of the Field Equations of Gravitation,” Conference Proceedings of Prussian Academy of Sciences, 1916. Translated from German by Alfred Engel in *Volume 6: The Berlin Years: Writings, 1914-1917 (English translation supplement)*.
- [16] P. R. Saulson, *Fundamentals of Interferometric Gravitational Wave Detectors*. World Scientific Publishing, Singapore, 1994.
- [17] J. A. Tyson and R. P. Giffard, “Gravitational-wave astronomy,” **16** (1978) 521–554.
- [18] B. Schutz, *A First Course in General Relativity, Second Edition*. Cambridge University Press, Cambridge, 2009.
- [19] K. Schwarzschild, “Über das Gravitationsfeld eines Massenpunktes nach der Einsteinschen Theorie,” *Sitzungsberichte der Königlich Preußischen Akademie der Wissenschaften (Berlin), 1916, Seite 189-196* (1916) .
- [20] F. Özel and P. Freire, “Masses, Radii, and the Equation of State of Neutron Stars,” **54** (Sept., 2016) 401–440, arXiv:1603.02698 [astro-ph.HE].
- [21] T. A. Thompson, M. D. Kistler, and K. Z. Stanek, “A High Rate of White Dwarf-Neutron Star Mergers Their Transients,” *ArXiv e-prints* (Dec., 2009) , arXiv:0912.0009 [astro-ph.HE].
- [22] P. Lorén-Aguilar, J. Guerrero, J. Isern, J. A. Lobo, and E. García-Berro, “Gravitational wave radiation from the coalescence of white dwarfs,” **356** (Jan., 2005) 627–636, astro-ph/0410356.
- [23] J. Centrella, J. G. Baker, B. J. Kelly, and J. R. van Meter, “Black-hole binaries, gravitational waves, and numerical relativity,” *Reviews of Modern Physics* **82** (Oct., 2010) 3069–3119, arXiv:1010.5260 [gr-qc].
- [24] C. D. Ott, “TOPICAL REVIEW: The gravitational-wave signature of core-collapse supernovae,” *Classical and Quantum Gravity* **26** no. 6, (Mar., 2009) 063001, arXiv:0809.0695.

- [25] B. P. Abbott, R. Abbott, T. D. Abbott, M. R. Abernathy, F. Acernese, K. Ackley, C. Adams, T. Adams, P. Addesso, R. X. Adhikari, *et al.*, “Prospects for Observing and Localizing Gravitational-Wave Transients with Advanced LIGO and Advanced Virgo,” *Living Reviews in Relativity* **19** (Feb., 2016) 1, arXiv:1304.0670 [gr-qc].
- [26] B. P. Abbott, R. Abbott, T. D. Abbott, M. R. Abernathy, F. Acernese, K. Ackley, C. Adams, T. Adams, P. Addesso, R. X. Adhikari, *et al.*, “All-sky search for short gravitational-wave bursts in the first Advanced LIGO run,” **95** no. 4, (Feb., 2017) 042003, arXiv:1611.02972 [gr-qc].
- [27] T. Damour and A. Vilenkin, “Gravitational radiation from cosmic (super)strings: Bursts, stochastic background, and observational windows,” **71** no. 6, (Mar., 2005) 063510, hep-th/0410222.
- [28] The LIGO Scientific Collaboration, the Virgo Collaboration, B. P. Abbott, R. Abbott, T. D. Abbott, F. Acernese, K. Ackley, C. Adams, T. Adams, P. Addesso, *et al.*, “GW170817: Implications for the Stochastic Gravitational-Wave Background from Compact Binary Coalescences,” *ArXiv e-prints* (Oct., 2017), arXiv:1710.05837 [gr-qc].
- [29] C. Cutler and K. S. Thorne, “An Overview of Gravitational-Wave Sources,” *ArXiv General Relativity and Quantum Cosmology e-prints* (Apr., 2002), gr-qc/0204090.
- [30] **LIGO Scientific Collaboration and Virgo Collaboration** Collaboration, J. Aasi, B. P. Abbott, R. Abbott, T. Abbott, M. R. Abernathy, F. Acernese, K. Ackley, C. Adams, T. Adams, T. Adams, *et al.*, “Narrow-band search of continuous gravitational-wave signals from Crab and Vela pulsars in Virgo VSR4 data,” *Phys. Rev. D* **91** (Jan, 2015) 022004. <https://link.aps.org/doi/10.1103/PhysRevD.91.022004>.
- [31] J. Aasi, B. P. Abbott, R. Abbott, T. D. Abbott, M. R. Abernathy, F. Acernese, K. Ackley, C. Adams, T. Adams, P. Addesso, *et al.*, “First low frequency all-sky search for continuous gravitational wave signals,” **93** no. 4, (Feb., 2016) 042007, arXiv:1510.03621 [astro-ph.IM].
- [32] B. P. Abbott, R. Abbott, R. Adhikari, P. Ajith, B. Allen, G. Allen, R. S. Amin, S. B. Anderson, W. G. Anderson, M. A. Arain, *et al.*, “LIGO: the Laser Interferometer Gravitational-Wave Observatory,” *Reports on Progress in Physics* **72** no. 7, (July, 2009) 076901, arXiv:0711.3041 [gr-qc].
- [33] H. Chen and D. E. Holz, “The Loudest Gravitational Wave Events,” *ArXiv e-prints* (2014), arXiv:1409.0522.

- [34] B. P. Abbott, R. Abbott, T. D. Abbott, M. R. Abernathy, F. Acernese, K. Ackley, C. Adams, T. Adams, P. Addesso, R. X. Adhikari, and et al., “Properties of the Binary Black Hole Merger GW150914,” *Physical Review Letters* **116** no. 24, (June, 2016) 241102, arXiv:1602.03840 [gr-qc].
- [35] F. Pretorius, “Evolution of Binary Black-Hole Spacetimes,” *Phys. Rev. Lett.* **95** (Sep, 2005) 121101.
<https://link.aps.org/doi/10.1103/PhysRevLett.95.121101>.
- [36] M. Campanelli, C. O. Lousto, P. Marronetti, and Y. Zlochower, “Accurate Evolutions of Orbiting Black-Hole Binaries without Excision,” *Phys. Rev. Lett.* **96** (Mar, 2006) 111101.
<https://link.aps.org/doi/10.1103/PhysRevLett.96.111101>.
- [37] J. G. Baker, J. Centrella, D.-I. Choi, M. Koppitz, and J. van Meter, “Gravitational-wave extraction from an inspiraling configuration of merging black holes,” *Phys. Rev. Lett.* **96** (Mar, 2006) 111102.
<https://link.aps.org/doi/10.1103/PhysRevLett.96.111102>.
- [38] L. Blanchet, “Gravitational radiation from post-newtonian sources and inspiralling compact binaries,” *Living Reviews in Relativity* **17** no. 1, (Feb, 2014) 2.
<https://doi.org/10.12942/lrr-2014-2>.
- [39] B. P. Abbott, R. Abbott, T. D. Abbott, F. Acernese, K. Ackley, C. Adams, T. Adams, P. Addesso, R. X. Adhikari, V. B. Adya, et al., “GW170817: Observation of Gravitational Waves from a Binary Neutron Star Inspiral,” *Physical Review Letters* **119** no. 16, (Oct., 2017) 161101, arXiv:1710.05832 [gr-qc].
- [40] J. Weber, “Detection and Generation of Gravitational Waves,” *Physical Review* **117** (Jan., 1960) 306–313.
- [41] J. Weber, “Gravitational-Wave-Detector Events,” *Physical Review Letters* **20** (June, 1968) 1307–1308.
- [42] J. Weber, “Evidence for Discovery of Gravitational Radiation,” *Physical Review Letters* **22** (June, 1969) 1320–1324.
- [43] A. A. Michelson and E. W. Morley, “On the Relative Motion of the Earth and of the Luminiferous Ether,” *Sidereal Messenger*, vol. 6, pp.306-310 **6** (Nov., 1887) 306–310.
- [44] R. L. Forward, “Wideband laser-interferometer gravitational-radiation experiment,” **17** (Jan., 1978) 379–390.

- [45] R. Weiss, “Electromagnetically coupled broadband gravitational antenna,” in *K.S. Thorne, “Gravitational radiation”, 300 Years of Gravitation, S W Hawking and W Israel, pp 330–458. University Press, 1972.*
- [46] B. F. Schutz, “Networks of gravitational wave detectors and three figures of merit,” *Classical and Quantum Gravity* **28** no. 12, (June, 2011) 125023, arXiv:1102.5421 [astro-ph.IM].
- [47] A. Abramovici, W. E. Althouse, R. W. P. Drever, Y. Gursel, S. Kawamura, F. J. Raab, D. Shoemaker, L. Sievers, R. E. Spero, and K. S. Thorne, “LIGO - The Laser Interferometer Gravitational-Wave Observatory,” *Science* **256** (Apr., 1992) 325–333.
- [48] B. Willke, P. Aufmuth, C. Aulbert, S. Babak, R. Balasubramanian, B. W. Barr, S. Berukoff, S. Bose, G. Cagnoli, M. M. Casey, D. Churches, D. Clubley, C. N. Colacino, D. R. M. Crooks, C. Cutler, K. Danzmann, R. Davies, R. Dupuis, E. Elliffe, C. Fallnich, A. Freise, S. Goßler, A. Grant, H. Grote, G. Heinzel, A. Heptonstall, M. Heurs, M. Hewitson, J. Hough, O. Jennrich, K. Kawabe, K. Kötter, V. Leonhardt, H. Lück, M. Malec, P. W. McNamara, S. A. McIntosh, K. Mossavi, S. Mohanty, S. Mukherjee, S. Nagano, G. P. Newton, B. J. Owen, D. Palmer, M. A. Papa, M. V. Plissi, V. Quetschke, D. I. Robertson, N. A. Robertson, S. Rowan, A. Rüdiger, B. S. Sathyaprakash, R. Schilling, B. F. Schutz, R. Senior, A. M. Sintes, K. D. Skeldon, P. Sneddon, F. Stief, K. A. Strain, I. Taylor, C. I. Torrie, A. Vecchio, H. Ward, U. Weiland, H. Welling, P. Williams, W. Winkler, G. Woan, and I. Zawischa, “The GEO 600 gravitational wave detector,” *Classical and Quantum Gravity* **19** no. 7, (2002) 1377. <http://stacks.iop.org/0264-9381/19/i=7/a=321>.
- [49] F. Acernese, M. Agathos, K. Agatsuma, D. Aisa, N. Allemandou, A. Allocca, J. Amarni, P. Astone, G. Balestri, G. Ballardin, and et al., “Advanced Virgo: a second-generation interferometric gravitational wave detector,” *Classical and Quantum Gravity* **32** no. 2, (Jan., 2015) 024001, arXiv:1408.3978 [gr-qc].
- [50] LIGO Scientific Collaboration, J. Aasi, B. P. Abbott, R. Abbott, T. Abbott, M. R. Abernathy, K. Ackley, C. Adams, T. Adams, P. Addesso, *et al.*, “Advanced LIGO,” *Classical and Quantum Gravity* **32** no. 7, (Apr., 2015) 074001, arXiv:1411.4547 [gr-qc].
- [51] Caltech/MIT/LIGO Lab, “Gravitational-Wave Observatories Across the Globe,” Feb., 2016. <https://www.ligo.caltech.edu/image/ligo20160211c>. Accessed: 2018-02-20.

- [52] Y. Aso, Y. Michimura, K. Somiya, M. Ando, O. Miyakawa, T. Sekiguchi, D. Tatsumi, and H. Yamamoto, “Interferometer design of the KAGRA gravitational wave detector,” **88** no. 4, (Aug., 2013) 043007, [arXiv:1306.6747](https://arxiv.org/abs/1306.6747) [gr-qc].
- [53] LIGO Scientific Collaboration, “Instrument Science White Paper,” tech. rep., 10, 2016. <https://dcc.ligo.org/T1600119/public>.
- [54] P. Amaro-Seoane, H. Audley, S. Babak, J. Baker, E. Barausse, P. Bender, E. Berti, P. Binetruy, M. Born, D. Bortoluzzi, J. Camp, C. Caprini, V. Cardoso, M. Colpi, J. Conklin, N. Cornish, C. Cutler, K. Danzmann, R. Dolesi, L. Ferraioli, V. Ferroni, E. Fitzsimons, J. Gair, L. Gesa Bote, D. Giardini, F. Gibert, C. Grimani, H. Halloin, G. Heinzl, T. Hertog, M. Hewitson, K. Holley-Bockelmann, D. Hollington, M. Hueller, H. Inchauspe, P. Jetzer, N. Karnesis, C. Killow, A. Klein, B. Klipstein, N. Korsakova, S. L. Larson, J. Livas, I. Lloro, N. Man, D. Mance, J. Martino, I. Mateos, K. McKenzie, S. T. McWilliams, C. Miller, G. Mueller, G. Nardini, G. Nelemans, M. Nofrarias, A. Petiteau, P. Pivato, E. Plagnol, E. Porter, J. Reiche, D. Robertson, N. Robertson, E. Rossi, G. Russano, B. Schutz, A. Sesana, D. Shoemaker, J. Slutsky, C. F. Sopuerta, T. Sumner, N. Tamanini, I. Thorpe, M. Troebis, M. Vallisneri, A. Vecchio, D. Vetrugno, S. Vitale, M. Volonteri, G. Wanner, H. Ward, P. Wass, W. Weber, J. Ziemer, and P. Zweifel, “Laser Interferometer Space Antenna,” *ArXiv e-prints* (Feb., 2017), [arXiv:1702.00786](https://arxiv.org/abs/1702.00786) [astro-ph.IM].
- [55] M. Armano, H. Audley, G. Auger, J. T. Baird, M. Bassan, P. Binetruy, M. Born, D. Bortoluzzi, N. Brandt, M. Caleno, L. Carbone, A. Cavalleri, A. Cesarini, G. Ciani, G. Congedo, A. M. Cruise, K. Danzmann, M. de Deus Silva, R. De Rosa, M. Diaz-Aguiló, L. Di Fiore, I. Diepholz, G. Dixon, R. Dolesi, N. Dunbar, L. Ferraioli, V. Ferroni, W. Fichter, E. D. Fitzsimons, R. Flatscher, M. Freschi, A. F. García Marín, C. García Marirrodriaga, R. Gerndt, L. Gesa, F. Gibert, D. Giardini, R. Giusteri, F. Guzmán, A. Grado, C. Grimani, A. Grynagier, J. Grzymisch, I. Harrison, G. Heinzl, M. Hewitson, D. Hollington, D. Hoyland, M. Hueller, H. Inchauspé, O. Jennrich, P. Jetzer, U. Johann, B. Johlander, N. Karnesis, B. Kaune, N. Korsakova, C. J. Killow, J. A. Lobo, I. Lloro, L. Liu, J. P. López-Zaragoza, R. Maarschalkerweerd, D. Mance, V. Martín, L. Martin-Polo, J. Martino, F. Martin-Porqueras, S. Madden, I. Mateos, P. W. McNamara, J. Mendes, L. Mendes, A. Monsky, D. Nicolodi, M. Nofrarias, S. Paczkowski, M. Perreux-Lloyd, A. Petiteau, P. Pivato, E. Plagnol, P. Prat, U. Ragnit, B. Raïs, J. Ramos-Castro, J. Reiche, D. I. Robertson, H. Rozemeijer, F. Rivas, G. Russano, J. Sanjuán, P. Sarra, A. Schleicher, D. Shaul, J. Slutsky, C. F. Sopuerta, R. Stanga, F. Steier, T. Sumner, D. Texier, J. I. Thorpe, C. Trenkel, M. Tröbs, H. B. Tu, D. Vetrugno, S. Vitale, V. Wand, G. Wanner, H. Ward, C. Warren, P. J. Wass, D. Wealthy, W. J. Weber, L. Wissel, A. Wittchen, A. Zambotti, C. Zandoni, T. Ziegler, and P. Zweifel,

- “Sub-Femto-g Free Fall for Space-Based Gravitational Wave Observatories: LISA Pathfinder Results,” *Physical Review Letters* **116** no. 23, (June, 2016) 231101.
- [56] B. P. Abbott, R. Abbott, T. D. Abbott, M. R. Abernathy, K. Ackley, C. Adams, P. Addesso, R. X. Adhikari, V. B. Adya, C. Affeldt, *et al.*, “Exploring the sensitivity of next generation gravitational wave detectors,” *Classical and Quantum Gravity* **34** no. 4, (Feb., 2017) 044001, arXiv:1607.08697 [astro-ph.IM].
- [57] M. Punturo, M. Abernathy, F. Acernese, B. Allen, N. Andersson, K. Arun, F. Barone, B. Barr, M. Barsuglia, M. Beker, *et al.*, “The Einstein Telescope: a third-generation gravitational wave observatory,” *Classical and Quantum Gravity* **27** no. 19, (Oct., 2010) 194002.
- [58] J. Miller, L. Barsotti, S. Vitale, P. Fritschel, M. Evans, and D. Sigg, “Prospects for doubling the range of Advanced LIGO,” **91** no. 6, (Mar., 2015) 062005, arXiv:1410.5882 [gr-qc].
- [59] R. A. Hulse and J. H. Taylor, “Discovery of a pulsar in a binary system,” *The Astrophysical Journal* **195** (1975) L51–L53.
- [60] J. M. Weisberg, J. H. Taylor, and L. A. Fowler, “Gravitational waves from an orbiting pulsar,” *Scientific American* **245** (1981) 74–81.
- [61] J. M. Weisberg and J. H. Taylor, “The Relativistic Binary Pulsar B1913+16: Thirty Years of Observations and Analysis,” in *Binary Radio Pulsars*, F. A. Rasio and I. H. Stairs, eds., vol. 328 of *Astronomical Society of the Pacific Conference Series*, p. 25. July, 2005. astro-ph/0407149.
- [62] B. P. Abbott, R. Abbott, T. D. Abbott, M. R. Abernathy, F. Acernese, K. Ackley, C. Adams, T. Adams, P. Addesso, R. X. Adhikari, and *et al.*, “GW151226: Observation of Gravitational Waves from a 22-Solar-Mass Binary Black Hole Coalescence,” *Physical Review Letters* **116** no. 24, (June, 2016) 241103, arXiv:1606.04855 [gr-qc].
- [63] B. P. Abbott, R. Abbott, T. D. Abbott, F. Acernese, K. Ackley, C. Adams, T. Adams, P. Addesso, R. X. Adhikari, V. B. Adya, *et al.*, “Multi-messenger Observations of a Binary Neutron Star Merger,” **848** (Oct., 2017) L12, arXiv:1710.05833 [astro-ph.HE].
- [64] B. P. Abbott, R. Abbott, T. D. Abbott, M. R. Abernathy, F. Acernese, K. Ackley, C. Adams, T. Adams, P. Addesso, R. X. Adhikari, *et al.*, “Prospects for Observing and Localizing Gravitational-Wave Transients with Advanced LIGO and Advanced Virgo,” *Living Reviews in Relativity* **19** (Feb., 2016) 1, arXiv:1304.0670 [gr-qc].

- [65] C. Berry, “Gravitational-wave sensitivity curves,” 2015.
<https://cplberry.com/2015/01/10/1408-0740/>. Accessed: 2018-01-31.
- [66] T. Bayes and R. Price, “An Essay Towards Solving a Problem in the Doctrine of Chances. By the late Rev. Mr. Bayes, communicated by Mr. Price, in a letter to John Canton, M.A. and F.R.S.,” *Philosophical Transactions of the Royal Society* (January, 1763) .
- [67] S. B. McGrayne, *The Theory That Would Not Die*. Yale University Press, New Haven & London, 2011.
- [68] E. T. Jaynes, *Probability Theory - The Logic of Science*. Cambridge University Press, Cambridge, UK, 2003.
- [69] H. Jeffreys, *The Theory of Probability*. Oxford Classic Texts in the Physical Sciences. OUP Oxford, 1998.
<https://books.google.co.uk/books?id=vh9Act9rtzQC>.
- [70] G. D’Agostini, “Bayesian inference in processing experimental data: principles and basic applications,” *Reports on Progress in Physics* **66** no. 9, (2003) 1383.
<http://stacks.iop.org/0034-4885/66/i=9/a=201>.
- [71] R. Munroe, “Frequentists vs. Bayesians,” 2012. <http://xkcd.com/1132/>.
Accessed: 2017-12-19.
- [72] R. Trotta, “Bayes in the sky: Bayesian inference and model selection in cosmology,” *Contemporary Physics* **49** (Mar., 2008) 71–104, arXiv:0803.4089.
- [73] J. Veitch and A. Vecchio, “Bayesian coherent analysis of in-spiral gravitational wave signals with a detector network,” **81** no. 6, (Mar., 2010) 062003, arXiv:0911.3820.
- [74] P. Gregory, *Bayesian Logical Data Analysis for the Physical Sciences: A Comparative approach with Mathematica Support*. Cambridge University Press, Cambridge, UK, 2005.
- [75] A. Liddle, *An Introduction to Modern Cosmology*. Wiley, West Sussex, 2003.
- [76] W. Herschel, “On the Construction of the Heavens.,” *Philosophical Transactions of the Royal Society of London Series I* **75** (1785) 213–266.
- [77] M. Blanton and SDSS, “SDSS Galaxy Map.”
<http://www.sdss.org/science/orangepie/>. Accessed: 2018-03-02.
- [78] P. J. E. Peebles, *Principles of Physical Cosmology*. Princeton University Press, Princeton, New Jersey, 1993.

- [79] E. Hubble, “A Relation between Distance and Radial Velocity among Extra-Galactic Nebulae,” *Proceedings of the National Academy of Science* **15** (Mar., 1929) 168–173.
- [80] A. Friedmann, “On the Curvature of Space,” *General Relativity and Gravitation* **31** (Dec., 1999) 1991.
- [81] A. Friedmann, “Über die Krümmung des Raumes,” *Zeitschrift für Physik* **10** (1922) 377–386.
- [82] A. Friedmann, “Über die Möglichkeit einer Welt mit konstanter negativer Krümmung des Raumes,” *Zeitschrift für Physik* **21** (Dec., 1924) 326–332.
- [83] S. Perlmutter, G. Aldering, G. Goldhaber, R. A. Knop, P. Nugent, P. G. Castro, S. Deustua, S. Fabbro, A. Goobar, D. E. Groom, I. M. Hook, A. G. Kim, M. Y. Kim, J. C. Lee, N. J. Nunes, R. Pain, C. R. Pennypacker, R. Quimby, C. Lidman, R. S. Ellis, M. Irwin, R. G. McMahon, P. Ruiz-Lapuente, N. Walton, B. Schaefer, B. J. Boyle, A. V. Filippenko, T. Matheson, A. S. Fruchter, N. Panagia, H. J. M. Newberg, W. J. Couch, and T. S. C. Project, “Measurements of Ω and Λ using 42 High-Redshift Supernovae,” *The Astrophysical Journal* **517** (1999) 565–586.
- [84] A. G. Riess, A. V. Filippenko, P. Challis, A. Clocchiatti, A. Diercks, P. M. Garnavich, R. L. Gilliland, C. J. Hogan, S. Jha, R. P. Kirshner, B. Leibundguut, M. M. Phillips, D. Riess, B. P. Schmidt, R. A. Schommer, R. C. Smith, J. Spyromilio, C. Stubbs, N. B. Suntzeff, and K. Tonry, “Observational evidence from supernovae for an accelerating universe and a cosmological constant,” *The Astronomical Journal* **119** (1998) 1009–1038.
- [85] A. Sandage, “The Change of Redshift and Apparent Luminosity of Galaxies due to the Deceleration of Selected Expanding Universes.,” **136** (Sept., 1962) 319.
- [86] A. Sandage, “Current Problems in the Extragalactic Distance Scale.,” **127** (May, 1958) 513.
- [87] V. M. Slipher, “The radial velocity of the Andromeda Nebula,” *Lowell Observatory Bulletin* **2** (1913) 56–57.
- [88] D. W. Hogg, “Distance measures in cosmology,” *ArXiv Astrophysics e-prints* (May, 1999), astro-ph/9905116.
- [89] T. Theuns, “Physical Cosmology.”
<http://icc.dur.ac.uk/~tt/Lectures/UA/L4/cosmology.pdf>.
- [90] J. L. Bernal, L. Verde, and A. G. Riess, “The trouble with H_0 ,” **10** (Oct., 2016) 019, arXiv:1607.05617.

- [91] C. Gordon, K. Land, and A. Slosar, “Cosmological Constraints from Type Ia Supernovae Peculiar Velocity Measurements,” *Physical Review Letters* **99** no. 8, (Aug., 2007) 081301, [arXiv:0705.1718](#).
- [92] N. Sugiura, N. Sugiyama, and M. Sasaki, “Anisotropies in Luminosity Distance,” in *Cosmological Parameters and the Evolution of the Universe*, K. Sato, ed., vol. 183 of *IAU Symposium*, p. 269. 1999.
- [93] Planck Collaboration, P. A. R. Ade, N. Aghanim, M. Arnaud, M. Ashdown, J. Aumont, C. Baccigalupi, A. J. Banday, R. B. Barreiro, J. G. Bartlett, *et al.*, “Planck 2015 results. XIII. Cosmological parameters,” **594** (Sept., 2016) A13, [arXiv:1502.01589](#).
- [94] A. A. Penzias and R. W. Wilson, “A Measurement of Excess Antenna Temperature at 4080 Mc/s.,” **142** (July, 1965) 419–421.
- [95] G. F. Smoot, C. L. Bennett, A. Kogut, E. L. Wright, J. Aymon, N. W. Boggess, E. S. Cheng, G. de Amici, S. Gulkis, M. G. Hauser, G. Hinshaw, P. D. Jackson, M. Janssen, E. Kaita, T. Kelsall, P. Keegstra, C. Lineweaver, K. Loewenstein, P. Lubin, J. Mather, S. S. Meyer, S. H. Moseley, T. Murdock, L. Rokke, R. F. Silverberg, L. Tenorio, R. Weiss, and D. T. Wilkinson, “Structure in the COBE differential microwave radiometer first-year maps,” **396** (Sept., 1992) L1–L5.
- [96] R. K. Sachs and A. M. Wolfe, “Perturbations of a Cosmological Model and Angular Variations of the Microwave Background,” **147** (Jan., 1967) 73.
- [97] D. J. Eisenstein, I. Zehavi, D. W. Hogg, R. Scoccimarro, M. R. Blanton, R. C. Nichol, R. Scranton, H.-J. Seo, M. Tegmark, Z. Zheng, S. F. Anderson, J. Annis, N. Bahcall, J. Brinkmann, S. Burles, F. J. Castander, A. Connolly, I. Csabai, M. Doi, M. Fukugita, J. A. Frieman, K. Glazebrook, J. E. Gunn, J. S. Hendry, G. Hennessy, Z. Ivezić, S. Kent, G. R. Knapp, H. Lin, Y.-S. Loh, R. H. Lupton, B. Margon, T. A. McKay, A. Meiksin, J. A. Munn, A. Pope, M. W. Richmond, D. Schlegel, D. P. Schneider, K. Shimasaku, C. Stoughton, M. A. Strauss, M. SubbaRao, A. S. Szalay, I. Szapudi, D. L. Tucker, B. Yanny, and D. G. York, “Detection of the Baryon Acoustic Peak in the Large-Scale Correlation Function of SDSS Luminous Red Galaxies,” **633** (Nov., 2005) 560–574, [astro-ph/0501171](#).
- [98] G. Hinshaw, D. Larson, E. Komatsu, D. N. Spergel, C. L. Bennett, J. Dunkley, M. R. Nolta, M. Halpern, R. S. Hill, N. Odegard, L. Page, K. M. Smith, J. L. Weiland, B. Gold, N. Jarosik, A. Kogut, M. Limon, S. S. Meyer, G. S. Tucker, E. Wollack, and E. L. Wright, “Nine-year Wilkinson Microwave Anisotropy Probe (WMAP) Observations: Cosmological Parameter Results,” **208** (Oct., 2013) 19, [arXiv:1212.5226](#).

- [99] C. L. Bennett, D. Larson, J. L. Weiland, N. Jarosik, G. Hinshaw, N. Odegard, K. M. Smith, R. S. Hill, B. Gold, M. Halpern, E. Komatsu, M. R. Nolta, L. Page, D. N. Spergel, E. Wollack, J. Dunkley, A. Kogut, M. Limon, S. S. Meyer, G. S. Tucker, and E. L. Wright, “Nine-year Wilkinson Microwave Anisotropy Probe (WMAP) Observations: Final Maps and Results,” **208** (Oct., 2013) 20, [arXiv:1212.5225](#).
- [100] Planck Collaboration, P. A. R. Ade, N. Aghanim, M. I. R. Alves, C. Armitage-Caplan, M. Arnaud, M. Ashdown, F. Atrio-Barandela, J. Aumont, H. Aussel, *et al.*, “Planck 2013 results. I. Overview of products and scientific results,” **571** (Nov., 2014) A1, [arXiv:1303.5062](#).
- [101] F. W. Bessel, “On the parallax of 61 Cygni,” **4** (Nov., 1838) 152–161.
- [102] Gaia Collaboration, T. Prusti, J. H. J. de Bruijne, A. G. A. Brown, A. Vallenari, C. Babusiaux, C. A. L. Bailer-Jones, U. Bastian, M. Biermann, D. W. Evans, *et al.*, “The Gaia mission,” **595** (Nov., 2016) A1, [arXiv:1609.04153](#) [astro-ph.IM].
- [103] W. L. Freedman and B. F. Madore, “The Hubble Constant,” **48** (Sept., 2010) 673–710, [arXiv:1004.1856](#).
- [104] B. F. Madore and W. L. Freedman, “The Cepheid distance scale,” **103** (Sept., 1991) 933–957.
- [105] H. S. Leavitt, “1777 variables in the Magellanic Clouds,” *Annals of Harvard College Observatory* **60** (1908) 87–108.3.
- [106] H. S. Leavitt and E. C. Pickering, “Periods of 25 Variable Stars in the Small Magellanic Cloud,” *Harvard College Observatory Circular* **173** (Mar., 1912) 1–3.
- [107] W. Baade, “The Period-Luminosity Relation of the Cepheids,” **68** (Feb., 1956) 5.
- [108] W. L. Freedman, “Correction: Cosmology at a crossroads,” *Nature Astronomy* **1** (June, 2017) 0169, [arXiv:1706.02739](#).
- [109] D. Branch and G. A. Tammann, “Type IA supernovae as standard candles,” **30** (1992) 359–389.
- [110] P. A. Mazzali, F. K. Röpke, S. Benetti, and W. Hillebrandt, “A Common Explosion Mechanism for Type Ia Supernovae,” *Science* **315** (Feb., 2007) 825, [astro-ph/0702351](#).
- [111] W. L. Freedman, B. F. Madore, B. K. Gibson, L. Ferrarese, D. D. Kelson, S. Sakai, J. R. Mould, R. C. Kennicutt, Jr., H. C. Ford, J. A. Graham, J. P. Huchra, S. M. G. Hughes, G. D. Illingworth, L. M. Macri, and P. B. Stetson, “Final Results from the Hubble Space

- Telescope Key Project to Measure the Hubble Constant,” **553** (May, 2001) 47–72, [astro-ph/0012376](https://arxiv.org/abs/astro-ph/0012376).
- [112] A. G. Riess, L. M. Macri, S. L. Hoffmann, D. Scolnic, S. Casertano, A. V. Filippenko, B. E. Tucker, M. J. Reid, D. O. Jones, J. M. Silverman, R. Chornock, P. Challis, W. Yuan, P. J. Brown, and R. J. Foley, “A 2.4% Determination of the Local Value of the Hubble Constant,” **826** (July, 2016) 56, [arXiv:1604.01424](https://arxiv.org/abs/1604.01424).
- [113] V. Bonvin *et al.*, “H0LiCOW V. New COSMOGRAIL time delays of HE0435-1223: H_0 to 3.8% precision from strong lensing in a flat Λ CDM model,” *Monthly Notices of the Royal Astronomical Society* **465** (2017) 4914–4930.
- [114] B. F. Schutz, “Determining the Hubble constant from gravitational wave observations,” *Nature* **323** (1986) 310–311.
- [115] S. Nissanke, D. E. Holz, N. Dalal, S. A. Hughes, J. L. Sievers, and C. M. Hirata, “Determining the Hubble constant from gravitational wave observations of merging compact binaries,” *ArXiv e-prints* (July, 2013), [arXiv:1307.2638](https://arxiv.org/abs/1307.2638) [astro-ph.CO].
- [116] D. E. Holz and S. A. Hughes, “Using Gravitational-Wave Standard Sirens,” **629** (Aug., 2005) 15–22, [astro-ph/0504616](https://arxiv.org/abs/astro-ph/0504616).
- [117] S. R. Taylor, J. R. Gair, and I. Mandel, “Hubble without the Hubble: Cosmology using advanced gravitational-wave detectors alone,” *Physical Review D* **85** no. 2, (2012) 023535.
- [118] B. P. Abbott, R. Abbott, T. D. Abbott, M. R. Abernathy, F. Acernese, K. Ackley, C. Adams, T. Adams, P. Addesso, R. X. Adhikari, *et al.*, “Binary Black Hole Mergers in the First Advanced LIGO Observing Run,” *Physical Review X* **6** no. 4, (Oct., 2016) 041015, [arXiv:1606.04856](https://arxiv.org/abs/1606.04856) [gr-qc].
- [119] F. Elavsky, LIGO, and Northwestern, “Masses in the Stellar Graveyard,” 2017. <https://media.ligo.northwestern.edu/gallery/mass-plot>. Accessed: 2018-02-06.
- [120] W. Del Pozzo, “Inference of cosmological parameters from gravitational waves: Applications to second generation interferometers,” **86** no. 4, (Aug., 2012) 043011, [arXiv:1108.1317](https://arxiv.org/abs/1108.1317).
- [121] S. R. Taylor and J. R. Gair, “Cosmology with the lights off: Standard sirens in the Einstein Telescope era,” *Physical Review D* **86** (2012) 023502.

- [122] H.-Y. Chen and D. E. Holz, “Finding the One: Identifying the Host Galaxies of Gravitational-Wave Sources,” *ArXiv e-prints* (Dec., 2016), arXiv:1612.01471 [astro-ph.HE].
- [123] N. Dalal, D. E. Holz, S. A. Hughes, and B. Jain, “Short GRB and binary black hole standard sirens as a probe of dark energy,” **74** no. 6, (Sept., 2006) 063006, astro-ph/0601275.
- [124] B. P. Abbott, R. Abbott, T. D. Abbott, F. Acernese, K. Ackley, C. Adams, T. Adams, P. Addesso, R. X. Adhikari, V. B. Adya, *et al.*, “A gravitational-wave standard siren measurement of the Hubble constant,” *ArXiv e-prints* (Oct., 2017), arXiv:1710.05835.
- [125] G. Dály, Z. Frei, G. Galgóczi, P. Raffai, and R. S. de Souza, “An Extended List of Galaxies for Gravitational-Wave Searches in the Advances Detector Era,” Presented at the 2015 September LIGO-Virgo Collaboration Meeting in Budapest, Hungary, September, 2015.
- [126] M. R. Blanton, D. W. Hogg, N. A. Bahcall, J. Brinkmann, M. Britton, A. J. Connolly, I. Csabai, M. Fukugita, J. Loveday, A. Meiksin, J. A. Munn, R. C. Nichol, S. Okamura, T. Quinn, D. P. Schneider, K. Shimasaku, M. A. Strauss, M. Tegmark, M. S. Vogeley, and D. H. Weinberg, “The Galaxy Luminosity Function and Luminosity Density at Redshift $z = 0.1$,” **592** (Aug., 2003) 819–838, astro-ph/0210215.
- [127] H. Oyaizu, M. Lima, C. E. Cunha, H. Lin, and J. Frieman, “Photometric Redshift Error Estimators,” **689** (Dec., 2008) 709–720, arXiv:0711.0962.
- [128] C. J. Conselice, A. Wilkinson, K. Duncan, and A. Mortlock, “The Evolution of Galaxy Number Density at $z \approx 8$ and Its Implications,” **830** (Oct., 2016) 83, arXiv:1607.03909.
- [129] C. J. Conselice, J. A. Blackburne, and C. Papovich, “The Luminosity, Stellar Mass, and Number Density Evolution of Field Galaxies of Known Morphology from $z = 0.5$ to 3,” **620** (Feb., 2005) 564–583, astro-ph/0405001.
- [130] D. J. White, E. J. Daw, and V. S. Dhillon, “A list of galaxies for gravitational wave searches,” *Classical and Quantum Gravity* **28** no. 8, (Apr., 2011) 085016, arXiv:1103.0695.
- [131] M. Tanaka, “Kilonova/Macronova Emission from Compact Binary Mergers,” *Advances in Astronomy* **2016** (2016) 634197, arXiv:1605.07235 [astro-ph.HE].
- [132] B. D. Metzger, “Kilonovae,” *Living Reviews in Relativity* **20** (May, 2017) 3, arXiv:1610.09381 [astro-ph.HE].

- [133] W. H. Lee and E. Ramirez-Ruiz, “The progenitors of short gamma-ray bursts,” *New Journal of Physics* **9** (Jan., 2007) 17, [astro-ph/0701874](#).
- [134] N. R. Tanvir, A. J. Levan, A. S. Fruchter, J. Hjorth, R. A. Hounsell, K. Wiersema, and R. L. Tunnicliffe, “A ‘kilonova’ associated with the short-duration γ -ray burst GRB 130603B,” **500** (Aug., 2013) 547–549, [arXiv:1306.4971 \[astro-ph.HE\]](#).
- [135] Binney, J. and Merrifield, M., *Galactic Astronomy*. Princeton University Press, Princeton, New Jersey, 1998.
- [136] H. Jerjen and G. A. Tammann, “Studies of the Centaurus cluster. III. Luminosity functions of individual Hubble-types as compared to Virgo and Fornax,” **321** (May, 1997) 713–723.
- [137] Z. Ivezić, J. A. Tyson, B. Abel, E. Acosta, R. Allsman, Y. AlSayyad, S. F. Anderson, J. Andrew, R. Angel, G. Angeli, others, and for the LSST Collaboration, “LSST: from Science Drivers to Reference Design and Anticipated Data Products,” *ArXiv e-prints* (May, 2008), [arXiv:0805.2366](#).
- [138] B. P. Abbott, R. Abbott, T. D. Abbott, M. R. Abernathy, F. Acernese, K. Ackley, C. Adams, T. Adams, P. Addesso, R. X. Adhikari, and et al., “The Rate of Binary Black Hole Mergers Inferred from Advanced LIGO Observations Surrounding GW150914,” **833** (Dec., 2016) L1, [arXiv:1602.03842 \[astro-ph.HE\]](#).
- [139] M. S. Fujii, A. Tanikawa, and J. Makino, “The detection rates of merging binary black holes originating from star clusters and their mass function,” **69** (Dec., 2017) 94, [arXiv:1709.02058 \[astro-ph.HE\]](#).
- [140] Caltech/MIT/LIGO Lab, “SkyMap,” Oct., 2017.
<https://www.ligo.caltech.edu/image/ligo20171016b>. Accessed: 2018-03-08.
- [141] B. P. Abbott, R. Abbott, T. D. Abbott, F. Acernese, K. Ackley, C. Adams, T. Adams, P. Addesso, R. X. Adhikari, V. B. Adya, *et al.*, “Gravitational Waves and Gamma-Rays from a Binary Neutron Star Merger: GW170817 and GRB 170817A,” **848** (Oct., 2017) L13, [arXiv:1710.05834 \[astro-ph.HE\]](#).
- [142] A. Goldstein, P. Veres, E. Burns, M. S. Briggs, R. Hamburg, D. Kocevski, C. A. Wilson-Hodge, R. D. Preece, S. Poolakkil, O. J. Roberts, C. M. Hui, V. Connaughton, J. Racusin, A. von Kienlin, T. Dal Canton, N. Christensen, T. Littenberg, K. Siellez, L. Blackburn, J. Broida, E. Bissaldi, W. H. Cleveland, M. H. Gibby, M. M. Giles, R. M. Kippen, S. McBreen, J. McEnery, C. A. Meegan, W. S. Paciesas, and M. Stanbro, “An Ordinary Short Gamma-Ray Burst with Extraordinary Implications: Fermi-GBM

Detection of GRB 170817A,” **848** (Oct., 2017) L14, arXiv:1710.05446 [astro-ph.HE].

- [143] V. Savchenko, C. Ferrigno, E. Kuulkers, A. Bazzano, E. Bozzo, S. Brandt, J. Chenevez, T. J.-L. Courvoisier, R. Diehl, A. Domingo, L. Hanlon, E. Jourdain, A. von Kienlin, P. Laurent, F. Lebrun, A. Lutovinov, A. Martin-Carrillo, S. Mereghetti, L. Natalucci, J. Rodi, J.-P. Roques, R. Sunyaev, and P. Ubertini, “INTEGRAL Detection of the First Prompt Gamma-Ray Signal Coincident with the Gravitational-wave Event GW170817,” **848** (Oct., 2017) L15, arXiv:1710.05449 [astro-ph.HE].